

SINGLE CRYSTAL POLARISED INFRARED
AND LASER RAMAN STUDIES OF SOME
INORGANIC COMPLEXES

By

HENRY AUGUSTINE BROWN-ACQUAYE

A Thesis submitted to the University of Glasgow in
fulfilment of the requirements for the Degree of
Doctor of Philosophy.

Department of Chemistry,
University of Glasgow,
GLASGOW G12 8QQ

July 1977

ProQuest Number: 13804117

All rights reserved

INFORMATION TO ALL USERS

The quality of this reproduction is dependent upon the quality of the copy submitted.

In the unlikely event that the author did not send a complete manuscript and there are missing pages, these will be noted. Also, if material had to be removed, a note will indicate the deletion.



ProQuest 13804117

Published by ProQuest LLC (2018). Copyright of the Dissertation is held by the Author.

All rights reserved.

This work is protected against unauthorized copying under Title 17, United States Code
Microform Edition © ProQuest LLC.

ProQuest LLC.
789 East Eisenhower Parkway
P.O. Box 1346
Ann Arbor, MI 48106 – 1346

SUMMARY

Single crystal polarized infra-red and Raman studies of some ionic transition metal complexes have been used to generate extremely accurate vibrational data, both with respect to frequency and symmetry assignments, and also investigate a variety of solid-state phenomena. The effects include static and dynamic crystal field splitting, order-disorder phenomena and first order phase transitions.

Extensive infra-red and Raman studies were undertaken for those complexes having the general formula A_2MX_4 and A_3MX_5 both of which contain isolated MX_4^{2-} tetrahedral ions. The spectra of these complexes clearly demonstrate the effects of distortion from perfect tetrahedral symmetry and both site and factor group splitting. In order to assist the assignment of a high frequency lattice mode, a Kramers-Kronig (K-K) analysis of the reflectivity data obtained from the A_3MX_5 complexes was undertaken.

The Raman spectra of the complexes $(RNH_3)_2MX_4$, $(Me_4N)_2MX_4$, $(Et_4N)_2MX_4$ and $(DMA)_3MX_5$ recorded at temperatures between 300°K and 77°K all show significant changes with temperature which can be attributed to orientational ordering of both the cations and anions. The $(RNH_3)_2MX_4$ complexes contain square planar MX_4 units which are linked together in 2-D sheets and hence their spectra differ from those characteristic of square-planar complexes.

Most of the copper complexes studied exhibit thermochromic behaviour but the cause is not attributed to any form of structural phase transition.

The single crystal Raman and infra-red reflectance spectra of some sodium perovskite fluorides having the GdFeO_3 structure have been investigated. The reflectivity data was subjected both to K-K and classical dispersion analysis to obtain the dispersion parameters. From consideration both of the factor group predictions and Raman and infra-red data, the centrosymmetric space group D_{2h}^{16} is confirmed for these NaMF_3 complexes.

Raman and infra-red spectra of K_2ZrF_6 and K_2HfF_6 are discussed in terms of the linked MF_8 dodecahedra in which both the zirconium and hafnium atoms are eight co-ordinate.

Owing to experimental difficulties, the first order phase transitions reported for some perchlorate complexes could not be detected from an investigation of their vibrational spectra. Only the room temperature Raman spectra could be recorded.

A C K N O W L E D G E M E N T S
=====

The work described in this thesis was carried out in the laboratories of the Department of Chemistry of the University of Glasgow.

The author wishes to express his sincere thanks to his supervisors, Drs. A.P. Lane and R.V. Emanuel, for their assistance and encouragement in this work.

The author would also like to thank Dr. A.V. Chadwick of the University of Kent at Canterbury for his help in the preparation of the single crystals of the NaMF_3 complexes, Mr. A. Mackie for writing the computer programmes for the K-K and Classical Dispersion analyses, Professor D.W.A. Sharp, head of the Chemistry Department and other staff and students of the department for their assistance and helpful discussion.

The financial assistance of the University of Glasgow is gratefully acknowledged.

---ooOoo---

C O N T E N T S

	Page
<u>CHAPTER 1 - THEORY</u>	1
1.1 Crystal Dynamics	2
1.2 Interaction of Electromagnetic radiation with matter	8
1.3 Infrared reflectance spectroscopy	11
1.4 Single crystal laser Raman spectroscopy	15
1.5 Selection rules	20
1.6 Rule of mutual exclusion	23
1.7 Non-centrosymmetric crystals	24
1.8 Group theory and crystal vibrations	27
<u>CHAPTER 2 - A_2MX_4 COMPLEXES</u>	40
2.1 Cs_2MCl_4 and $(NMe_4)_2MCl_4$ complexes	41
2.2 $(NEt_4)_2MX_4$ complexes	64
<u>CHAPTER 3 - A_3MX_5 COMPLEXES</u>	75
<u>CHAPTER 4 - $(C_nH_{2n+1}NH_3)_2MX_4$ COMPLEXES</u>	96
4.1 $(C_nH_{2n+1}NH_3)_2MCl_4$ complexes	97
4.2 Thermochromism in copper complexes	120
<u>CHAPTER 5 - PEROVSKITE-TYPE $NaMF_3$ COMPLEXES</u>	124
<u>CHAPTER 6 - K_2ZrF_6 AND K_2HfF_6 COMPLEXES</u>	148

<u>CHAPTER 7 - PERCHLORATES</u>	159
7.1 $M(ClO_4)_2 \cdot 6H_2O$ complexes	160
7.2 $Ni(ClO_4)_2 \cdot 6NH_3$ complex	164
<u>CHAPTER 8 - GENERAL EXPERIMENTAL METHODS</u>	170
8.1 Far infrared interferometers	171
8.2 Laser Raman spectrometer	174
8.3 Preparation of single crystals	177
8.4 Determination of crystallographic axes	179

A list of references is given at the end of each chapter.

-----ooOoo-----

LIST OF TABLES

<u>TABLE</u>		<u>PAGE</u>
1.1	32
1.2	33
2.1	45
2.2	45
2.3	47
2.4	48
2.5	49
2.6	52
2.7	53
2.8	54
2.9	55
2.10	56
2.11	57
2.12	58
2.13	59
2.14	60
2.15	66
2.16	66
2.17	67
2.18	67
2.19	68
2.20	69
3.1	79
3.2	80
3.3	84

TABLEPAGE

3•4	85
3•5	89
3•6	93
4•1	104
4•2	104
4•3	105
4•4	109
4•5	109
4•6	110
4•7	110
4•8	111
4•9	111
4•10	112
4•11	113
4•12	113
4•13	114
4•14	114
4•15	114
4•16	121
5•1	136
5•2	136
5•3	137
5•4	138
5•5	138
5•6	140
5•7	142

TABLE

PAGE

6.1	151
6.2	151
6.3	155
6.4	156
7.1	163
7.2	163
7.3	166

LIST OF FIGURES

<u>FIGURE</u>		<u>PAGE</u>
1.1	4
1.2	7
1.3	7
2.1	43
3.1	82
3.2	83
3.3	91
4.1	99
4.2	107
4.3	107
4.4	108
5.1	128
5.2	133
5.3	134
5.4	135
5.5	143
6.1	153

CHAPTER 1 - THEORY

- 1.1 Crystal Dynamics
- 1.2 Interaction of Electromagnetic Radiation with Matter.
- 1.3 Infrared Reflectance Spectroscopy
- 1.4 Single Crystal Laser Raman Spectroscopy
- 1.5 Selection Rules
- 1.6 Rule of Mutual Exclusion
- 1.7 Non-Centrosymmetric Crystals
- 1.8 Group Theory and Crystal Vibrations

1.1 CRYSTAL DYNAMICS

A crystal may be regarded as an infinite array of molecules so that the study of crystal vibrations grows out of the study of molecular vibrations. A crystal lattice consists of a regular array of unit cells each containing a similar group of nuclei and electrons. If a nucleus is displaced from its equilibrium position, a restoring force will act on it, but in a crystal lattice nuclei are coupled by interatomic forces so that they cannot vibrate independently of one another. The vibrations depend on the form and magnitude of the binding energy between adjacent nuclei. Because of their much smaller mass, the electrons will arrange themselves in nearly equilibrium configuration for each nuclear displacement so that the movements of the nuclei could be discussed without explicitly discussing the movements of the valence electrons. This approach is known as the Adiabatic Approximation, introduced by Born and Oppenheimer (1).

As in many other fields of physics, the understanding of crystal vibrations in general is greatly aided by the discussion of model cases capable of explicit solutions. The simplest possible approximation is usually referred to as the Einstein model (2) where it is assumed that the particles in a simple lattice vibrate independently of each other, each isotropically about its mean position so that all the vibrational frequencies are equal. However there is a tendency for the motion of adjacent particles to be

correlated. To obtain the spectrum of the whole lattice the local forces must be considered and the motions described completely. This would be an impossible problem were it not for the Translational Invariance of the lattice.

A crystal, considered as a mechanical system of nN particles, where n is the number of particles per unit cell and N is the number of unit cells contained in the whole crystal, will have $3nN$ degrees of freedom of which $3nN-3$ are linearly independent normal modes of oscillations of the crystal and three are pure translations. Each normal mode has an angular frequency ω , a wave vector k and a polarization vector e . Because the number of modes belonging to a macroscopic piece of a crystal is very large ($\sim 10^{24}$) it is necessary to describe the frequency spectrum in terms of a frequency distribution.

The frequency spectrum of the nuclear motions in a solid can be determined by constructing the classical equations of motions for the lattice points and obtaining the solutions of the normal modes as plane waves. The $3n$ roots of the secular equation involving the wave vector $k(=2\pi/\lambda)$ which may take N values, give the vibrational frequencies. A simple model due originally to Born and Karman (3) will be used to illustrate the normal vibrations. The model consists of an infinite diatomic lattice labelled so that the atoms designated even have mass M and those designated odd have mass m (Fig. 1.1). They have a regular spacing a and only nearest-neighbour interactions are assumed so that the binding forces between two atoms determine the elastic force constant, f , of the vibration.

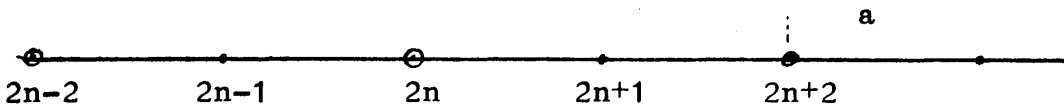


Fig. 1.1

The vibrations of two kinds of atoms are thus described by two differential equations, each representing elastic oscillations of one kind of atom in the linear chain.

If the displacement of atom M at $2n$ position is denoted by X_{2n} and the displacements of its neighbours are denoted by X_{2n+1} and X_{2n-1} , both chains may be described by the two differential equations of the form:-

$$M \frac{d^2 X_{2n}}{dt^2} = f (X_{2n-1} + X_{2n+1} - 2X_{2n}) \quad (1)$$

$$m \frac{d^2 X_{2n+1}}{dt^2} = f (X_{2n} + X_{2n+2} - 2X_{2n+1}) \quad (2)$$

The solution of both equations for both kinds of atoms will be found in the form of plane travelling waves:

$$X_{2n}(t) = X_M \cos (Wt - 2nka) \quad (3)$$

$$X_{2n+1}(t) = X_m \cos (Wt - (2n+1)ka) \quad (4)$$

By substituting solutions (3) and (4) into equations (1) and (2) a system of two equations is obtained to find the amplitudes X_M and X_m .

$$(MW^2 - 2f) X_M + (2f \cos ka) X_m = 0 \quad (5)$$

$$(2f \cos ka) X_M + (mW^2 - 2f) X_m = 0 \quad (6)$$

This has a solution for X_M and X_m if the determinant set up from the coefficients of these variables is zero, i.e. if

$$\begin{vmatrix} MW^2 - 2f & 2f \cos ka \\ 2f \cos ka & mW^2 - 2f \end{vmatrix} = 0 \quad (7)$$

By solving equation (7) a relation for the square of the angular frequency W , is obtained:

$$W^2 = \frac{f}{\mu} \pm f \left[\frac{1}{\mu^2} - \frac{4 \sin^2 ka}{Mm} \right]^{\frac{1}{2}} \quad (8)$$

where μ is the reduced mass, $\frac{m+M}{mM}$.

Since W must be positive, each value of W^2 leads only to a single value of W . But owing to the positive or negative terms in the right-hand side of equation (8), to each value of the wave vector k there corresponds two values of W . The relationship between the wave vector k and the frequency of the waves W , is referred to as the Dispersion Relationship. From equation (8) it is evident that the angular frequencies W_{\pm} are periodic functions of the wave-vector. If a finite length of $2Na$ is chosen for the lattice, it will restrict the possible values of k in the region $-a \leq k \leq +a$. The region between these limits of k is termed the First Brillouin Zone (4). A plot of W_{\pm} as a function of k gives two branches in the First Brillouin Zone (Fig. 1.2). The lower branch corresponds to W_- and is called the Acoustical Branch and the upper one W_+ is called the Optical Branch. Since it is the vibrations within the body of the crystal which are being discussed and not surface effects, the surfaces are removed by imposing periodic boundary conditions $k = \pm \pi/2a$. If $k=0$ the following relations are observed:

$$(W_+)_{\max} = \left(\frac{2f}{\mu} \right)^{\frac{1}{2}} ; W_- = 0 \quad (9)$$

when $k = \pm \pi/2a$ (boundary condition)

$$(W_-)_{\max} = \left(\frac{2f}{M} \right)^{\frac{1}{2}} ; (W_+)_{\min} = \left(\frac{2f}{m} \right)^{\frac{1}{2}} \quad (10)$$

Between both branches W_+ and W_- there is a region of frequencies which are not allowed to pass through the linear chain. The minimum width of the band of "forbidden frequencies" is at the boundary of the Brillouin zone and

has the value

$$\Delta W = (W_+)_{\min} - (W_-)_{\max} = \left[2f \left(\frac{1}{m} - \frac{1}{M} \right) \right]^{\frac{1}{2}} \quad (11)$$

which increases with the ratio of masses M/m of both atoms, while the width of the optical branch, measured by the difference $(W_+)_{\max} - (W_+)_{\min}$ is inversely proportional to M/m .

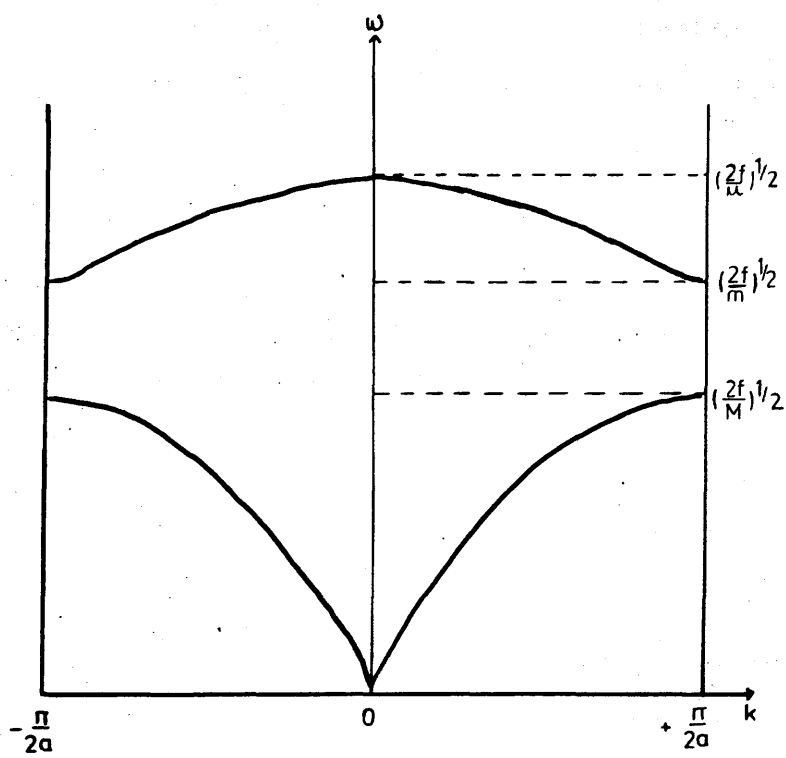
Some idea of the physical significance of the existence of the two branches may be obtained by looking at the amplitude of vibrations of very small wave vector k . In the limit of $k=0$, it may be calculated that for the acoustical branch $X_M = X_m$ and for the optical branch

$$\frac{X_M}{X_m} = - \frac{m}{M} \quad (12)$$

This implies that in the acoustical branch the two types of atoms may be considered as vibrating in phase whereas in the optical branch they vibrate out of phase, keeping their centre of mass fixed.

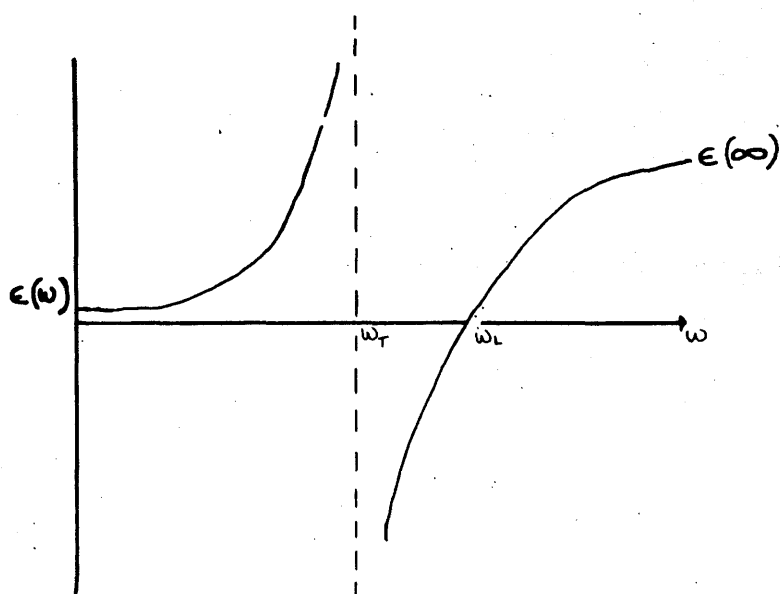
If the atoms are electrically charged (i.e. an ionic crystal) the vibrations of the optical branch will be associated with an oscillating electric dipole in the crystal which can interact with the electric component of electromagnetic radiation. Because of this infrared absorption is good evidence that sodium chloride really contains Na^+ and Cl^- ions. With some mathematical complexity these arguments can be extended to three dimensional systems (3).

FIGURE 1.2



Dispersion relation for a linear diatomic chain

FIGURE 1.3



Variation of dielectric constant with zero damping

1.2 INTERACTION OF ELECTROMAGNETIC RADIATION
WITH MATTER

The interaction of lattice vibrations and electromagnetic radiation manifests itself in a large number of effects which collectively provide one of the principal sources of detailed experimental information on phonon dispersion relations. The optical properties of crystals are due primarily to the interaction of light waves with the optical branches of the phonon spectrum. Lattice waves and electromagnetic waves can interact only when their respective wave vectors and frequencies are equal. Since the maximum lattice frequency is about 10^{13}sec^{-1} , the magnitude of the wave vector ($q = k = \omega/c$) should be only about 300cm^{-1} and this is negligible compared to the total range of q from the zone centre to the zone boundary which is about 10^8cm^{-1} . Thus the wavelength of the radiation is very much longer than the interionic spacing and the wave vector associated with the electromagnetic field in the infrared region is therefore essentially zero. These correspond to the conservation of energy and momentum, i.e.

$$\hbar\omega(q) = \hbar\omega(k) \quad (1)$$

$$\hbar q = \hbar k \quad (2)$$

The optical lattice vibrations of large wavelengths can be considered on a macroscopic bases (5). Such optical vibrations are important chiefly in ionic crystals owing to the strong electric moments associated with the motion. It is known in the electromagnetic theory of light that the square of the refractive index is equal to the dielectric constant; the phenomenon of dispersion follows directly from a frequency-dependent dielectric constant. In ionic

crystals two contributions to the dielectric constant are distinguished:- the electronic part and the ionic part. The former depends entirely on the response of the electrons to the field and is denoted by $\epsilon(\infty)$ since it remains almost constant up to frequencies in the optical region of the electromagnetic spectrum ($\omega/2\pi \sim 10^{15} \text{ sec}^{-1}$). The other contribution, the ionic part, comes from the relative displacement of the positive and negative ions. Resonant frequencies are associated with the electronic polarisation (ω_{uv} in the ultraviolet) and with the ionic polarisation (ω_{ir} in the far i.r.). The value of the dielectric constant in the low frequency region $\omega \ll \omega_{ir}$ is denoted by ϵ_0 and is known as the static dielectric constant. The dispersion formula then is most conveniently written as follows (4):

$$\epsilon(\omega) = \epsilon(\infty) + \omega_T^2 \frac{(\epsilon(0) - \epsilon(\infty))}{\omega_T^2 - \omega^2} \quad (3)$$

where ω_T is the infrared dispersion frequency at which the refractive index and the dielectric constant become infinitely large. In practice this is measured as the absorption frequency of a thin film of the crystal, and is the frequency of the transverse optic mode. Function (3) is shown in Figure 1.3. The curve represents a typical dispersion effect, with zero damping associated with the resonance at $\omega = \omega_T$. At this frequency $\epsilon(\omega)$ exhibits an infinite discontinuity and remains negative up to $\omega = \omega_L$, where ω_L is the frequency of the longitudinal optic mode. Thus in the macroscopic theory of Huang (5), the independent vibrational modes can be taken as transverse and longitudinal

plane waves of different wave-numbers and directions of propagation: all the transverse waves vibrate with the i.r. dispersion frequency ω_T and all the longitudinal waves vibrate with the higher frequency ω_L . A consequence of the dielectric function (6) is that electromagnetic waves will not propagate in a forbidden frequency region and thus

$$\omega_T^2 < \omega^2 < \omega_L^2 \quad \equiv \quad \omega_T^2 \frac{\epsilon(0)}{\epsilon(\infty)} \quad (4)$$

which defines ω_L . The frequencies ω_T and ω_L differ because in a transverse wave the electric field vanishes everywhere and the vibration frequency is solely determined by the local elastic restoring force whereas in a longitudinal wave there is an electric field which contributes an additional restoring force. This difference was first pointed out by Lyddane and Herzfeld (6) and Frohlich and Mott (7). Since the dynamic equations of lattice motion reveal the frequency of ω_L to be that of the Longitudinal Optic Mode (LO) in the limit of long wavelengths, equation (3) may be written as

$$\epsilon(\omega) = \epsilon(\infty) \frac{\omega_L^2 - \omega^2}{\omega_T^2 - \omega^2} \quad (5)$$

and that

$$\frac{\omega_T^2}{\omega_L^2} = \frac{\epsilon(\infty)}{\epsilon(0)} \quad (6)$$

Equation (6) is called Lyddane-Sachs-Teller relation (8).

1.3 INFRARED REFLECTANCE SPECTROSCOPY

To obtain absorption spectra on which to base a structural analysis, it is essential to have a very thin section of a single crystal to allow the intensity of absorption to be measured accurately. Generally for ionic crystals the thickness has to be less than 1μ and this is difficult to attain. Measurements of the reflected radiation from optically polished surfaces of bulk specimens can, however, be used and the reflected spectrum converted into an absorption spectrum (9). It is known that surface reflectivity and internal absorption become very strong in the vicinity of fundamental oscillator frequencies, but whereas the absorption band is reasonably well centred on the oscillator frequency, the reflectivity band can be highly asymmetrical in the region of resonance. This is because for most crystals the dielectric constant $\epsilon(\omega)$ is in general complex and is the square of the complex refractive index whose real part is the refractive index commonly associated with refractometry and geometrical optics; its imaginary part is the extinction coefficient that describes the dissipation of energy from an electromagnetic wave as a function of frequency as it proceeds through a crystal. The extinction coefficient K , is related to the more familiar absorption coefficient, α appearing in Lambert's Law $T = e^{-\alpha x}$ where T is the fractional transmission and x is the sample thickness. The refractive index n , and the extinction coefficient K , are the optical constants, functions of frequency. Fresnel's equations

provide the connection between the optical constants and the reflected and transmitted intensities of a wave as it encounters the boundary between two dissimilar media such as air/optically polished crystal surface. The reflected and transmitted intensities are measurable quantities, the optical constants are nonmeasurable quantities which have direct physical significance.

$$N^2 = (n - iK)^2 = \epsilon(W) = \epsilon_1(W) - i\epsilon_2(W) \quad (1)$$

where n and K are the conventional refractive index and extinction coefficient respectively. The real and imaginary parts of equation (1) are

$$n^2 - K^2 = \epsilon_1(W), \quad 2nK = \epsilon_2(W) \quad (2)$$

When an electromagnetic wave is reflected, the reflectivity and the accompanying phase shift are not entirely independent quantities. The coefficient called 'reflectivity' $r(W)$ is a complex physical quantity connecting linearly the electric field amplitude of the reflected wave to the amplitude of the electric field of the incident wave, thus

$$E_{\text{ref}} = r(W)E_{\text{inc}} \quad (3)$$

Such a relation is one example of various physical phenomena which can be treated using linear response theory (10, 11). Kramers and Kronig(12) have formulated a whole family of relations which show that the real and imaginary parts of the refractive index and those of the dielectric constant are related rather than independent quantities. Physically they represent two aspects of the same phenomena and quantitatively the relation is so close that a knowledge of the real part can be used to yield the imaginary parts and vice-versa. They are known as the Kramers-Kronig relations and the following is the statement of the relations. The amplitude

and phase of the complex reflection coefficient are related by (13, 14)

$$\theta(W) = \frac{2W}{\pi} \int_0^{\infty} \frac{\ln|r(W)/dW_i}{W^2 - W_i^2} \quad (4)$$

Therefore, from a measurement over the frequency spectrum, which needs extrapolating the experimental values to $W \rightarrow \infty$ and $W=0$, of the amplitude of the reflected wave, the value $\theta(W)$ can be obtained from the equation

$$|r(W)|e^{i\theta} = \frac{n-1 - iK}{n+1 - iK} \quad (5)$$

The real and imaginary parts of the dielectric constant and those of the refractive index are given by equations (1) and (2).

Another method of studying the reflectivity data is known as the Classical Dispersion Analysis which has been associated with the names of Helmholtz, Lorentz and Drude (15). The method regards the crystal as an assembly of one or more sets of damped oscillators, each of which is defined by its three 'dispersion parameters' which are its resonant frequency W_j , strength ρ_j and width γ_j . The assumption is that each mode can be excited independently of the other normal modes. From classical dispersion theory of crystals (16) the refractive index n and extinction coefficient K are given by the equations:

$$n^2 - K^2 = \epsilon_0 + \sum_j 4\pi\rho_j W_j^2 \frac{W_j^2 - W^2}{(W_j^2 - W^2)^2 + \gamma_j^2 W^2} \quad (6)$$

$$nK = \sum_j 2\pi\rho_j W_j^2 \frac{\gamma_j W}{(W_j^2 - W^2)^2 + \gamma_j^2 W^2} \quad (7)$$

where the summation is over the lattice oscillators. Since each peak in the plot of ϵ'' vs energy in the K-K analysis represents a resonance, the dispersion parameters can be

obtained from the K-K analysis of each peak and these adjusted quantitatively in the measured reflection spectrum until the closest fit is obtained. Spitzer and Kleinman (15) employed a trial and error technique which was later found unsuitable by Jaspere, Kahan, Plendl and Mitra (17). Other techniques for the Classical Dispersion Analysis of the I.R. reflectance data have been developed by various researchers. (18, 19).

1.4 SINGLE CRYSTAL LASER RAMAN SPECTROSCOPY

Raman spectroscopy is a scattering process in which the incident radiation of angular frequency W_i interacts with the crystal to create or destroy one or more lattice quanta (phonons) and the energy to W gained or lost is compensated by a decrease or increase in the frequency W_s of the scattered light: ($W_s = W_i \pm W$). This phenomena predicted by Smekal (20) was later demonstrated by Raman (21) in 1928. The same effect was observed in quartz later by Landsberg and Mandelstam(22) working independently. This effect differed from the earlier known radiation scattering effects for particles (Tyndall) and for molecules (Rayleigh) (23,24). Nevertheless the understanding of the nature of the Raman effect is inseparable from a knowledge of the nature of Rayleigh scattering. The theory of light scattering is based on the fact that the incident light wave with electric vector E , oscillating with frequency W and represented by

$$E = E_0 \cos 2\pi Wt \quad (1)$$

where E_0 is the amplitude and t the time, induces an oscillating dipole moment P in the molecule

$$P = [\alpha]E = [\alpha]E_0 \cos 2\pi Wt \quad (2)$$

where $[\alpha]$ represents the polarizability. Thus the scattered radiation arises from electromagnetic waves emitted by the vibrating dipole, the intensity being dependent on the polarizability which in a molecule is due almost entirely to the displacements of the electrons under the influence of the oscillating field of the incident light beam. From classical electromagnetic theory(25), the total intensity or the average rate of total radiation is given by

$$I = \frac{16\pi^4}{3c^3} W^4 P_o^2 \quad (3)$$

where c is the velocity of light and P_o is the amplitude of P , i.e. αE_o . The term W^4 implies that I varies rapidly with frequency.

Since the irradiated molecule may itself be executing periodic motion (perhaps thermally excited) the molecular polarizability α will vary with time and may be expressed to a first approximation by

$$\alpha = \alpha_o + \left(\frac{d\alpha}{dQ_1} \right)_o Q_1 + \dots \quad (4)$$

for small oscillations about the equilibrium position. Q_1 is a displacement co-ordinate, that is, its value is zero in the equilibrium position. The polarizability in the equilibrium configuration of the molecule is α_o and therefore $\left(\frac{d\alpha}{dQ_1} \right)_o$ is the rate of change of polarizability with Q_1 . Since the molecule vibrates with frequency W_1 , the displacement Q_1 is also a function of time so that

$$Q_1 = Q_1^o \cos(2\pi W_1 t) \quad (5)$$

where Q_1^o is the maximum value of the displacement from equilibrium and thus is the vibrational amplitude. Hence

$$P = E_o \cos(2\pi W_o t) \left[\alpha_o + \left(\frac{d\alpha}{dQ_1} \right)_o Q_1 \cos(2\pi W_1 t) \right] \quad (6)$$

$$P = E_o \alpha_o \cos(2\pi W_o t) + E_o Q_1^o \left(\frac{d\alpha}{dQ_1} \right)_o (\cos 2\pi W_o t) \cos(2\pi W_1 t) \quad (7)$$

Using the trigonometric identity

$$\cos \alpha \cos \beta = \frac{1}{2} \left\{ \cos(\alpha + \beta) + \cos(\alpha - \beta) \right\}$$

equation 7 becomes

$$P = E_o \alpha_o \cos(2\pi W_o t) + \frac{1}{2} E_o Q_1^o \left(\frac{d\alpha}{dQ_1} \right)_o \left\{ \cos[2\pi(W_o + W_1)t] + \cos[2\pi(W_o - W_1)t] \right\} \quad (8)$$

Equation (8) shows that the induced dipole moment can be regarded as the superposition of three periodically changing moments having frequencies W_0 , (W_0+W_1) and (W_0-W_1) . The first term in equation (8) corresponds to scattering without change of frequency and in phase with the incident light, i.e. coherent Rayleigh scattering, its intensity depends only on the molecular polarizability. The second and third terms correspond to scattering with change of frequency, i.e. Raman scattering; the high frequency term, by analogy with fluorescence is called the Anti-Stokes line and the low frequency term the Stokes line. Thus while the polarizability of a molecule gives rise to Rayleigh scattering, it is the changes of polarizability during molecular motions, that are responsible for the Raman effect. Rayleigh scattering is an elastic process while Raman scattering is inelastic. Raman effects are relatively inefficient processes since about 10^{-3} of the intensity of the incident radiation appears as Rayleigh while approximately 10^{-6} as Raman lines. Classical physics is unable to offer explanation as to why the anti-Stokes lines are weaker than their Stokes companions. From the application of quantum mechanics to molecular motion, it is known (26) that for any molecule there is a large number of possible energy states each characterizable by suitable labels. In thermal equilibrium the molecules of a gaseous sample will be distributed among these possible levels according to the function

$$N_E = N_0 e^{-E/KT} \quad (9)$$

where N_E is the number in the state E . Thus under the influence of the electromagnetic field the number of molecules available for Stokes scattering will be larger than that for anti-Stokes scattering because of this Boltzmann factor, since only excited molecules can give anti-Stokes scattering.

Generally, the induced dipole moment need not point in the same direction as the incident electric vector. The polarizability is a tensor because the induced dipole and the field strength are vectors and the two are related as follows:

$$\begin{aligned} P_x &= \alpha_{xx} E_x + \alpha_{xy} E_y + \alpha_{xz} E_z \\ P_y &= \alpha_{yx} E_x + \alpha_{yy} E_y + \alpha_{yz} E_z \\ P_z &= \alpha_{zx} E_x + \alpha_{zy} E_y + \alpha_{zz} E_z \end{aligned} \quad (9)$$

where the coefficients α_{xx} , α_{xy} etc are the polarizability tensors. The polarizability α can be resolved into two parts, a symmetric or isotropic part α^s , and the anisotropic part α^a such that $\alpha = \alpha^s + \alpha^a$ (10)

$$\text{where } 3\alpha^s = (\alpha_{xx} + \alpha_{yy} + \alpha_{zz}) \quad (11)$$

$$\text{and } 2[\alpha^a]^2 = [(\alpha_{xx} - \alpha_{yy})^2 + (\alpha_{yy} - \alpha_{zz})^2 + (\alpha_{zz} - \alpha_{xx})^2 + 6(\alpha_{xy}^2 + \alpha_{yz}^2 + \alpha_{zx}^2)] \quad (12)$$

Hence the total polarizability is given by the sum of two matrices:

$$\begin{vmatrix} \alpha_{xx}^s + \alpha_{xx}^a & \alpha_{xy}^a & \alpha_{xz}^a \\ \alpha_{yx}^a & \alpha_{yy}^s + \alpha_{yy}^a & \alpha_{yz}^a \\ \alpha_{zx}^a & \alpha_{zy}^a & \alpha_{zz}^s + \alpha_{zz}^a \end{vmatrix} = \begin{vmatrix} \alpha_{xx}^s & 0 & 0 \\ 0 & \alpha_{yy}^s & 0 \\ 0 & 0 & \alpha_{zz}^s \end{vmatrix} + \begin{vmatrix} \alpha_{xx}^a & \alpha_{xy}^a & \alpha_{xz}^a \\ \alpha_{yx}^a & \alpha_{yy}^a & \alpha_{yz}^a \\ \alpha_{zx}^a & \alpha_{zy}^a & \alpha_{zz}^a \end{vmatrix} \quad (13)$$

The values of α^s and $(\alpha^a)^2$ are the invariants of the polarizability tensor. The matrix elements α_{ij} , although dependent on the directions of the co-ordinate axes within the molecule, are independent of the directions of E and P. Thus in a molecule there exists a set of axes such that all the off diagonal elements of the polarizability tensor are zero. From the symmetry of the unit cell of the single crystal the Raman tensor may be aligned with the crystallographic axes for orthorhombic and higher symmetries (27). For less symmetrical crystal classes, orthogonal axes are chosen. Damien, Porto and Tell(28) have introduced a notation by which the spectrum is defined by four symbols. Thus $i(yz)j$ implies that the light incident along the i -direction with the electric vector in the y -direction is scattered and the Raman light is observed from the j -direction with the analyser so placed that it passes light with the electric vector along the z -direction.

Group theory predicts the number of frequencies which are Raman or I.R. active for all molecules provided that the shape of the molecule or its 'point group' is known. For each normal mode those polarizability tensor components which change during the vibrational motion are also predicted by Group Theory.

1.5 SELECTION RULES

The basis of infrared spectroscopy is the absorption of photons by matter, which is a resonant process. The first requirement is that the energy of the photons match the energy difference between the initial state ψ_i and the final state ψ_f involved in the transition. The transition moment for infrared absorption is given by:

$$\psi_{if} = \int \psi_i \mu \psi_f dQ$$

where ψ_i and ψ_f are respectively the wave functions of the initial and final state; μ is the electric dipole moment of the molecule as a function of Q which is the normal co-ordinate of the vibrational mode. The integral is to be extended over the whole co-ordinate range. Since the dipole moment of a molecule is a vector quantity, the symmetry properties of μ are those of a vector, in particular, it goes into minus itself if the molecule is subjected to a symmetry operation such as inversion or reflection in an appropriate plane. The condition that the integral for the component μ_i (where i denotes x , y or z) shall not vanish is that the integrand $\psi_i \mu_i \psi_f$ shall be totally symmetric i.e. shall be transformed into itself by all the symmetry operations of the molecular point group. Since ψ_i , the ground vibrational state, is known always to be symmetric (29) it follows that the product $\mu_i \psi_f$ must be totally symmetric. This can only happen if both factors belong to the same symmetry species. For a transition to occur, it will suffice if this is so for at least one of the components of μ . However, ψ_f always belongs to the same symmetry species as does the vibration itself(29). Thus the infrared absorption selection rule for fundamentals can be stated as follows(30).

A fundamental is permitted in infrared absorption only if its species is the same as that of at least one of the components of the electric dipole moment.

The species of the dipole-moment components are the same as those of the corresponding translations and are given in the point group character tables.

Raman spectroscopy depends on a scattering process, so that the intrinsic dipole moment μ of the molecule is not what is considered but rather the dipole moment P which is induced in the molecule by the electric field E of the incident radiation. This is given by

$$P = \alpha E \quad (2)$$

where α is the molecular polarizability. For a fundamental Raman transition the transition moment is given by

$$P_{if} = \int \psi_i \alpha E \psi_f dQ = E \int \psi_i \alpha \psi_f dQ$$

The polarizability tensor α is conveniently represented as a 3-by-3 matrix.

$$\left\{ \begin{array}{ccc} \alpha_{xx} & \alpha_{yx} & \alpha_{zx} \\ \alpha_{xy} & \alpha_{yy} & \alpha_{zy} \\ \alpha_{xz} & \alpha_{yz} & \alpha_{zz} \end{array} \right\}$$

Since the matrix is symmetric it has only 6 independent parameters. The selection rule for Raman scattering can therefore be stated as follows.

A fundamental is permitted in Raman scattering only if its species is the same as that of at least one of the components of the polarizability tensor.

A component α_{ij} transforms in the same way as does the product of translations T_i and T_j . The species of the

components of α_{ij} are also given in the point-group character tables so that it is an easy matter to read off the selection rules for vibration of any species.

1.6 RULE OF MUTUAL EXCLUSION

One of the satisfying features of vibrational spectroscopy is the extraordinary complementarity of infrared absorption and Raman scattering, due partly to the contrasting sensitivities of the two methods to ionic and covalent bonds and partly to the contrasting symmetry properties of the two operators, i.e. the vector $\underline{\mu}$ and the ellipsoid $\underline{\alpha}$. This complementarity attains its most rigorous expressions in centrosymmetric molecules. The rule can be expressed as "For molecules with a centre of symmetry, transitions that are allowed in the infrared are forbidden in the Raman spectrum," and conversely, "transitions that are allowed in the Raman spectrum are forbidden in the infrared." (30) This is because for a transition to be allowed, the corresponding transition-moment integral must be non-zero; to be non-zero, it must remain unchanged on application of all symmetry operations appropriate to the molecule. Quantities fulfilling this requirement are described as totally symmetric. The inversion operation \underline{i} will always send a vector into minus itself and the polarizability ellipsoid into plus itself. Thus if ψ_f and ψ_i are such that $\langle \psi_f / \underline{\mu} / \psi_i \rangle$ remains unchanged on application of \underline{i} , $\langle \psi_f / \underline{\alpha} / \psi_i \rangle$ must go into minus itself and vice versa with the result that the transition $\psi_i \rightarrow \psi_f$ must be forbidden in either the Raman or Infrared. This rule is however, not inviolable since some breakdown may take place when spectra are recorded on liquids or solids when molecular complexity increases.

1.7 NON-CENTROSYMMETRIC CRYSTALS

A vibrational mode, phonon, in a crystal can be both Raman and Infrared active only in non-centrosymmetric crystals. Of the 32 classes of crystals, ten have centres of symmetry and the rest lack centres of symmetry and hence are piezoelectric. Fundamental Raman vibrations which are also infrared active are 'anomalous' in that more first-order Raman lines are observed than predicted by factor-group selection rules. This experimental observation has been explained by a detailed treatment of the perturbation of lattice waves by the radiation, (31,32). It has been found that in piezoelectric crystals each Raman-active fundamental predicted by factor-group analysis leads to a pair of Raman lines at frequencies ω_{LO} and ω_{TO} while only the band at ω_{TO} appears in infrared absorption. Even though they correspond to the same mechanical vibrational mode, the two offspring phonons scatter at different frequencies because the macroscopic electric field associated with the longitudinal phonon serves to stiffen the force constant of the phonon and thereby raise the frequency of the LO over that of the TO. This phenomena is discussed by Born and Huang (4) for cubic diatomic crystals and has been generalised by Loudon (27) and others (33). Two modes were observed by Couture-Mathieu and Mathieu (34) for the cubic diatomic crystal ZnS, instead of the one predicted by the theory when the photons are neglected. Poulet (31) subsequently explained the measurements. The separation in frequency is determined to an extent by the dipole-dipole interaction. In simple cubic systems the

LO-TO splitting is very large. However the situation is far more complicated in uniaxial crystals as it becomes necessary to consider simultaneously two independent forces: the long-range electrostatic forces responsible for the LO-TO splitting and the short-range interatomic forces, which exhibit the anisotropy of the force constants and which require the phonons to follow group theoretical selection rules. (27). In examining the Raman spectra of ZnO, Porto (32) emphasises the conservation of both energy and momentum in the Raman spectra of solids. From factor-group analysis a doubly degenerate phonon E_1 is both Raman and I.R. active. When i.r. active in the x-direction the polarizability tensor $\alpha_{xz} \neq 0$. This component can be obtained if the incident light is in the z-direction and the observation is made in the y-direction. A phonon will be produced in the yz plane with x polarization. This phonon will have a propagation direction perpendicular to its polarization and will be a transverse optical mode (TO). However, if the observation is made in the x-direction a phonon will be produced in the xz plane with x polarization. This observed phonon will be both transverse, propagation perpendicular to polarization, (TO) and longitudinal (LO). Hence in the z(xz)y spectrum only one line is observed, the TO phonon, while in the z(xz)x spectrum two lines are obtained, the TO and LO phonons. Lyddane-Sachs-Teller relationship (35) expresses the relations between the LO and TO.

$$\epsilon_0 = \epsilon_\infty \left(\frac{W_{LO}}{W_{TO}} \right)^2$$

where ϵ_0 is the static dielectric constant and ϵ_∞ is the

high-frequency dielectric constant.

Many reviews have been written on the Raman effect. However Placzek's (36) work is still regarded as a standard text on the subject for the pre-laser period. The advent of the laser adrenalised research in Raman spectroscopy and the book by Gilson and Hendra (37) treats the subject in detail.

1.8 GROUP THEORY AND CRYSTAL VIBRATIONS

The internal oscillations of any physical system whose components are linked by simple harmonic forces (i.e. forces proportional to displacement) may be analysed into uncoupled normal modes. Each of these forms a complex pattern of vibration at a definite frequency. By 'uncoupled' is meant that if such a system is set oscillating in a particular normal mode the motion will continue in this mode and no other modes will be excited. Group theory may then be applied to determine the numbers, symmetry and degeneracy of the normal modes. In the application of group theory to crystals it is convenient to deal with finite rather than infinite groups. This is because real crystals are finite in size. The space group describes the internal structure of the crystal rather than its size and shape. This group includes translational operations as well as the point symmetry operations. But these two kinds of symmetry operations do not, in general commute, so that in a given space group it is necessary to select those operations which represent pure translations. They form a subgroup of the space group. The existence of a translational subgroup implies that the crystal may be built up by repeated basic primitive translations of some recognizable unit called the Bravais unit cell. Since it is only the modes of zero wave-vector i.e. the ones corresponding to the centre of the Brillouin zone, that may be optically active as fundamentals, consideration to the vibrations of the Bravais unit cell rather than the crystal as a whole is justified. The group of symmetry operations which remains after primitive translations have

everywhere been equated to the identity operation is called the FACTOR GROUP. A factor group is always isomorphous with one of the 32 crystallographic point groups and therefore the irreducible representations of a factor group are the same as those of its isomorphous point group.

Bhagavantam and Venkatarayudu(38) and Halford (39) have been pioneers in the developments of methods for the determination of vibrational modes which are optically active. In the first method the motions of the crystallographic unit cell are considered while in the other method attention is focussed on the motions of individual molecules within the crystal. Hornig (40) has shown that starting from the method of Halford the results of Bhagavantam and Venkatarayudu could be obtained. However both methods have been shown(41) to be derived from a treatment which considers the motions of a crystal segment composed of an arbitrary number of unit cells and subject to the Born-Karman cyclic boundary conditions (42).

The method of Bhagavantam and Venkarayudu, later modified by Mitra(43), when applied to crystals in which discrete polyatomic ions or molecules can be distinguished, gives the optical activity and symmetry of the internal vibrations of the discrete polyatomic units and the external or lattice vibrations between the discrete structural units of the crystal. The external modes which occur at lower frequencies than the internal ones can be further subdivided into Translatory and Rotatory types, which in the limit of vanishing forces among the groups correspond to pure translations and rotations respectively. The rotatory

lattice modes are often referred to as librational modes, and may be associated with any polyatomic group in a crystal.

Using the symbolism of Mitra, the procedure consists of first determining W_R , the number of atoms in the Bravais cell invariant under the symmetry operation R . The character $X_j'(n_i)$ of the reducible representation with the cartesian co-ordinates of the atoms of the unit cell as a basis are given by

$$X_j'(n_i) = W_R (\pm 1 + 2 \cos \phi_R) \quad (1)$$

where ϕ_R is the rotation angle for the operation R and is defined as follows.

- a) Where E is a proper rotation $\phi = 0^\circ$
- b) (+) used for proper rotations C_n , $\phi = \frac{360}{n}$
- c) (-) used for improper rotations S_n , $\phi = \frac{360}{n}$
- d) σ_h is an improper rotation with $\phi = 0$.
- e) i is an improper rotation with $\phi = 180^\circ$.

The characters $X_j'(T)$ of the reducible representation with the translational movements of the Bravais cell as a whole as a basis are given by

$$X_j'(T) = \pm 1 + 2 \cos \phi_R \quad (2)$$

These characters could, however, be obtained from character tables as the sum of the corresponding characters for the components of the translational movements, T_x , T_y and T_z along the cartesian axes.

The characters $X_j'(T')$ of the reducible representation with the translational lattice modes as a basis are given by

$$X_j'(T') = [W_R(S)-1] [\pm 1 + 2 \cos \phi_R] \quad (3)$$

where $W_R(S)$ is the number of discrete structural groups invariant under the operation R (rotation of the group about its centre of mass or reflection in a plane passing through its centre of mass does not constitute movement when the group as a whole is being considered).

The characters $X_j'(R')$ of the reducible representation with the rotational lattice modes as a basis are given by

$$X_j'(R') = [W_R(S-P)] X_j'(P) \quad (4)$$

where $W_R(S-P)$ is the number of polyatomic structural groups invariant under the operation R ; $X_j'(P)$ is equal to $(1 \pm 2 \cos \phi_R)$ for non-linear polyatomic groups, or $\pm 2 \cos \phi_R$ for the operations $C(\phi_R)$ and $S(\phi_R)$ for a linear polyatomic group, or zero for the operation $C_2(\phi)$ and σ_v for a linear polyatomic group.

The reduction of the various reducible representations to irreducible representations to obtain the symmetry species of the normal modes of vibration of different kinds can be carried out by means of the equation:

$$N_K = \frac{1}{N} \sum h_j X_K(R) X_j'(R) \quad (5)$$

where

N_K is the number of times a particular irreducible representation Γ_K is contained in another representation of Γ , N is the order of the group and h_j the number of group operations contained in the j th subgroup; $X_K(R)$ and $X_j'(R)$ are respectively, the characters of the group operation R in the representations Γ_K and Γ_1 .

The computations required are rather tedious so that the introduction of a set of tables developed by Adams and Newton (44) has been of great help. These give the irreducible representations for each set of Wyckoff (45) sites in all the 230 space groups. Table 1.1 illustrates the use of these tables for the A_2MX_4 complexes and provides a key to the symbols used.

The alternative method developed by Halford uses the 'site' approximation in which the local symmetry of a molecular group in the unit cell is considered. The molecule is located on a point which is left invariant by some operations of the space group. Those operations may be shown to constitute a group which is called the Site Group, and is a subgroup of both the molecular and the crystallographic point group. There is a relationship between the representations of a group and those of its subgroup which is expressed by the Correlation theorem (46). This states that any basis for an irreducible representation of a group is also a basis for a representation (not necessarily irreducible) of any of its subgroups. Thus the representations in the unit cell may be obtained from those of the site group by a reverse use of the theorem. An illustration of the theorem is provided by considering the vibrations of the WO_4 unit in $CaWO_4$ which crystallises in the space group $I 41/a (C_{4h}^6)$ and has two formula units per unit cell (47). The isolated WO_4 units have T_d symmetry. The vibrations of one T_d WO_4 unit spans $A_1 + E + 2T_2$ (Table 1.2). These vibrations associated with the isolated molecule are perturbed to account for their environment in the crystal since each W

Table 1.1 Example of the Use of the Tables of
Adams and Newton for the Factor Group
Analysis of the A_2MX_4 Complexes

Space Group D_{2h}^{16} No. 62 ($z = 4$)

Point Group D_{2h}

Wyckoff sites	A_g	B_{1g}	B_{2g}	B_{3g}	A_u	B_{1u}	B_{2u}	B_{3u}	
A(1) 4C	2	1	2	1	1	2	1	2	(1)
A(2) 4C	2	1	2	1	1	2	1	2	(2)
M 4C	2	1	2	1	1	2	1	2	(3)
X(1) 4C	2	1	2	1	1	2	1	2	(4)
X(2) 4C	2	1	2	1	1	2	1	2	(5)
X(3) 8d	3	3	3	3	3	3	3	3	(6)
Total n_i	13	8	13	8	8	13	8	13	(7)
(1)+(2)+(3) = T + T'	6	3	6	3	3	6	3	6	(8)
T	0	0	0	0	0	1	1	1	(9)
(8)-(9) T'	6	3	6	3	3	5	2	5	(10)
R	1	2	1	2	2	1	2	1	(11)
(7)-(8)-(11) n'_i	6	3	6	3	3	6	3	6	(12)

n_i = total number of zone-centre ($k=0$) modes.

T = acoustic modes (translations)

T' = translatory lattice modes

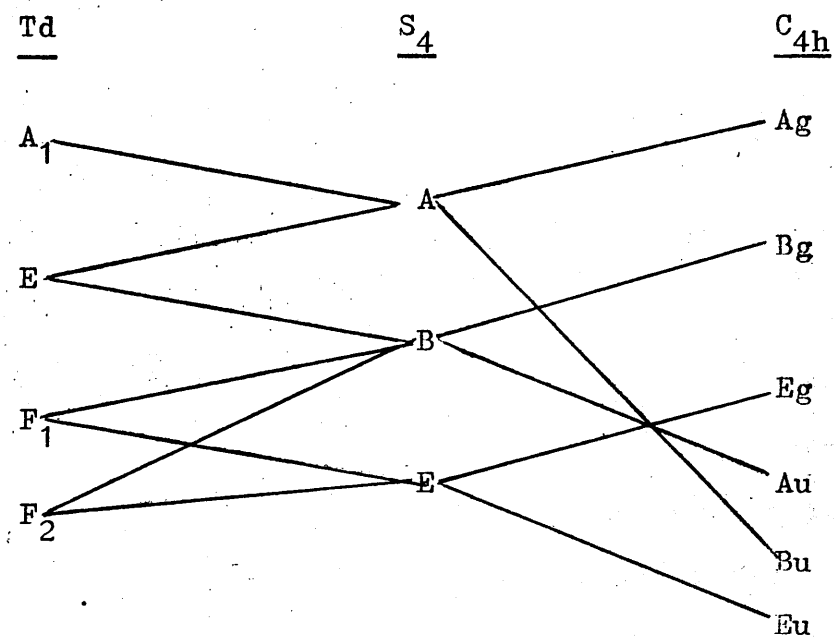
R = rotatory lattice modes (in complexes with structured cations and anions, these are denoted by R_+ and R_- respectively).

n'_i = internal modes of polyatomic groups.

Selection rules: Raman: A_g x^2, y^2, z^2 B_{2g} xz
 B_{1g} xy B_{3g} yz

I.r. B_{1u} - z , B_{2u} - y , B_{3u} - x .

Table 1.2 Correlation Diagram Between the Unit Cell Group, Site Group and Molecular Point Group in Calcium Tungstate, CaWO_4



atom lies on a site of S_4 symmetry. In this site the vibrations span $2A + 3B + 2E$. Since there are two units of WO_4 in the unit cell, each representation of S_4 must cover vibrations from both WO_4 units so that the representations spanned by both WO_4 units are $4A + 6B + 4E$ in S_4 . These then correlate with the unit cell group as shown in Table 1.2. The measure of the influence which the surrounding lattice, in its equilibrium configuration, exerts on the molecule is known as STATIC FIELD EFFECT (48). It may give rise to shifts and splittings of frequencies, the latter if a site group of lower symmetry than the molecular group leads to removal of degeneracies. The interaction of the number of molecules in the unit cell gives rise to the 'Dynamic Field Effect' (48). A complete list of Correlation Tables is given in Appendix X-8 of the book by Wilson, Decius and Cross (9).

The group theoretical analysis, however, does not indicate the extent to which the molecule and its environment deviates from the molecular point symmetry. If this deviation is small, the vibrational spectra of the molecule may, for all practical purposes, be the spectra expected of an isolated molecule. As the deviations increase two effects become apparent. Firstly, because of the lower symmetry the selection rules may change and a band may be observed which corresponds to a vibration. For example, the A_1 stretching vibration of a tetrahedral XY_4 molecule is Raman active only but both I.R. and Raman active in C_{3v} (A_1). Secondly, the results of site symmetry lowering may be the

splitting of degenerate vibrations. This effect together with the change in selection rules is observed in the study of the ion $[\text{Ni}(\text{CN})_4]^{2-}$ in various salts. In $\text{Na}_2[\text{Ni}(\text{CN})_4] \cdot 3\text{H}_2\text{O}$, the E_u vibrations are split into two clearly resolved bands [2128 and 2132cm^{-1} for $\nu(\text{C-N})$] (49).

References

1. Adiabatic Approximation - introduced by Born and Oppenheimer (1927) - Ann. Phys., 84, 457.
2. Lattice Vibration - Einstein model - Ann. d. Phys., [4], 22, 180, (1907), A. Einstein.
3. Diatomic Chain - Born and Karman - Phys. Zeit., 13, 297, (1912).
4. M. Born and K. Huang, Dynamical Theory of Crystal Lattices (Oxford), page 84.
5. K. Huang, E.R.A. Report L/T 239 (1950); Proc. Roy. Soc. A, 208, 352, (1951).
6. R.H. Lyddane and K.F. Herzfeld; Phys. Rev. 54, 846 (1938).
7. H. Fröhlich and N.F. Mott; Proc. Roy. Soc. A, 171, 496, (1939).
8. R.H. Lyddane, R.G. Sachs and E. Teller; Phys. Rev., 59, 673, (1941).
9. T.S. Robinson and W.C. Price; Molecular Spectroscopy, edited by G. Sell (The Institute of Petroleum, London, 1955); Proc. Phys. Soc. (London), B66, 969 (1953).
10. R. Kubo, J. Phys. Soc., Japan, 12, 570 (1957)
11. S.H. Glarum, J. Chem. Phys., 33, 1371 (1960).
12. H.A. Kramers, Att. Cong. Intern. Fis., (Como), 2, 545, (1927); Physik Z., 30, 522 (1929).
13. J.S. Plaskett and P.N. Schatz; J. Chem. Phys., 38, 612, (1963).
14. P.N. Schatz, Shiro Maeda and Kunio Kozima, J. Chem. Phys., 38, 2658 (1963).
15. W.G. Spitzer and D.A. Kleinman, Phys. Rev., 121, 1324, (1961); W.G. Spitzer, R.C. Miller, D.A. Kleinman and L.E. Howarth; Phys. Rev., 126, (5), 1710 (1962).

16. F. Seitz, Modern Theory of Solids (McGraw-Hill Book Company Inc., New York, 1940), Chap. 17.
17. J.R. Jasperse, A. Kahan, J.N. Plendl and S.S. Mitra; Phys. Rev., 145, 526 (1966).
18. H.W. Verleur, J. Opt. Soc. Am., 58, 1356 (1968).
19. L.R. Brantley, G. Andermann and P. Sakamoto, Spectroscopy Letters, 4(314), 47 (1971)
20. A. Smekal, Naturwiss, 11, 873 (1923)
21. C.V. Raman, Indian J. Physics, 2, 387 (1928);
C.V. Raman, and K.S. Krishnan, Nature, 121, 501 (1928).
22. G. Landsberg and L. Mandelstam, Naturwiss, 16, 57 (1928).
23. Tyndall, Phil. Mag., 37, 384 (1869).
24. Lord Rayleigh, Phil. Mag., 47, 375, (1899), Coll. papers IV, 397.
25. J.C. Slater and N.H. Frank, Introduction to Theoretical Physics; McGraw-Hill, New York, (1933) Page 293.
26. L. Pauling and E.B. Wilson, Jr , - Introduction to Quantum Mechanics, McGraw-Hill, New York, 1935.
27. R. Loudon, Adv. Phys., 13, 423 (1964).
28. T.C. Damien, S.P.S. Porto and B. Tell, Phys. Rev., 142, 570 (1966).
29. F.A. Cotton, Chemical Applications of Group Theory, Interscience (London) 1963.
30. G. Herzberg, - Infrared and Raman Spectra, D. Van Nostrand Company, New York (1945), page 256.
31. H. Poulet, Ann. Phys., (Paris), 10, 908, (1955).
32. S.P.S. Porto, Light Scattering with Laser Sources, Chap. A-1 in "Light Scattering of Solids" (1969) Springer-Verlag, Berlin (G.B. Wright, ed).

33. L. Merten, Z. Naturforsch, A15, 47 (1960).
34. L. Couture-Mathieu and J.P. Mathieu, C.R. Acad. Sci., (Paris), 236, 371 (1953).
35. R.H. Lyddane, R.G. Sachs, and E. Teller, Phys. Rev., 59, 673 (1941).
36. G. Placzek, 'Marx's Handbuch der Radiologie VI', 2, 209 (1934), English Translation: U.S. At Energy Comm., UCRL - 256(L) (1962).
37. T.R. Gilson and P.J. Hendra, Laser Raman Spectroscopy; Wiley-Interscience (London) (1970).
38. S. Bhagavantam and T. Venkatarayudu; Proc. Indian Acad. Sci., 9A, 224 (1939).
39. R.S. Halford, J. Chem. Phys., 14, 8 (1946).
40. D.F. Hörnig, J. Chem. Phys., 16, 1063, (1948).
41. H. Winston and R.S. Halford, J. Chem. Phys., 17, 607 (1949).
42. M. Born, Proc. Phys. Soc. London, 54, 362 (1942)
43. S.S. Mitra and P.J. Crielisse, Progress in Infrared Spectroscopy (ed. H. Szymanski) Plenum Press, New York, (1963).
44. D.M. Adams and D.C. Newton, "Tables for Factor Group and Point Arrays Analysis" Beckman-RIIC Ltd., Croydon, 1970; J. Chem. Soc. (A), 1970, 2822.
45. R.W.G. Wyckoff, "Crystal Structures", Interscience, New York, 2nd edn., 1965, vol. 1.
46. E.B. Wilson, J.C. Decius and P.C. Cross, "Molecular Vibrations", McGraw-Hill, New York, 1955.
47. S.P.S. Porto and J.F. Scott, Phys. Rev., 157, 716 (1967); J.F. Scott, J. Chem. Phys., 48, 872 (1968).

48. W. Vedder and D.F. Hornig, *Advances in Spectroscopy*,
Vol. 2, ed. Thompson H.W. page 189.
49. R.L. McCullough, L.H. Jones and G.A. Crosby, *Spectrochim
Acta.*, 16, (1960).

CHAPTER 2 - A_2MX_4 COMPLEXES

2.1 Cs_2MCl_4 and $(NMe_4)_2MCl_4$ complexes

2.2 $(NEt_4)_2MX_4$ complexes

CHAPTER 2

2.1 A₂MX₄ Complexes

A = Cs, NMe₄ where Me = CH₃; M = Co, Zn, Cu; X = Cl

The crystal structure of Cs₂ZnCl₄ has been reported (1) to be isomorphous with that of Cs₂CoCl₄ which has four molecules in the orthorhombic unit cell of space group Pnma (D_{2h}¹⁶) (2,3). Cs₂CuCl₄ has a similar structure (4-7). The tetramethylammonium complexes are isostructural and are similar to their caesium analogues except that there is evidence of orientational disordering of both the cations and anions (5-10).

In all these complexes there are A cations and discrete [MX₄]²⁻ anions which are distorted from perfect tetrahedral geometry. This geometry in the solid state depends on many factors including crystal field stabilization, ligand-ligand repulsion, Jahn-Teller distortion and van der Waals forces. The distortion for the zincate and the cobaltate is apparently mainly due to crystal packing effects and these anions are reported to possess either C_s crystallographic symmetry (11,12) or approximately D_{2d} symmetry (17,27). Because of the inherent Jahn-Teller distortion, the [CuCl₄]²⁻ anion is very much distorted from perfect tetrahedral geometry and is often referred to as the 'flattened' tetrahedron with nearly or exactly D_{2d} symmetry. This is intrinsically more stable than a complex with either T_d (regular tetrahedral) or D_{4h} (square planar) geometry (13-15). For complexes of type A₂CuCl₄, a distorted tetrahedral anion of D_{2d} symmetry is expected when A is a large bulky cation which prevents the [CuCl₄]²⁻ anion from interacting to produce distorted square-pyramidal or octahedral co-ordination (16).

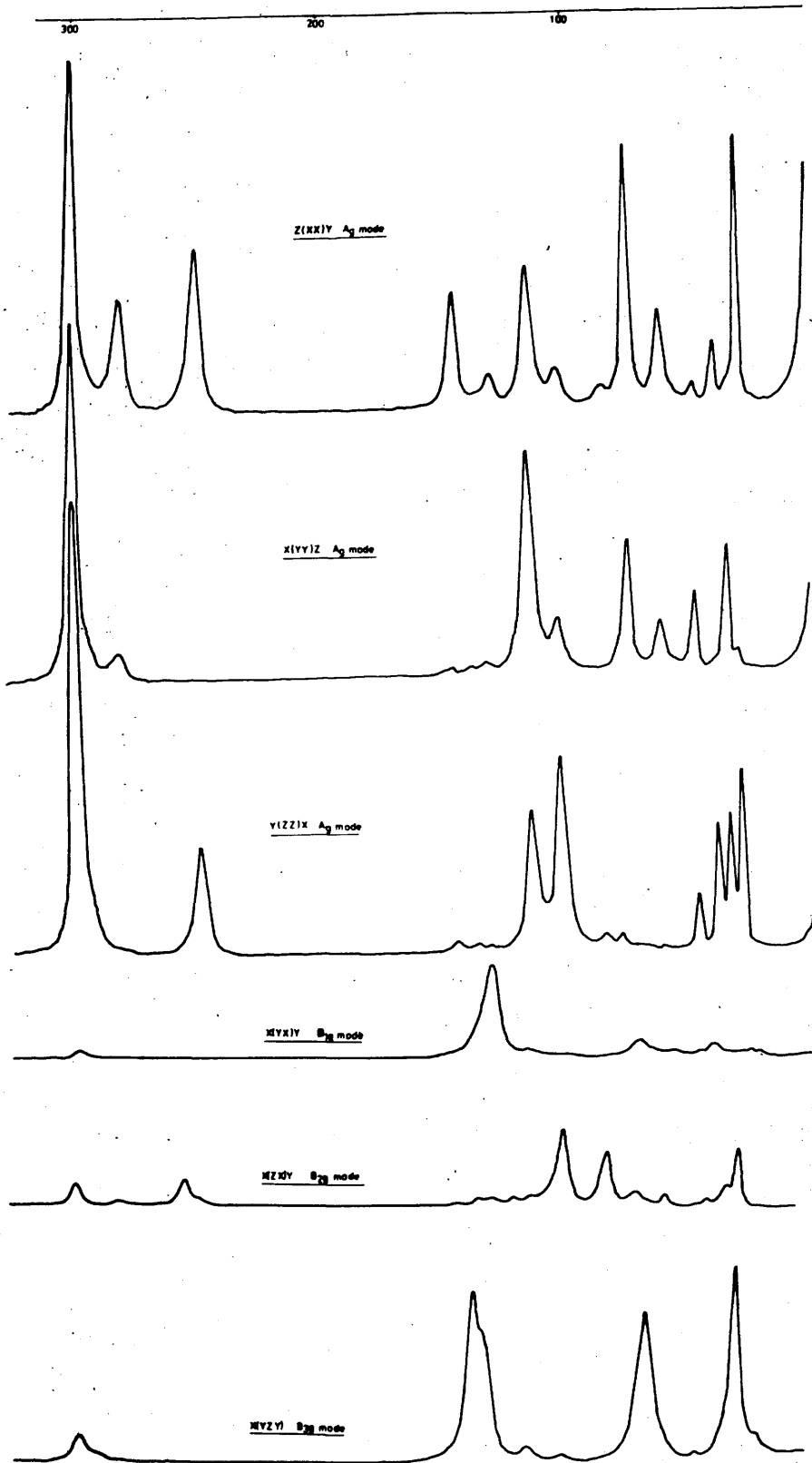
The vibrational spectra of these complexes have been extensively studied. I.r. data both from powdered solids (17-20) and single crystals (21) have been reported. Raman spectra of the aqueous solution of the tetrachlorozincate and that in the solid state as tetraalkylammonium, caesium and sodium salts have been investigated (22-26) but single crystal Raman spectra have been reported only for Cs_2CuCl_4 (27) and Cs_2ZnCl_4 (12,27). Although the single crystal Raman and i.r. spectra of Cs_2CuCl_4 and Cs_2ZnCl_4 have already been reported (12,21,27) it was decided to investigate the Raman spectra of both complexes together with that of Cs_2CoCl_4 especially at 77°K to benefit from the decrease in line width and the increase in the signal to noise ratio. It was hoped that additional information would be obtained to enable more complete vibrational assignments to be made and this would be of great assistance when interpreting the spectra of the $(\text{NR}_4)_2\text{MX}_4$ complexes where $\text{R} = \text{CH}_3, \text{C}_2\text{H}_5$.

RESULTS AND DISCUSSION

The Raman spectra of the three complexes were recorded at 77°K for the six non-equivalent tensor components. Typical of the results are those of Cs_2CuCl_4 which are shown in Figure 2.1 from which it is evident that the spectroscopic data is excellent. The spectra could easily be recorded from 10 cm^{-1} and are typical of the orthorhombic crystal system. Those spectra originating from scattering from the diagonal tensor components give the symmetric A_g modes of the point group D_{2h} of which the tensor has the form,

$$\begin{vmatrix} a & 0 & 0 \\ 0 & b & 0 \\ 0 & 0 & c \end{vmatrix}$$

FIGURE 2.1



Raman Spectra for Cs_2CuCl_4 at 77°K .

The intensity of a Raman band is proportional to the square of its tensor component and this implies that scattering from the diagonal tensor components, while producing bands of the same symmetry and frequency, will result in a variation in intensity of the observed bands. This is clearly demonstrated by the spectra in Figure 2.1.

The next nearest and other neighbour interactions in a crystal, together with the primary co-ordination sphere decide the site symmetry of the ion. In these complexes, the $[\text{MCl}_4]^{2-}$ anions occupy sites having only a plane of symmetry (C_s site symmetry), in consequence of which the double and triple degeneracies of the ν_2 and of the ν_3 and ν_4 modes of a tetrahedral configuration would be completely lifted. Deviations from perfect tetrahedral geometry may also remove the degeneracies. The four fundamental modes of vibration of a perfect tetrahedron are:

symmetric stretch ν_1 of symmetry species A,

symmetric deformation, ν_2 of symmetry species E and anti-

symmetric stretch and deformation ν_3 and ν_4 respectively, both of symmetry species F_2 .

All four are Raman-active but only the $2F_2$ are i.r. active.

The factor group analysis is summarised in Table 2.1 and from it the number and symmetry species of the Raman active internal and lattice modes are given by representations (2.1) and (2.2).

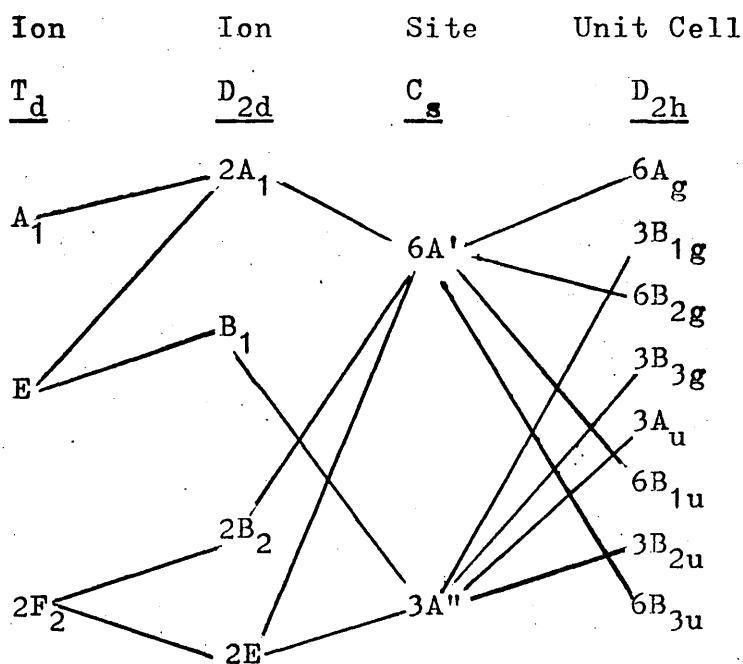
$$\Gamma_{\text{internal}} = 6A_g + 3B_{1g} + 6B_{2g} + 3B_{3g} \quad (2.1)$$

$$\Gamma_{\text{lattice}} = 7A_g + 5B_{1g} + 7B_{2g} + 5B_{3g} \quad (2.2)$$

Table 2.1 Factor Group Analysis of A_2MCl_4 Complexes
with space group D_{2h}^{16}

D_{2h}	n_i	T	T'	R_+	R_-	n_i'
A_g	13	0	6	3	1	6
B_{1g}	8	0	3	3	2	3
B_{2g}	13	0	6	3	1	6
B_{3g}	8	0	3	3	2	3
A_u	8	0	3	3	2	3
B_{1u}	13	1	5	3	1	6
B_{2u}	8	1	2	3	2	3
B_{3u}	13	1	5	3	1	6

Table 2.2 Correlation Table for A_2MCl_4 Complexes with
Space Group D_{2h}^{16}



The Raman frequencies, recorded at 77°K, polarization intensity data and symmetry assignments for the three cesium complexes are given in Tables 2.3 - 2.5. In making assignments of the bands, group theoretical predictions, the expected frequency range of the various T_d modes and the intensities of the bands are taken into account. From previous studies (17) it is known that both ν_1 and ν_3 occur around 300 cm^{-1} while ν_2 and ν_4 are found in the region 140 cm^{-1} to 115 cm^{-1} . For each of the cesium complexes three bands of A_g symmetry species are found in the 300 cm^{-1} region corresponding to one from ν_1 and two from ν_3 as predicted from the site group analysis shown in Table 2.2. Similarly three bands of A_g symmetry species are also found in the region for ν_2 and ν_4 , one of which is a ν_2 component and the other two are ν_4 components. The components of the ν_2 mode in the i.r. arise from an i.r.-inactive mode of the isolated tetrahedron and are thus observed as weak bands in the lower frequency region where ν_2 and ν_4 occur (21). Accordingly the bands around 140 cm^{-1} are assigned to the ν_4 modes while those of the lower frequencies, about 115 cm^{-1} , are assigned to ν_2 components. Similar arguments could be used to distinguish the ν_1 component from ν_3 since the ν_1 components in the i.r. also arise from an i.r. inactive mode of the isolated tetrahedron and would be observed as weak i.r. bands. However, the ν_1 modes have not been definitely observed in the i.r. spectra. The three bands of A_g symmetry in the Raman spectra have very comparable intensities so that it is difficult to distinguish the ν_1 from the ν_3 . The B_{1g} and B_{3g} modes arise only for the ν_3 and could be used to make the distinction, but they are observed as very weak bands

Table 2.3 Raman Frequencies (cm^{-1}), Recorded at 77°K
Polarization Intensity Data and Symmetry
Assignments for Cs_2CoCl_4

Frequency cm^{-1}	Scattering Geometry						Assignment
	x(yy)z	x(yx)z	z(xx)y	z(xz)y	y(zz)x	y(zy)x	
318	32	4	7	5	16	5	$\underline{A}_g + \underline{B}_{1g} + \underline{B}_{2g} + \underline{B}_{3g}$
308	19	0	8	5	8	0	$\underline{A}_g + \underline{B}_{2g}$
285	116	16	96	30	71	18	$\underline{A}_g + \underline{B}_{2g}$
142	51	9	112	20	15	9	$\underline{A}_g + \underline{B}_{2g} + \underline{B}_{3g}$
127	78	27	46	30	56	25	$\underline{A}_g + \underline{B}_{1g} + \underline{B}_{2g}$
113	107	0	60	0	50	80	$\underline{A}_g + \underline{B}_{3g}$
108	0	0	0	84	0	0	\underline{B}_{2g}
105	0	90	0	0	0	0	\underline{B}_{1g}
89	0	5	0	0	4	11	$\underline{B}_{1g} + \underline{B}_{3g}$
80	55	14	0	0	14	14	$\underline{A}_g + \underline{B}_{1g}$
75	0	0	0	10	0	0	\underline{B}_{2g}
70	11	0	0	0	13	16	$\underline{A}_g + \underline{B}_{3g}$
59	27	7	9	5	0	13	$\underline{A}_g + \underline{B}_{2g} + \underline{B}_{3g}$
46	25	0	29	32	12	13	$\underline{A}_g + \underline{B}_{2g} + \underline{B}_{3g}$
42	0	37	0	0	0	0	\underline{B}_{1g}
31	20	0	0	0	0	0	\underline{A}_g
21	0	7	9	9	30	12	$\underline{A}_g + \underline{B}_{1g} + \underline{B}_{2g}$

Table 2.4 Raman Frequencies (cm^{-1}), Recorded at 77°K,
Polarization Intensity Data and Symmetry
Assignments for Cs_2ZnCl_4

Frequency cm^{-1}	Scattering Geometry						Assignment
	x(yy)z	x(yx)z	z(xx)y	z(xz)y	y(zz)x	y(zy)x	
301	81	36	106	13	98	31	$A_g + B_{1g}$
290	0	0	12	8	0	17	$B_{2g} + B_{3g}$
286	158	34	14	0	166	30	A_g
275	106	23	55	12	170	21	A_g
138	89	15	4	5	112	16	$A_g + B_{2g} + B_{3g}$
125	33	33	21	8	23	40	$B_{1g} + B_{2g} + B_{3g}$
122	28	0	48	2	20	0	A_g
114	52	92	24	44	47	31	$A_g + B_{1g} + B_{2g}$
106	0	0	0	0	22	46	B_{3g}
86	0	9	2	3	0	0	$B_{1g} + B_{2g}$
75	14	0	10	1	19	8	$A_g + B_{3g}$
68	0	16	6	5	12	7	$B_{1g} + B_{2g} + B_{3g}$
54	9	0	2	0	16	0	A_g
45	19	12	7	3	16	4	$A_g + B_{1g} + B_{2g}$
40	30	12	5	2	31	25	$A_g + B_{3g}$
29	11	2	9	1	10	0	A_g
23	0	14	1	9	9	5	$B_{1g} + B_{2g} + B_{3g}$
17	45	9	25	3	51	11	A_g

Table 2.5 Raman Frequencies, Recorded at 77°K,
Polarization Intensity Data and Symmetry
Assignments for Cs₂CuCl₄

<u>Frequency</u> cm ⁻¹	<u>Scattering Geometry</u>						<u>Assignment</u>
	y(xx)z	y(xy)z	z(yy)x	z(yz)x	x(zz)y	x(zx)y	
302	178	0	182	15	250	6	A _g
298	0	4	0	0	0	0	B _{1g}
284	0	0	0	0	0	2	B _{2g}
282	56	0	14	0	0	0	A _g
258	0	0	0	0	0	7	B _{2g}
252	82	0	0	0	54	2	A _g
148	58	0	3	0	5	0	A _g
140	0	0	4	89	4	0	B _{3g}
135	17	46	6	0	3	0	A _g +B _{1g}
126	0	0	0	0	0	3	B _{2g}
118	72	0	114	0	71	4	A _g
106	20	0	27	0	98	36	A _g +B _{2g}
89	11	0	8	0	0	25	B _{2g}
78	134	0	8	0	67	5	A _g
74	0	9	0	0	0	0	B _{1g}

Table 2.5 (cont'd)

Frequency cm ⁻¹	Scattering Geometry						Assignment
	y(xx)z	y(xy)z	z(yy)x	z(yz)x	x(zz)y	x(zx)y	
70	0	0	0	79	0	0	B _{3g}
65	49	0	2	0	25	4	A _g
61	0	4	0	0	0	0	B _{1g}
52	12	3	28	7	40	0	A _g
48	0	0	0	0	0	2	B _{2g}
44	33	7	63	0	6	0	A _g
41	0	0	0	0	0	9	B _{2g}
39	0	0	68	0	61	0	A _g
36	0	0	0	0	0	18	B _{2g}
35	0	4	0	104	0	0	B _{3g}
34	138	0	90	0	9	0	A _g
30	0	0	0	0	0	0	B _{1g}
26	0	4	0	17	0	0	B _{3g}

and occur in the same region and could, in some cases, be leakages from the intense A_g modes. Force constant calculations would prove very useful in solving this problem. The Raman frequencies, recorded at 77°K, together with the polarization intensity data and the symmetry assignments for the tetramethyl (TMA) complexes are given in Tables 2.6-2.8.

The earlier Raman studies on Cs_2ZnCl_4 by Beattie and co-workers (27) interpreted the observed splitting of the ν_3 mode in terms of tetragonal (D_{2d}) distortion in the $[ZnCl_4]^{2-}$ anion, although Jahn-Teller effects, which are responsible for the distortion in $[CuCl_4]^{2-}$ anions, do not occur in complexes of metal ions with d^{10} configuration (28). Wong, however, recently attributed the cause of the splitting to a planar (C_s) distortion of the $[ZnCl_4]^{2-}$ ions in Cs_2ZnCl_4 (12).

The assignments of the frequencies observed to the various internal modes for the cesium complexes are given in Tables 2.9 - 2.11 while those for the (TMA) complexes are given in Tables 2.12 - 2.14.

The spectral features of the cuprate complexes differ from those of the zincate and cobaltate complexes in that in both the stretching and bending regions the peaks are better resolved and separated in the cuprates than in the others. This might reflect the differences in the nature of the distortions of the anions. From the correlation table (Table 2.2) it is observed that for the copper complexes the triply degenerate F_2 mode in T_d (tetrahedral) symmetry splits into an E and a B_2 mode when compressed along one of the S_4 axes to form a species of D_{2d} symmetry. The amount of splitting is reported to be proportional to the extent of the compression (29).

Table 2.6 Raman Frequencies (cm^{-1}) Recorded at 77°K,
Polarization Intensity Data and Symmetry
Assignments for $(\text{NMe}_4)_2\text{CoCl}_4$

Frequencies cm^{-1}	Scattering Geometry						Assignments
	y(xx)z	y(xy)z	x(zz)y	x(zx)y	z(yy)x	z(yz)x	
324	0	0	0	0	10	0	A_g
303	0	0	3	0	6	0	A_g
280	41	11	48	10	74	28	A_g
137	20	19	32	18	82	0	$A_g + B_{1g} + B_{2g}$
135	0	0	0	0	0	80	B_{3g}
126	0	0	0	22	0	0	B_{2g}
123	32	24	0	0	0	0	$A_g + B_{1g}$
118	0	0	0	0	37	0	A_g
95	0	0	85	0	15	0	A_g
86	0	0	70	0	0	0	A_g
83	37	0	0	0	0	0	A_g
75	0	0	0	15	0	0	B_{2g}
64	0	0	60	16	11	15	$A_g + B_{3g}$

Table 2.7. Raman Frequencies (cm^{-1}) Recorded at 77°K ,
Polarization Intensity Data and Symmetry
Assignments for $(\text{NMe}_4)_2\text{ZnCl}_4$

Frequency cm^{-1}	Scattering Geometry						Assignment
	x(yy)z	x(yx)z	z(xx)y	z(xz)y	y(zz)x	y(zy)x	
313	0	0	10	4	8	6	$B_{3g} + A_g$
306	0	0	8	6	8	7	B_{2g}
296	0	0	8	7	17	8	B_{2g}
278	142	35	150	14	117	16	A_g
269	70	0	66	12	0	0	A_g
131	27	0	35	0	59	0	A_g
129	0	0	0	27	0	25	$B_{2g} + B_{3g}$
126	0	31	0	0	0	0	B_{1g}
122	0	45	0	41	0	31	$B_{1g} + B_{2g} + B_{3g}$
117	36	0	52	0	0	0	A_g
112	0	0	0	19	0	11	$B_{2g} + B_{3g}$
104	12	0	17	0	0	0	A_g
88	0	0	16	0	0	0	A_g
79	0	0	0	0	16	0	A_g
76	38	0	0	0	0	0	A_g
67	37	0	40	0	0	0	A_g
58	33	0	30	0	10	0	A_g
49	0	0	0	0	8	0	A_g
45	0	5	12	15	0	7	$B_{1g} + B_{2g} + B_{3g}$

Table 2.8 Raman Frequencies (cm^{-1}) Recorded at 77°K,
Polarization Intensity Data and Symmetry
Assignments for $(\text{NMe}_4)_2\text{CuCl}_4$

Frequency cm^{-1}	Scattering Geometry						Assignment
	x(yy)z	x(yx)z	z(xx)y	z(xz)y	y(zz)x	y(zy)x	
311	12	4	10	0	13	3	$B_{3g} + B_{2g}$
302	19	7	23	10	0	0	$B_{1g} + B_{2g}$
295	0	0	15	7	16	8	B_{2g}
283	109	10	82	12	158	14	A_g
278	180	46	159	28	117	15	A_g
237	0	0	0	8	0	0	B_{2g}
233	31	10	26	4	37	4	A_g
150	0	15	58	45	13	26	$B_{1g} + B_{2g} + B_{3g}$
140	45	22	99	57	35	33	$A_g + B_{2g} + B_{3g}$
133	28	0	0	0	44	0	A_g
120	57	17	60	0	17	0	$A_g + B_{1g}$
114	0	0	0	17	0	0	B_{2g}
104	26	0	0	0	17	0	A_g
96	38	10	40	0	31	0	A_g
66	0	0	9	0	26	0	A_g
58	0	10	35	0	0	0	$A_g + B_{1g}$
54	40	15	0	16	55	15	$A_g + B_{2g}$
50	46	16	35	0	0	0	A_g
39	11	16	25	19	42	14	$A_g + B_{1g} + B_{2g}$
33	0	0	68	0	25	16	$A_g + B_{3g}$
24	17	5	39	11	53	13	$A_g + B_{2g}$
21	50	17	81	11	46	12	A_g

Table 2.9 Assignments of the Bands in the Low
Temperature Spectra of Cs₂CoCl₄

Frequency cm ⁻¹	Crystal mode	Site Group mode	T _d mode
318	A _g }	A'	F ₂ (ν ₃)
318	B _{2g} }	A'	
318	B _{1g} }	A''	
318	B _{3g} }	A''	
308	A _g }	A'	A ₁ (ν ₁)
308	B _{2g} }	A'	
285	A _g }	A'	F ₂ (ν ₄)
285	B _{2g} }	A'	
142	A _g }	A'	E(ν ₂)
142	B _{2g} }	A''	
142	B _{3g} }	A''	
127	B _{1g} }	A''	
127	A _g }	A'	E(ν ₂)
127	B _{2g} }	A'	
113	B _{3g} }	A''	
105	B _{1g} }	A''	
113	A _g }	A'	
108	B _{2g} }	A'	

Table 2.10 Assignments of the Bands in the Low
Temperature Spectra of Cs_2ZnCl_4

Frequency cm^{-1}	Crystal mode	Site Group mode	T_d mode
301	A_g	A'	$F_2(\nu_3)$
-	B_{2g}	A''	
301	B_{1g}	A'	
290	B_{3g}	A''	$F_2(\nu_3)$
290	B_{2g}	A'	
275	A_g	A'	$A_1(\nu_1)$
286	A_g	A'	
-	B_{2g}	A''	$F_2(\nu_4)$
138	A_g	A'	
138	B_{2g}	A''	
138	B_{3g}	A'	$F_2(\nu_4)$
125	B_{1g}	A''	
125	B_{2g}	A'	$E(\nu_2)$
122	A_g	A''	
125	B_{3g}	A''	$E(\nu_2)$
114	B_{1g}	A'	
114	A_g	A''	$E(\nu_2)$
114	B_{2g}	A'	

Table 2:11

Assignments of the Bands in the Low
Temperature Spectra of Cs_2CuCl_4

Frequency cm^{-1}	Crystal mode	Site Group mode	D_{2d} mode	T_d mode
302	A_g	A'	A_1	A_1 (ν_1)
-	B_{2g}			
298	B_{1g}	A''	E	F_2 (ν_3)
-	B_{3g}			
284	B_{2g}	A'	B_2	F_2 (ν_3)
282	A_g			
258	B_{2g}	A'	B_2	F_2 (ν_3)
252	A_g			
148	A_g	A'	E	F_2 (ν_4)
-	B_{2g}			
140	B_{3g}	A''	E	F_2 (ν_4)
135	B_{1g}			
135	A_g	A'	B_2	F_2 (ν_4)
126	B_{2g}			
118	A_g	A'	A_1	E (ν_2)
106	B_{2g}			
-	B_{1g}	A''	B_1	E (ν_2)
-	B_{3g}			

Table 2•12 Assignments of the Bands in the Low
Temperature Spectra of $(\text{NMe}_4)_2\text{CoCl}_4$

Frequency cm^{-1}	Crystal mode	Site Group mode	T_d mode
324	A_g	A'	$F_2(\nu_3)$
-	B_{2g}		
-	B_{1g}	A''	
-	B_{3g}		
303	A_g	A'	$F_2(\nu_3)$
-	B_{2g}		
280	A_g	A'	$A_1(\nu_1)$
-	B_{2g}		
137	A_g	A'	$F_2(\nu_4)$
137	B_{2g}		
137	B_{1g}	A''	
135	B_{3g}		
126	B_{2g}	A'	$F_2(\nu_4)$
123	A_g		
118	A_g	A'	$E(\nu_2)$
-	B_{2g}		
-	B_{3g}	A''	
-	B_{1g}		

Table 2•13 Assignment of the Bands in the Low
Temperature Spectra of $(\text{NMe}_4)_2\text{ZnCl}_4$

Frequency cm^{-1}	Crystal mode	Site Group mode	T_d mode
313	A_g }	A'	$F_2(\nu_3)$
306	B_{2g} }	A''	
313	B_{3g} }	A''	$F_2(\nu_3)$
-	B_{1g} }	A'	
269	A_g }	A'	$A_1(\nu_1)$
-	B_{2g} }		
278	A_g }	A'	$A_1(\nu_1)$
-	B_{2g} }		
131	A_g }	A'	$F_2(\nu_4)$
129	B_{2g} }	A''	
129	B_{3g} }	A''	
126	B_{1g} }	A'	
122	B_{2g} }	A'	$E(\nu_2)$
117	A_g }		
122	B_{3g} }	A''	
122	B_{1g} }	A''	
112	B_{2g} }	A'	$E(\nu_2)$
104	A_g }	A'	

Table 2.14 Assignments of the Bands in the Low
Temperature Spectra of $(\text{NMe}_4)_2\text{CuCl}_4$

Frequency cm^{-1}	Crystal mode	Site Group mode	D_{2d} mode	T_d mode
311	B_{3g}	A''	E	$F_2(\nu_3)$
302	B_{1g}			
302	B_{2g}	A'	B_2	
283	A_g			
237	B_{2g}	A'	A_1	
233	A_g			
295	B_{2g}	A'	A_1	
278	A_g			
150	B_{3g}	A''	E	$F_2(\nu_4)$
150	B_{1g}			
150	B_{2g}	A'	B_2	
140	A_g			
140	B_{2g}	A'	B_2	
133	A_g			
140	B_{3g}	A''	B_1	$E(\nu_2)$
120	B_{1g}			
120	A_g	A'	A_1	
114	B_{2g}			

The site, C_{2v} , further splits the E mode. Thus for the $[CuCl_4]^{2-}$ anion, there is a large B_2 -E splitting with a smaller $A'(E) - A''(E)$ splitting resulting from the static crystal field. However when the ν_3 (and ν_4) mode of the tetrahedral symmetry splits into ($B_2 + E$) modes under D_{2d} , it is not obvious which of the two should be at the higher frequency. From the correlation that, by further compression of the D_{2d} symmetry to a square planar configuration, the B_2 mode becomes A_{2u} which is a bending mode in D_{4h} symmetry, the B_2 mode is expected to be of lower symmetry than the E vibration (30). To calculate the amount of splitting it is necessary to consider both the Raman and I.r. multiplet components. However a rough estimate can be obtained by considering only the A_g modes since one each derives from the B_2 and E modes. There is thus a separation of 30 cm^{-1} between $A_g(E)$ and $A_g(B_2)$ for ν_3 for the cesium and 50 cm^{-1} for the TMA cuprate complexes. The corresponding separation for the ν_4 modes are 13 cm^{-1} and 7 cm^{-1} for the cesium and TMA salts respectively. The presence of the D_{2d} anion symmetry is confirmed even in solution by the observation of strong i.r. bands near 280 cm^{-1} and 240 cm^{-1} and weaker ones at 119 cm^{-1} and 84 cm^{-1} when salts of the $[CuCl_4]^{2-}$ anion are dissolved in non-co-ordinating solvent (20). Although the $[CuCl_4]^{2-}$ anion in the TMA complex is similar to that of the cesium complex different ordering of the B_2 -E modes were made by Lane (21,29) from i.r. results. McGinnety, nevertheless, suggests that the splitting might be due to a more complete breakdown of the isolated anion approximation (31).

In the case of the zincate and cobaltate complexes, the distortion is towards C_{2v} symmetry which is the same symmetry as that of the site. Hence the $A'(F_2)$ and $A''(F_2)$ separation could be used as a measure of the splitting accompanying the

distortion. Here also separation between the $A_g(A')$ and $A_g(A'')$ modes give a rough estimate of the splitting. Owing to the low site symmetry there is a lot of mixing of the modes. The splitting of ν_3 is found to be 26 cm^{-1} and 24 cm^{-1} for the cesium and TMA zincate complexes. The ν_4 splittings are 16 cm^{-1} and 9 cm^{-1} respectively for the cesium and TMA salts. For the cobaltates the ν_3 splittings are 10 cm^{-1} and 11 cm^{-1} and the ν_4 splittings are 15 cm^{-1} and 14 cm^{-1} for the cesium and TMA complexes respectively. Thus the greater distortion in the cuprates is manifested by larger splittings of the ν_3 modes.

The lattice modes are generally much weaker than the internal modes and are often found below 100 cm^{-1} . The bending region is often complicated by mixing with the lattice modes. In Cs_2CuCl_4 the band at 106 cm^{-1} of both A_g and B_{2g} symmetry species is assigned as the B_{2g} component of ν_2 and also as a lattice mode of A_g species. In the TMA complexes the cation rotatory modes should be taken into account and these are given by the additional representation (2.3)

$$\Gamma_{\text{cation}}^{\text{rot}} = 3A_g + 3B_{1g} + 3B_{2g} \quad (2.3)$$

Thus in the lattice region of the TMA complexes a total of thirty-three bands are expected but most of them could not be observed. They are either too weak or possibly more than one band occurs at the same frequency.

In general there were some spectral differences between the cesium and the TMA complexes which mainly arise due to the fact that the TMA complexes are reported to be disordered

at room temperature. Even at 77°K, the lack of effective polarization as compared to that in the cesium complexes might suggest that some disorder still remains. At room temperature the TMA complexes show none of the predicted splitting of the internal modes though they do so at 77°K. The temperature dependent spectral changes observed in the TMA complexes can be attributable to the orientational disorder of both the cations and anions in these complexes. Thus at room temperature a situation exists whereby there are a number of sites on which the cation or anion may reside all having the same energy and it is this fact which gives rise to the large thermal parameters reported in the x-ray studies of these complexes. On lowering the temperature, these thermal parameters decrease and the system gradually becomes ordered and thus all the bands predicted from a factor group analysis based on the proposed space group are observed. The broad bands observed at room temperature are due to a breakdown in the zone-centre ($k = 0$) approximation with the result that all the modes in the Brillouin zone are allowed to interact with the incident radiation. The spectra observed at room temperature are analogous to solution spectra. The effect of lowering the temperature in the cesium complexes is only to make the bands much sharper and this is expected from consideration of the Boltzmann distribution which is 'kT' dependent.

2.2 (NEt₄)₂MX₄ Complexes

M = Co, Cu, X = Cl, Br, Et = C₂H₅

(NEt₄)₂CoCl₄ has been reported to be isostructural with (NEt₄)₂NiCl₄ and to belong to the tetragonal space group P4₂/nmc (D_{4h}¹⁵) with two molecules in the unit cell (32). The bromide complex is assumed to have a similar structure but there is no structural data for (NEt₄)₂CuCl₄. Here too there is evidence of orientational disorder of both the cations and anions. The [MX₄]²⁻ anion is distorted from the tetrahedral geometry but unlike the (NMe₄)₂MCl₄ complexes it is not flattened but tetragonally elongated, giving in the case of the (NEt₄)₂NiCl₄ for instance, two angles of 106.83° and four 110.81° for the [NiCl₄]²⁻ ion.

Some groups of researchers have reported the i.r. transmission spectra of (NEt₄)₂MX₄ complexes (17-19) but there are some discrepancies between the published frequencies and also as to the number of bands observed for the metal-halogen stretching vibrations for some of the complexes. The powder Raman spectra of (NEt₄)₂CuCl₄ has been reported (22) together with that of the nickel complex (23) and in the latter three bands at 271 cm⁻¹, 100 cm⁻¹ and 88 cm⁻¹ have been assigned to ν₁, ν₄ and ν₂ respectively.

In this work single crystal Raman spectra are reported for the complexes (NEt₄)₂CoCl₄, (NEt₄)₂CoBr₄ and (NEt₄)₂CuCl₄ all recorded at 77°K.

RESULTS AND DISCUSSION

Owing to the higher symmetry the factor group analysis

of D_{4h}^{15} is simpler than that for the orthorhombic D_{2h}^{16} complexes and is summarised in Table 2.15. A correlation diagram for the anions on D_{2d} sites is also shown in Table 2.16. The number and symmetry of the Raman-active internal and lattice modes are given by the representations (2.4) and (2.5)

$$\Gamma_{\text{internal}} = 2A_{1g} + 1B_{1g} + 2B_{2g} + 2E_g \quad (2.4)$$

$$\Gamma_{\text{lattice}} = A_g + A_{2g} + 2B_{2g} + 4E_g \quad (2.5)$$

The rotatory lattice modes of the cation are given by the additional representation (2.6)

$$\Gamma_{\text{cat}}^{\text{rot}} = A_{2g} + B_{1g} + 2E_g \quad (2.6)$$

From the correlation table, Table 2.16, it is seen that in the i.r. spectra only one component each of ν_3 and ν_4 should be present in each of the A_{2u} and E_u spectra while none of either ν_1 and ν_2 will be observed. Thus Raman spectra are the only sources for the observation of the ν_1 and ν_2 modes of vibration.

The Raman frequencies, recorded at 77°K, the polarization intensity data and their symmetry assignments for the complexes $(\text{NEt}_4)_2\text{CoCl}_4$, $(\text{NEt}_4)_2\text{CoBr}_4$ and $(\text{NEt}_4)_2\text{CuCl}_4$ are given in Tables 2.17 - 2.19. The assignments to the internal modes of the tetrahedral $[\text{MX}_4]^{2-}$ anion are given in Table 2.20. Only the E_g component of ν_3 could not be observed for the cobalt complexes. The Raman frequencies together with those from the i.r. spectra already reported (29) for $(\text{NEt}_4)_2\text{CoCl}_4$ are given in Table (2.20) to enable the effects of the correlation coupling to be observed. The correlation field effects in these systems are still difficult to observe since for ν_1 and ν_2 the i.r. components

Table 2·15 Factor Group Analysis of $(\text{NEt}_4)_2\text{MX}_4$
 Complexes with Space Group D_{4h}^{15}

D_{4h}	n_i	T	T'	R_+	R_-	n_i'
A_{1g}	3	0	1	0	0	2
A_{2g}	2	0	0	1	1	0
B_{1g}	2	0	0	1	0	1
B_{2g}	4	0	2	0	0	2
E_g	8	0	3	2	1	2
A_{1u}	2	0	0	1	0	1
A_{2u}	4	1	1	0	0	2
B_{1u}	3	0	1	0	0	2
B_{2u}	2	0	0	1	2	0
E_u	8	1	2	2	1	2

Table 2·16 Correlation diagram for the $[\text{MX}_4]^{2-}$ ions
 in the $(\text{NEt}_4)_2\text{MX}_4$ Complexes

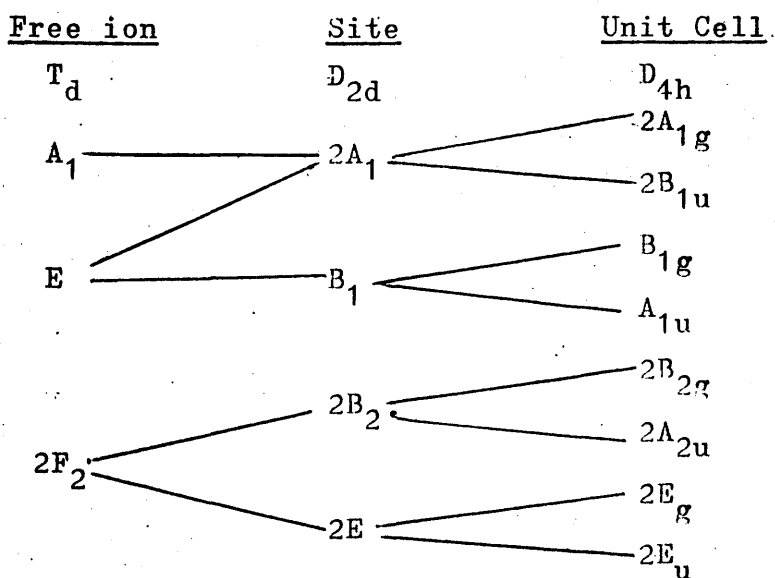


Table 2-17 Raman Frequencies (cm^{-1}) Recorded at 77°K ,
Polarization Intensity Data and Symmetry
Assignments for $(\text{NEt}_4)_2\text{CoCl}_4$

Frequency cm^{-1}	Scattering Geometry				Assignment
	x(zz)y	x(zx)y	y(xx)z	y(xy)z	
272	48	14	25	21	$A_g + B_{2g}$
135	0	0	45	20	B_{1g}
130	0	0	0	30	B_{2g}
127	23	30	72	0	$A_g + E_g$
110	0	0	53	0	B_{1g}
69	0	0	19	0	B_{1g}
58	0	0	25	0	B_{1g}
56	0	7	0	0	E_g

Table 2-18 Raman Frequencies (cm^{-1}) Recorded at 77°K
Polarization Intensity Data and Symmetry
Assignments for $(\text{NEt}_4)_2\text{CoBr}_4$

Frequency cm^{-1}	Scattering Geometry				Assignment
	x(zz)y	x(zx)y	y(xx)z	y(xy)z	
172	100	18	40	41	$A_g + B_{2g}$
101	0	0	38	31	B_{1g}
95	0	0	26	25	B_{2g}
90	57	13	27	20sh	A_g
79	57	16	12	5	A_g
75	0	15	0	0	E_g
71	0	0	18	10	B_{2g}
65	31	53	17	10	$E_g + B_{2g}$
51	17	11	8	0	$E_g + B_{1g}$
41	68	27	0	0	A_g
29	0	19	27	12	$E + B_{1g}$

Table 2•19 Raman Frequencies Recorded at 77°K,
Polarization Intensity Data and Symmetry
Assignments for (NEt₄)₂CuCl₄

<u>Frequency</u> cm ⁻¹	<u>Scattering Geometry</u>				<u>Assignment</u>
	x(zz)y	x(zx)y	z(yy)x	z(yz)x	
280	20	11	50	16	} $\nu_1 + \nu_3$
273	0	0	15	0	
262	0	0	4	5	
237	0	0	0	7	
134	8	5	12	10	} $\nu_2 + \nu_4$
124	0	0	18	0	
114	10	25	21	35	
89	0	0	7	0	} Lattice
75	10	6	0	0	
72	0	0	0	10	
69	0	0	5	0	
61	13	0	0	0	
35	0	0	0	11	

Table 2.20 Assignments of the Bands in the Low
Temperature Spectra of $(\text{NEt}_4)_2\text{CoBr}_4$
and $(\text{NEt}_4)_2\text{CoCl}_4$

Free ion	Site	Crystal mode	Frequency		
			$(\text{NEt}_4)_2\text{CoCl}_4$	$(\text{NEt}_4)_2\text{CoBr}_4$	
T_d	D_{2d}	D_{4h}			
ν_1	A	A ₁	A _{1g}	272	172
			B _{1u}	-	-
ν_2	E	A ₁	A _{1g}	127	90
			B _{1u}	-	-
		B ₁	B _{1g}	135	101
			A _{1u}	-	-
ν_3	E	B ₂	B _{2g}	272	172
			A _{2u}	304	-
		E	E _g	-	-
			E _u	299	-
ν_4	E	B ₂	B _{2g}	130	95
			A _{2u}	133	-
		E	E _g	127	-
			E _u	127	-

are inactive. There is, however, a splitting of 8 cm^{-1} between $A_{1g}(A_1)$ and $B_{1g}(B_1)$ components of $\nu_2(E)$. The splitting of the ν_4 mode into (B_2+E) is found to be only 4 cm^{-1} . It is not possible to calculate the splitting for ν_3 since the E_g component could not be observed. However from the amount of splitting of the ν_2 and ν_4 , it can be concluded that there is very little perturbation due to the site and the factor group. The ν_1 mode has been calculated to be at 260 cm^{-1} from a complex transmission spectrum of a thin $(\text{NEt}_4)_2\text{CoCl}_4$ crystals above 400 cm^{-1} in which a group of three sharp weak bands were observed at 593 , 556 and 537 cm^{-1} . These were assigned to two-phonon combinations of Co-Cl stretching modes, being $2\nu_3$, $\nu_1+\nu_3$ and $2\nu_1$ respectively. (34). Owing to the heavier mass of the bromide, there is a shift to lower frequencies in the spectra of $(\text{NEt}_4)_2\text{CoBr}_4$.

The crystals of the copper complex were of poor quality so that the spectra were not very good. Four bands were found in the region between 237 cm^{-1} and 280 cm^{-1} . Under the site group analysis for the tetragonal complexes of space group D_{4h}^{15} only three bands are predicted, one for the ν_1 component and the remaining two for the ν_3 components. The presence of the extra band would indicate a structure other than D_{4h}^{15} . Clark and Dunn (17) had also observed three components of ν_3 in the i.r. powder spectrum of $(\text{NEt}_4)_2\text{CuCl}_4$. The results of other workers (19,20) however are compatible with its being isostructural with the cobalt and nickel complexes. The assignments of the bands are therefore made for the regions where the various vibrational modes of the tetrahedral molecule are expected.

The lattice region in the cobalt and copper complexes showed fewer bands than predicted. In the bromide complex there is a lot of mixing of the modes. The copper complex showed only six bands in the lattice region. The disorder in these complexes at room temperature is manifest by the fact that the lattice region in the room temperature spectra is featureless.

EXPERIMENTAL

Crystals of Cs_2MCl_4 and $(\text{NMe}_4)_2\text{MCl}_4$ complexes were grown by slow evaporation of saturated aqueous solutions containing the appropriate molar ratio of the constituent chlorides. The tetraethylammonium complexes were prepared according to the literature (35) by mixing anhydrous ethanol solution of the metal halides and the ethylammonium halides.

The spectra were recorded at room temperature and at 77°K at 2 cm^{-1} resolution for most and 5 cm^{-1} resolution for a few. The various exciting lines of the Ar^+ and Kr^+ lasers were used:

488.0nm	for	Cs_2ZnCl_4 , $(\text{NMe}_4)_2\text{ZnCl}_4$
476.1nm	for	Cs_2CoCl_4 , $(\text{NMe}_4)_2\text{CoCl}_4$, $(\text{NEt}_4)_2\text{CoCl}_4$
496.5nm	for	$(\text{NEt}_4)_2\text{CoBr}_4$
647.1nm	for	Cs_2CuCl_4 , $(\text{NEt}_4)_2\text{CuCl}_4$
568.2nm	for	$(\text{NMe}_4)_2\text{CuCl}_4$ at L.T.
647.1nm	for	$(\text{NMe}_4)_2\text{CuCl}_4$ at R.T.

References

1. B. Brehler, Z. Krist., 109, 68 (1957)
2. M.A. Porai-Koshits, Sov. Phys. Crystallog. 1, 224, (1956), Trudy Inst. Krist. Akad. Nauk SSSR, 10, 117 (1954).
3. G.N. Tischenko and Z.G. Pinsker, Dokl. Akad. Nauk. SSSR, 100, 913 (1955)
4. J. McGinnety, J. Amer. Chem. Soc., 94, 8406 (1972)
5. B. Morosin and E.C. Lingafelter, J. Phys. Chem., 65, 50 (1961)
6. L. Helmholtz and R.F. Kruh, J. Amer. Chem. Soc., 74, 1176 (1952)
7. D.P. Mellor, Z. Krist., 101, 160 (1939)
8. J.R. Wisner, R.C. Srivastava, C.H.L. Kennard, M. DiVaira and E.C. Lingafelter, Acta Cryst., 23 565 (1967)
9. B. Morosin and E.C. Lingafelter, Acta Cryst., 12 611 (1959)
10. G.B. Guthrie and J.P. McCullough, J. Phys. Chem. Solid., 18, 53 (1961)
11. W. De Harrocks and D.A. Burlone, J. Amer. Chem. Soc., 98, 6512 (1976)
12. P.T.T. Wong, J. Chem. Phys., 64, 2191 (1976)
13. D.W. Smith, J. Chem. Soc. A., 2529 (1969)
14. D.W. Smith, J. Chem. Soc. A., 2900 (1970)
15. J. Demnynck, A. Veillard and U. Wahlgren, J. Amer. Chem. Soc., 95, 5563 (1973)
16. R.L. Harlow, W.J. Wells III, G.W. Watt and S.H. Simonsen, Inorg. Chem. 14 1768 (1975)

17. R.J.H. Clark and T.M. Dunn, *J. Chem. Soc.* (1963)
1198
18. D.M. Adams, J. Chatt, J.M. Davidson and J. Gerratt,
J. Chem. Soc. (1963), 2189
19. A. Sabatini and L. Sacconi, *J. Amer. Chem. Soc.*, 86
17 (1964)
20. D. Forster, *Chem. Comm.*, 113 (1967)
21. J.T.R. Dunsmuir and A.P. Lane, *J. Chem. Soc. (A)* 1971,
404.
22. J.S. Avery, C.D. Burbridge and D.M.L. Goodgame,
Spectrochim Acta., 24A, 1721 (1968)
23. D.F.C. Morris, E.L. Short and D.N. Waters, *J. Inorg.*
Nuclear Chem., 25, 975 (1963)
24. M.L. Delwaulle, *C.R. Acad. Sci.*, 240 2132 (1955)
25. C.O. Quicksall, T.G. Spiro, *Inorg. Chem.*, 5, 2232 (1966)
26. G.L. Cessac, R.K. Khanna, E.R. Lippincott and A.R. Bandy,
Spectrochim Acta., A28, 917 (1972)
27. I.R. Beattie, T.R. Gilson and G.A. Ozin, *J. Chem. Soc. (A)*,
534, (1969)
28. L.E. Orgel, 'An Introduction to Transition-metal
Chemistry Ligand-Field Theory' Wiley, New York (1960).
29. J.T.R. Dunsmuir and A.P. Lane, *J. Chem. Soc (A)*, 2781, 1971
30. R.D. Willet, J.R. Ferraro and M. Choca, *Inorg. Chem.*,
13, 2919 (1974)
31. J. McGinnety, *Inorg. Chem.*, 13, 1057 (1974)
32. G.D. Stucky, J.B. Folkers and T.J. Kistenmachers,
Acta Cryst., 23, 1064 (1967)

33. A. Mooney, R.H. Nuttal and W.E. Smith, J. Chem.Soc. (Dalton), 1096 (1972)
34. J.T.R. Dunsmuir, Ph.D. Thesis, Glasgow University, (1972)
35. N.S. Gill and R.S. Nyholm, J.Chem. Soc., 3997 (1959)

APPROXIMATE - 1972

CHAPTER 3 - A₃MX₅ COMPLEXES

CHAPTER 3

A_3MX_5 COMPLEXES

$A = Cs, M = Co, Ni, Cu, Zn; X = Cl, Br; Rb_3CoCl_5$ and $(DMA)_3CuCl_5$ where $DMA = (CH_3)_2NH_2$

Introduction

Despite the stoichiometry of these complexes, which might suggest pentacoordination they are all reported to contain isolated MX_4^{2-} tetrahedra with free halide ion in the lattice (1).

Up to the present, the vibrational studies of the A_3MX_5 complexes have been confined to the i.r. spectra ($40 - 700cm^{-1}$) of powdered samples (2,3). The single crystal work reported is that of the reflectance spectra of Cs_3CoCl_5 (2) where two bands of almost similar intensity were observed in the M-X bending region although only one is predicted.

The aims of the present studies, like those of the previous chapter, were to employ polarised Raman and i.r. studies of oriented single crystals to make unambiguous assignment of the multiplet components arising from the distortion, the site and factor group splittings of the internal modes. It is also intended to carry out Kramers-Kronig analysis on the reflectivity data to resolve the uncertainty as to which of the two bands in the M-X bending region should be assigned to the E_u component of ν_4 . It has been suggested that the other band is a lattice mode of a rather high frequency. Another objective is to extend the vibrational studies to cover other complexes, in the A_3MX_5 series.

With the exception of $(\text{DMA})_3\text{CuCl}_5$, all the complexes in the series are isostructural and crystallize in the tetragonal space group $I \underline{m} \underline{c} \underline{m}$ (D_{4h}^{18}), $Z = 4$. (4-8). Cs_3CoCl_5 has been subjected to very detailed crystallographic studies (4,6) which reveal the presence of CoCl_4^{2-} groups in approximately tetrahedral configuration. The fifth chlorine atom is present as a free Cl^- ion and is far removed from the cobalt atom. The Co-Cl bond length is 2.252°A and the Cl-Co-Cl angles are 106.1° and 111.2° . The deviation from perfect tetrahedral symmetry is seen to involve angular distortions rather than bond stretching or contraction. The CoCl_4^{2-} unit thus approaches D_{2d} symmetry with two pairs of equal angles, each angle in the pair being related by a crystallographic plane of symmetry.

The crystal structure data for Cs_3CuCl_5 is incomplete (7), but from the similarity of its i.r. spectrum to that of Cs_2CuCl_4 (2) it is reasonable to assume that it also contains isolated CuCl_4^{2-} units. For tetrahedral Cu^{2+} (d^9) complexes, Jahn-Teller effects are expected to produce extensive deviation from T_d symmetry.

Cs_3NiCl_5 is stable only above 690°K and from X-ray diffraction patterns on samples quenched from a temperature above 417°C to room temperature, the compound was found to be isostructural with Cs_3CoCl_5 . (7)

Willet (9) reports that $(\text{DMA})_3\text{CuCl}_5$ crystallises in the less symmetric space group $\underline{P} \underline{n} \underline{m} \underline{a}$ (\underline{D}_{2h}^{16}) $Z = 4$ and also contains discrete CuCl_4^{2-} and a lattice chloride ion.

The Cu-Cl bond distances in this complex are all equal and two of the Cl-Cu-Cl angles are 98° while the other two are 136° and thus this unit has the largest reported distortion from T_d symmetry of the chlorocuprates(II). The DMA groups are all involved in hydrogen bonding of the type N-H...Cl and this causes the lattice chloride and one of the DMA ions to be disordered. This complex exhibits thermochromic behaviour, being yellow at room temperature but turning green when cooled to liquid nitrogen temperature.

Results and Discussion

The results of Factor Group Analysis on the complexes with space group D_{4h}^{18} are given in Table 3.1 and from it the number and symmetry species of the optically active internal modes and lattice modes are given by the representations 3.1 and 3.2

$$\Gamma_{\text{internal}} = 2A_{1g} + B_{1g} + 2B_{2g} + 2E_g + 2A_{2u} + 2E_u \quad (3.1)$$

$$\Gamma_{\text{lattice}} = A_{1g} + B_{1g} + 2B_{2g} + 4E_g + 3A_{2u} + 6E_u \quad (3.2)$$

The correlations between the internal modes of vibration of the MX_4^{2-} unit with the modes of isolated T_d and the factor group are identical to those in Table 2.16.

The Factor Group Analysis for the $(\text{DMA})_3\text{CuCl}_5$ complex based on the proposed structure and treating the DMA ions as point groups is given in Table 3.2 where \underline{R}^- gives the symmetry species of the rotatory lattice modes associated with the CuCl_4^{2-} ion. The torsional vibrations of the DMA ions is given by the representation (3.3)

Table 3.1 Factor-group analysis for A_3MCl_5 complexes
with space group D_{4h}^{18}

D_{4h}	n_i	T	T'	R	α	n'_i	activity
A_{1g}	3		1		2	2	$x^2 + y^2, z^2$
A_{2g}	3		2	1			
B_{1g}	2		1		1	1	$x^2 - y^2$
B_{2g}	4		2		1	2	xy
E_g	6		3	1	1	2	(xz, yz)
A_{1u}	2		1			1	
A_{2u}	6	1	3			2	z
B_{1u}	3					2	
B_{2u}	1			1			
E_u	9	1	5	1		2	(x, y)

TABLE 3.2

Factor group analysis for $(DMA)_3CuCl_5$

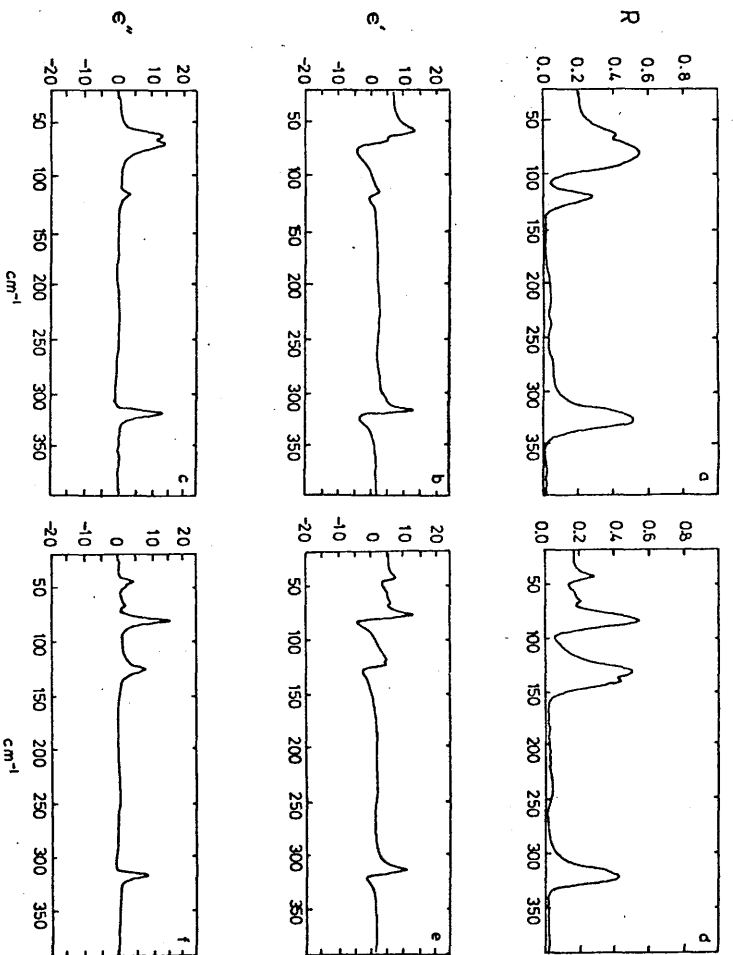
\underline{D}_{2h}	\underline{n}_i	\underline{T}	\underline{T}'	\underline{R}	$\underline{\alpha}$	\underline{n}'_i	activity
\underline{A}_g	14		7	1	3	6	$\underline{x}^2, \underline{y}^2, \underline{z}^2$
\underline{B}_{1g}	10		5	2	1	3	\underline{xy}
\underline{B}_{2g}	14		7	1	1	6	\underline{xz}
\underline{B}_{3g}	10		5	2	1	3	\underline{yz}
\underline{A}_u	13		8	2		3	
\underline{B}_{1u}	17	1	10	1		6	\underline{z}
\underline{B}_{2u}	13	1	8	2		3	\underline{y}
\underline{B}_{3u}	17	1	10	1		6	\underline{x}

$$\Gamma_R^+ = 4A_g + 5B_{1g} + 4B_{2g} + 5B_{3g} + 5A_u + 4B_{1u} + 5B_{2u} + 4B_{3u} \quad (3.3)$$

Since the Cu atoms are located on sites of C_s symmetry, the site group analysis for this complex is identical to that given in Table 2.2 for Cs_2MCl_4 complexes having the same space group.

Single crystals of good optical quality were obtained for Cs_3CoCl_5 and Cs_3CoBr_5 which permitted a complete polarised i.r. and Raman studies to be undertaken. Representative spectra of the chloride complex, recorded at 77°K are given in Figures 3.1 and 3.2. They show the i.r. reflectance spectra recorded for both the ordinary and extraordinary rays, together with their respective variation of the real and imaginary parts of the dielectric constant with frequency as calculated from Kramers-Kronig analysis. The Raman spectra of the four pertinent tensor components are shown in Figure 3.2. The Raman intensity data for both complexes are given in Table 3.3 and the observed frequencies and their symmetry assignments are shown in Table 3.4. These frequencies, which were recorded at 77°K in order to benefit from the decrease in spectral band width, differed only by about 4cm^{-1} from those recorded at room temperature.

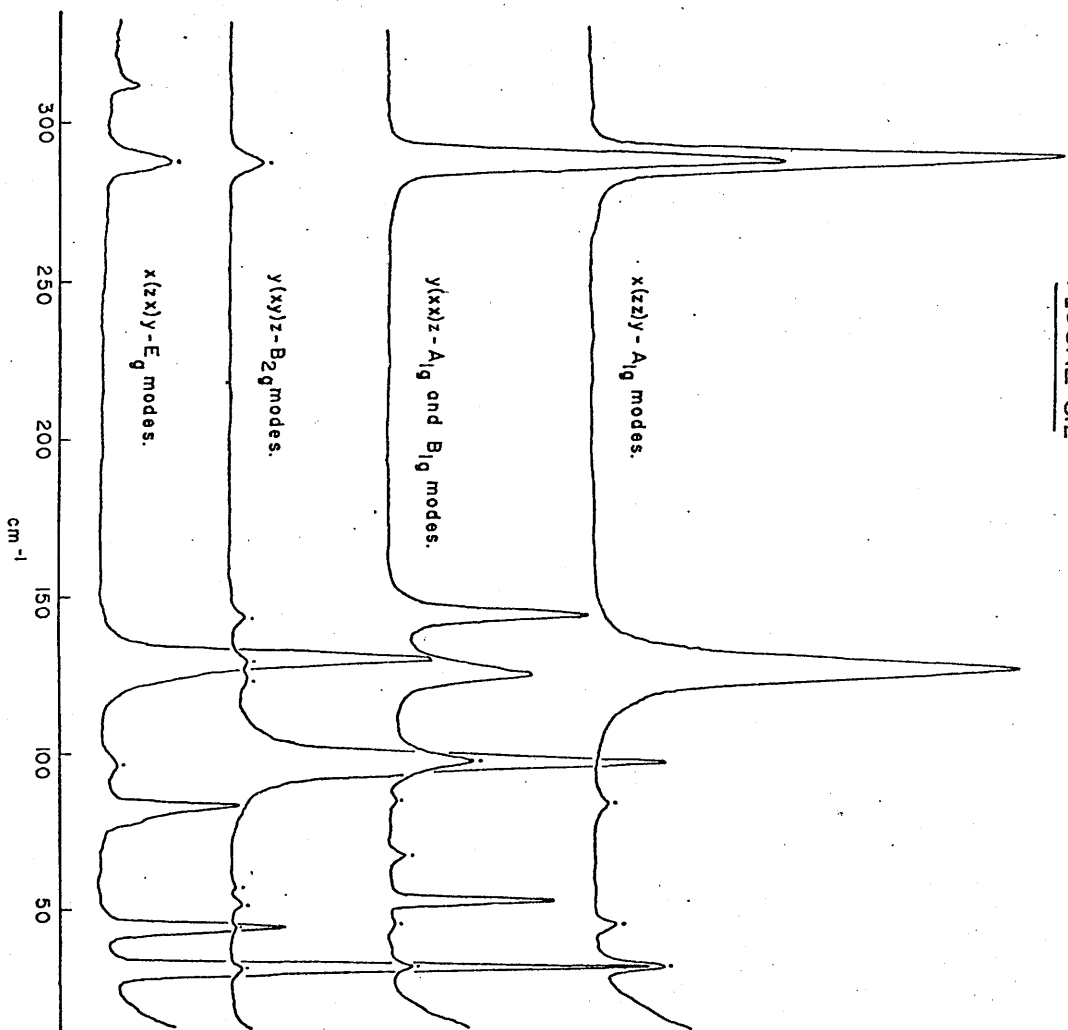
The symmetric stretching vibration ν_1 has no i.r. component and therefore, unlike the A_2MCl_4 complexes, its assignment from the Raman data is straightforward. The symmetric bending vibration ν_2 is split under D_{2d} symmetry into A_1 and B_1 and have no i.r. components. Their assignments are also straightforward. The asymmetric stretching and bending vibrations, ν_3 and ν_4 are split under D_{2d} and have i.r. components. From the Raman data only two E_g modes



Infrared Reflectance Spectra and K-K Analysis
for Cs_3CoCl_5 (at 77°K)

- a. Extraordinary Ray Spectrum - A_{2u} modes.
- b. Real dielectric response for A_{2u} modes.
- c. Imaginary dielectric response for A_{2u} modes.
- d. Ordinary Ray Spectrum - A modes.
- e. Real dielectric response for A modes.
- f. Imaginary dielectric response for A modes.

FIGURE 3.2



Raman Spectra for CsCoCl_2 at 77°K . indicates polarization leakage.

T A B L E 3•3 Raman polarization intensity data (arbitrary units)
for Cs_3CoCl_5 and Cs_3CoBr_5

	Frequency cm^{-1}	Scattering Geometry				Assignment
		$y(xx)z$	$x(zz)y$	$y(xy)z$	$x(zx)y$	
Cs_3CoCl_5	31	7	24	5	178	E_g
	44	2	8	2	60	E_g
	51	53	0	4	0	B_{1g}
	65	5	0	1	0	A_{1g}
	83	3	5	0	45	E_g
	96	27	0	138	6	B_{2g}
	125	47	136	5	30	A_{1g}
	130	0	0	0	110	E_g
	142	65	0	5	0	B_{1g}
	289	128	163	11	22	A_{1g}
	313	0	0	0	12	E_g
Cs_3CoBr_5	26	5	14	8	36	E_g
	31	5	24	0	10	A_{1g}
	41	22	10	6	23	E_g
	54	21	6	95	6	B_{2g}
	59	0	14	0	31	E_g
	63	40	9	13	0	B_{1g}
	67	46	12	185	21	B_{2g}
	83	77	168	13	16	A_{1g}
	90	14	49	12	68	E_g
	100	127	5	13	6	B_{1g}
	181	167	146	15	10	A_{1g}

† A B L E 3•4. Observed vibrational frequencies (cm^{-1}) and assignments for Cs_3CoCl_5 and Cs_3CoBr_5 recorded at 77°K

Free Ion T_d	Unit cell D_{4h}	Cs_3CoCl_5	Cs_3CoBr_5
$\nu_3(T_2)$	A_{2u}	320	248
	E_u	316	242
	E_g	313	-
$\nu_1(A_1)$	B_{2g}	-	-
	A_{1g}	289	181
$\nu_2(E)$	B_{1g}	142	100
	A_{1g}	125	83
$\nu_4(T_2)$	A_{2u}	132	76
	E_u	128	90
	E_g	130	90
	B_{2g}	-	-
Lattice Modes	E_u	136	92
	B_{2g}	96	67
	A_{2u}	88	54
	E_g	83	59
	E_u	82	64
	B_{2g}	-	54
	A_{2u}	79	
	A_{1g}	65	31
	E_u	66	42
	B_{1g}	51	63
E_g	44	41	
E_g	31	26	

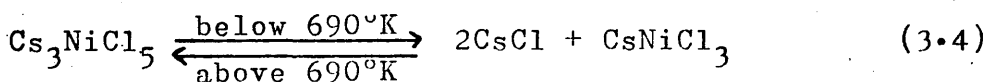
could be observed and the mode at 313cm^{-1} is assigned to ν_3 while that at 130cm^{-1} is assigned to ν_4 for the chloride complex. Apart from the B_{2g} modes and, for Cs_3CoBr_5 , the weak E_g component of ν_3 all of the internal modes and eleven of the seventeen predicted lattice modes were observed for both complexes. From the infrared the two predicted A_{2u} and E_u modes associated with both the ν_3 and ν_4 were clearly observed and there is no difficulty in assigning the bands at 320cm^{-1} and 316cm^{-1} to ν_3 . The A_{2u} band at 132cm^{-1} is also assigned to ν_4 without difficulty. The only difficulty in assignment of the observed bands to the crystal components of the free ion modes arose for the ordinary ray spectra. Here two bands were observed, at 128cm^{-1} and 136cm^{-1} for Cs_3CoCl_5 and at 90cm^{-1} and 92cm^{-1} for Cs_3CoBr_5 , one of which could be assigned to the E_u component of ν_4 while the other is a high frequency lattice mode. For both complexes the spectral features in these regions were typical of those arising from the interaction of a weak oscillator on the high frequency side of a strong oscillator thereby causing inversion of the latter (10,11) and therefore, in order to substantiate this a Kramers-Kronig analysis of the reflectivity data was undertaken. The results, for Cs_3CoCl_5 , shown in Figure 3.1, give the variation with frequency for both the real ϵ' and imaginary ϵ'' parts of the dielectric constant. The plot of ϵ' with frequency for the ordinary ray clearly shows two bands in the 130cm^{-1} region but in the ϵ'' spectrum, in which the frequency and intensity of the calculated maxima reflect, respectively, the true frequency and strength of the oscillators, only one peak at 128cm^{-1} was observed. Failure to observe a peak at around 136cm^{-1}

indicates the weakness of the high frequency mode.

[The frequencies of 136cm^{-1} and 92cm^{-1} quoted for the E_u modes in the chloride and bromide complexes respectively were taken at the minimum of the main reflectance bands (11)]. Since in both complexes the A_{2u} components of ν_4 is of medium intensity and for the tetragonal complexes $(\text{NEt}_4)_2\text{MCl}_4$ ($\text{Et} = \text{C}_2\text{H}_5$; $\text{M} = \text{Co}, \text{Ni}$) both the A_{2u} and E_u components of ν_4 appear as strong reflectance maxima (12), the main bands at 128cm^{-1} for the chloride and 90cm^{-1} for the bromide are assigned to ν_4 and the weak high frequency bands at 136cm^{-1} and 92cm^{-1} for the chloride and bromide complexes respectively are assigned to the lattice modes. Generally lattice modes in complex halides are rarely found much higher than 120cm^{-1} . The existence of this one at 136cm^{-1} could be explained from consideration of the structure of the complex. The lattice is composed of layers of Cs_2Cl and $\text{Cs}(\text{CoCl}_4)$ which alternate so that it is likely to have a lattice mode involving displacements of atoms in the Cs_2Cl layers only. Thus this mode is confined entirely to the free chloride ion and would produce a higher frequency than if the massive CoCl_4^{2-} ions are involved.

From the assignments in the spectra of Cs_3CoCl_5 it is observed that, in the absence of the frequency for the B_{2g} components of ν_3 and ν_4 an indication of the degree of splitting is given by considering the frequencies for A_{2u} and E_u . There is only a splitting of 4cm^{-1} for each of ν_3 and ν_4 . Thus it is likely that the splitting is due to the factor group instead of the distortion from perfect tetrahedral geometry.

For those complexes where single crystals could not be obtained, namely Cs_3MCl_5 ($\text{M} = \text{Ni}, \text{Cu}, \text{Zn}$) and Rb_3CoCl_5 , Raman spectra of powdered samples were recorded both at 300°K and 77°K and the observed frequencies together with assignments based on the single crystal data for Cs_3CoCl_5 are given in Table 3.5. The spectral features for Cs_3MCl_5 ($\text{M} = \text{Ni}, \text{Zn}$) and Rb_3CoCl_5 were very similar to the powder spectrum of Cs_3CoCl_5 and thus substantiate the x-ray studies which indicate that these complexes are isostructural. It is known (7) that, because of the enhanced crystal field stabilization due to octahedral coordination in d^8 systems, Cs_3NiCl_5 undergoes a solid state transformation at 690°K decomposing to CsCl and the octahedral complex CsNiCl_3 , according to the equation



blue

yellow

The results of the Raman spectrum are given in Table 3.5. The Raman spectrum of Cs_3NiCl_5 showed none of the bands reported (12) for CsNiCl_3 ; in particular the intense \underline{E}_{2g} mode at 195cm^{-1} was totally absent. This negligible lack of decomposition can be attributed to the fact that the quenched sample was stored at 77°K and only briefly allowed to reach room temperature for loading into the cryostat.

The Raman spectrum of Cs_3CuCl_5 differs markedly from those of the other complexes in that three bands of medium intensity are observed between 240cm^{-1} and 300cm^{-1} . The relative intensity and frequency of these bands are very similar to those found in Cs_2CuCl_4 discussed in Chapter 2

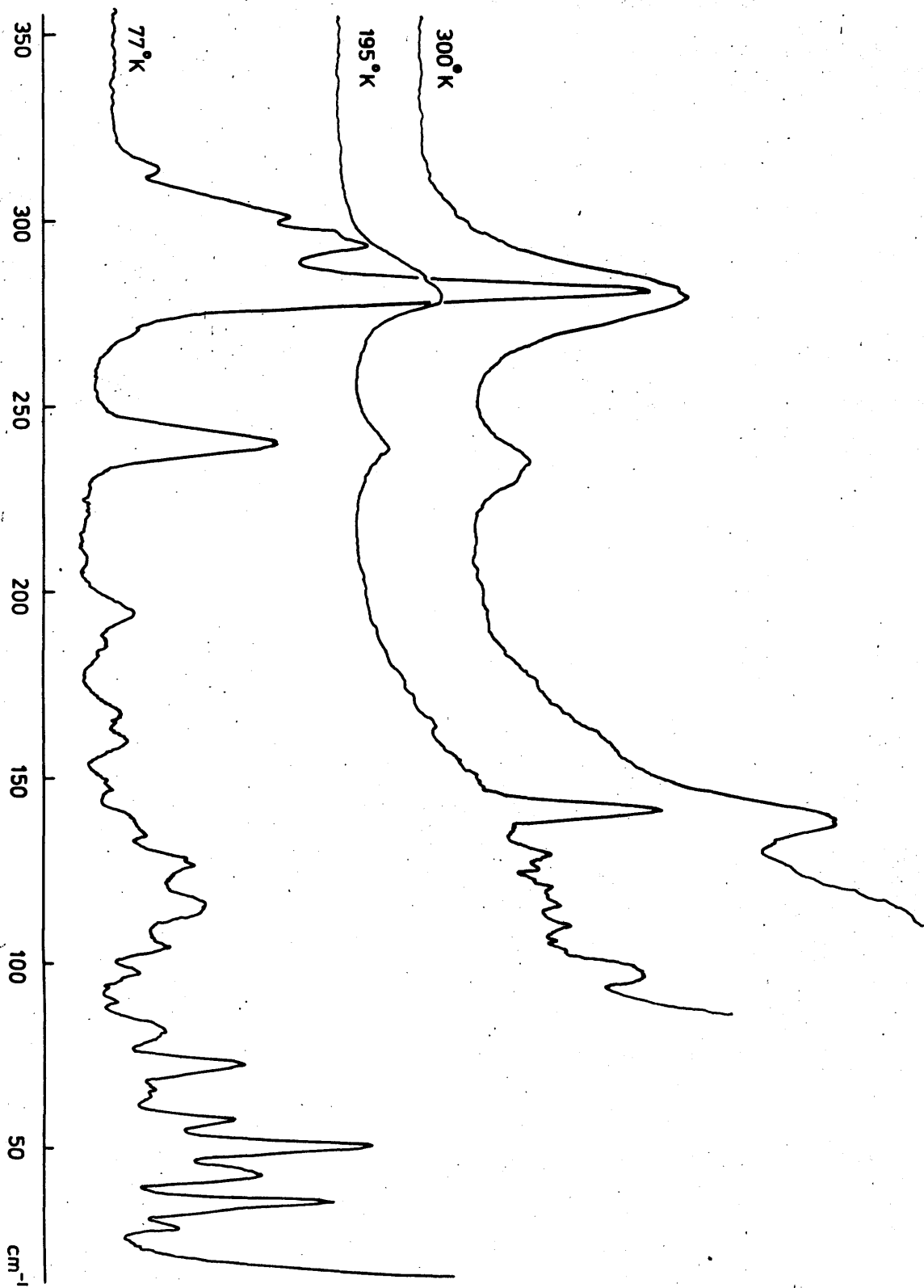
Table 3.5 Observed Raman frequencies (cm^{-1}), recorded at 77°K , and proposed assignments for A_3MCl_5 complexes.

Cs_3CoCl_5	Cs_3NiCl_5	Cs_3ZnCl_5	Cs_3CuCl_5	Rb_3CoCl_5	Assignment
	314		298, 250		ν_3
283	289	297	273	239	ν_1
137		142	115	142	ν_2
123	128	133	135, 131	125	ν_4
117	119			119	ν_2
91	103	102	102	84	} lattice modes
84	77	81	85	75	
66	66	65	79	66	
48	55	50	60	51	
42	49	43	48	44	
33	42	29	33	32	
	26				

and $(\text{DMA})_3\text{CuCl}_5$ suggesting that Cs_3CuCl_5 is not tetragonal, accordingly the vibrational assignments given in Table 3.5 are based on those for the orthorhombic complex Cs_2CuCl_4 . The 48cm^{-1} splitting of the ν_3 Raman active crystal mode is larger than that found for Cs_2CuCl_4 , indicating substantial distortion of the CuCl_4^{2-} ions from tetrahedral symmetry.

The Raman spectra of the $(\text{DMA})_3\text{CuCl}_5$ complex were recorded for the six non-equivalent scattering geometries at 300°K , 195°K and 77°K and typical of the results obtained, the ~~zz~~ tensor components are shown in Figure 3.3. At 300°K , the lattice region, below 100cm^{-1} , is featureless and this is due to the orientational disorder of a DMA and the free chloride ions which cause a breakdown in the zone centre approximation ($\underline{k} = 0$). This effect is less pronounced for the ordered CuCl_4^{2-} vibrations and three distinct broad bands are observed at 281cm^{-1} , 236cm^{-1} and 139cm^{-1} corresponding respectively to the $(\nu_1 + \nu_3)$, ν_3 and $(\nu_4 + \nu_2)$ vibrations of the tetrahedral anion. Preliminary differential thermal analysis and broadline n.m.r. experiments (9) indicate that two minor phase changes occur below 300°K and these have been attributed to hindered rotation of the methyl groups and order-disorder phenomena in the $\text{N-H}\cdots\text{Cl}$ hydrogen bonding system. The spectrum at 195°K , apart from some additional weak bands between 130cm^{-1} and 90cm^{-1} shows little evidence of this ordering but at 77°K significant changes are observed; the bands at 281cm^{-1} and 139cm^{-1} are split into several components, new bands appear between 200cm^{-1} and 150cm^{-1} and in the lattice region, eleven sharp bands are observed down to 28cm^{-1} .

FIGURE 33

Raman Spectra for (DMFA)₃CuCl₅ at 300, 195 and 77 °K

These sharp spectral features are certainly indicative of substantial ordering of the DMA and chloride ions at 77°K. Further analysis of the data provides little information as to the exact location of these ions in the lattice. If they were situated on the elements of symmetry required by the proposed space group, then the region from 320cm^{-1} to 240cm^{-1} , where the crystal modes of ν_1 and ν_3 are observed, should be similar to that found in the Raman spectrum of Cs_2CuCl_4 recorded at 77°K where three major peaks are observed. This is, however, not the case in $(\text{DMA})_3\text{CuCl}_5$ since there are at least four bands of medium to strong intensity in this region which suggests enlargement of the proposed tetramolecular unit cell at 77°K. The observed Raman frequencies for this complex recorded at 77°K, polarization intensity for the six scattering geometries used and the proposed vibrational assignments are given in Table 3.6. Despite care in alignment of the crystal axes and repeated measurements, it can be seen from the intensity data that polarization leakage between diagonal and off-diagonal tensor components was very large and this prevented accurate symmetry assignments. In most cases, therefore, the assignments are limited to the crystal components of the CuCl_4^{2-} vibrations and the lattice modes. Large polarization leakage of this kind is normally not encountered in ordered crystals and must, therefore, be due to inherent disorder still remaining at 77°K causing scrambling of the polarized radiation. Similar effects have been observed in the i.r. reflectance (13) and the Raman spectra discussed in Chapter 2 of $(\text{NMe}_4)_2\text{MCl}_4$ ($\text{M} = \text{Co}, \text{Zn}, \text{Cu}$) complexes recorded at 77°K.

Table 3.6 Observed Raman frequencies (cm^{-1}), recorded at 77°K , polarization intensity data (arbitrary units) and vibrational assignments for $(\text{DMA})_3\text{CuCl}_5$

Frequency	Scattering Geometry						Assignment ¹
	z(xx)y	z(xz)y	x(yy)z	x(yx)z	y(zz)x	y(zy)x	
312	0	0	26	25	0	0	} $\nu_3 + \nu_1$
302	70	17	70	0	0	0	
294	142	30	97	34	94	30	
282	203	59	192	74	157	44	
241	56	21	65	24	57	15	
195	25	4	17	8	0	0	} ν_3
186	12	0	9	8	0	0	
167	18	4	12	23	0	0	
160	28	7	15	22	14	12	
146	0	0	9	18	12	0	} ν_4
136	0	4	20	20	0	0	
126	0	0	37	16	0	0	
120	0	8	0	0	0	0	} ν_2
115	13	0	42	21	30	9	
105	5	0	28	15	0	0	} lattice
96	13	0	18	20	0	0	
83	61	12	28	20	0	0	
78	0	0	0	0	31	11	
722	58	28	55	26	0	12	
58	45	16	51	47	139	26	
51	121	22	85	29	0	22	
43	33	10	48	30	41	20	
41	0	0	0	38	0	0	
35	20	14	85	43	85	22	
32	0	0	0	30	0	0	
28	0	0	34	14	0	0	

Experimental

Crystals of Cs_3CoCl_5 and Cs_3CoBr_5 were obtained from aqueous solution by the method of Powell and Wells (4), using a six-fold excess of the cesium halide for the chloride complex and a 1:1 molar ratio for the bromide complex.

$(\text{DMA})_3\text{CuCl}_5$ crystals were obtained by slow evaporation, in an N_2 atmosphere, of an ethanolic solution containing stoichiometric quantities of the constituent chlorides.

All the remaining complexes were prepared by fusion of stoichiometric quantities of the alkali metal chloride and the anhydrous transition metal dichloride contained in an evacuated silica tube; the melting points for the Cu, Ni and Zn, complexes were taken as 491°C , 547°C and 601°C respectively (14) while that for Rb_3CoCl_5 was 600°C (5).

In the case of Cs_3NiCl_5 , the tube was removed from the furnace at 500°C and immediately quenched to 0°C .

The laser excitation frequencies found to be most suitable for recording the Raman spectra of these complexes were 496.5nm for Cs_3CoBr_5 , 472.7nm for Cs_3CoCl_5 , 476.5nm for Cs_3NiCl_5 and 488.0nm for Cs_3ZnCl_5 and Rb_3CoCl_5 . For $(\text{DMA})_3\text{CuCl}_5$ the 568.2nm line was used at 300°K while at low temperatures a change to the 514.5nm line was necessary due to the thermochromism exhibited by this complex (9), the same excitation frequencies were used to record the Raman spectra of Cs_3CuCl_5 at 300°K and 77°K .

References

1. A.F. Wells, 'Structural Inorganic Chemistry', 4th Edition, Clarendon Press, Oxford, 1975.
2. J.T.R. Dunsmuir and A.P. Lane; *J. Chem. Soc. (A)*, 404 (1971).
3. R.J.H. Clark and T.M. Dunn; *J. Chem. Soc.*, 1198 (1963)
4. H.M. Powell and A.F. Wells; *J. Chem. Soc.*, 369 (1935)
5. A. Engberg and H. Soling; *Acta. Chem. Scand.*, 21, 168 (1967).
6. B.N. Figgis, M. Gerloch and R. Mason; *Acta Cryst.*, 17, 506 (1964).
7. E. Ibers, R. Gut and D.M. Gruen; *J. Phys. Chem.*, 66, 65 (1962).
8. R.P. Van Staplele, H.G. Belgers, P.F. Bongers and H. Zijlstra; *J. Chem. Phys.*, 44, 3719 (1966).
9. R.D. Willet and M.L. Larsen; *Inorganica Chimica Acta.*, 5, 175 (1971).
10. J.D. Black, J.T.R. Dunsmuir, I.W. Forrest and A.P. Lane; *Inorg. Chem.*, 14, 1257 (1975).
11. W.G. Spitzer and D. Kleinman; *Phys. Rev.*, 121, 1324 (1961).
12. J.T.R. Dunsmuir, Ph.D. Thesis, Glasgow University (1972).
13. A. Chadwick, J.T.R. Dunsmuir, S. Fernando, I.W. Forrest and A.P. Lane; *J. Chem. Soc. (A)*, 2794 (1971).
14. J.T.R. Dunsmuir and A.P. Lane, *J. Chem. Soc. (A)* 2781 (1971)
15. G.N. Papatheodorou; *J. Inorg. and Nucl. Chem.*, 35, 465 (1973).

CHAPTER 4 - $(C_n H_{2n+1} NH_3)_2 MX_4$ COMPLEXES

4.1 $(C_n H_{2n+1} NH_3)_2 MCl_4$ complexes

4.2 Thermochromism in Copper complexes

CHAPTER 4

 $(C_nH_{2n+1}NH_3)_2MCl_4$ ComplexesM = Cu, Mn, n = 1, 2, 3.Introduction

The complexes of the above general formula have been studied in solid state physics and chemistry because of their interesting layer-structure with hexa-coordinated metal ions (1), luminescence phenomena (2) and quasi two-dimensional magnetic ordering at low temperatures. (3,4,5)

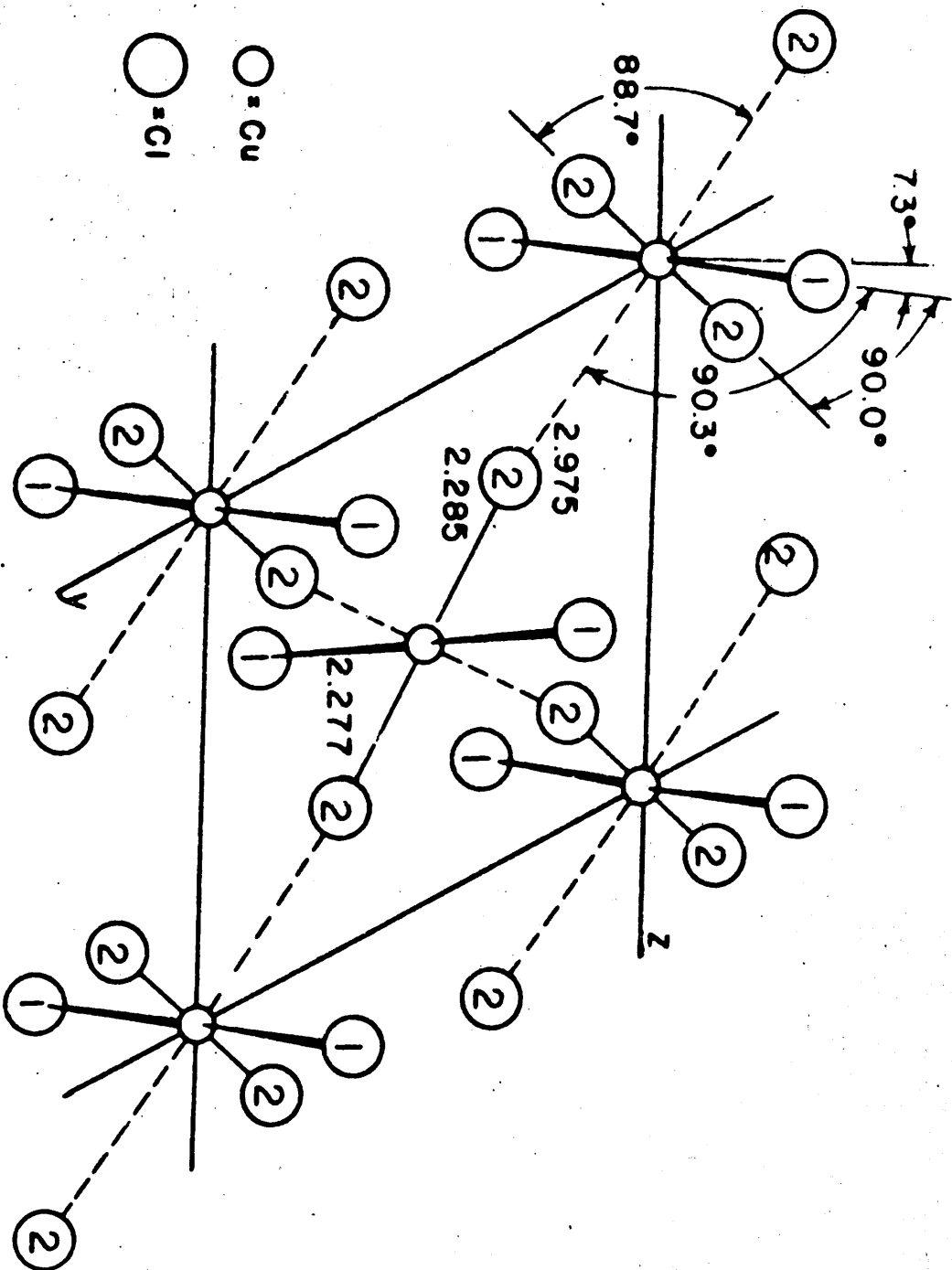
Two slightly different structural types at room temperature are reported; a more symmetric one for the manganese complexes which leads to the space group $Cmca$ ($= D_{2h}^{18}$) with two formula units in the primitive cell (6,7), and a less symmetric one for the copper complexes leading to the space group $Pbca$ ($= D_{2h}^{15}$) with four formula units in the unit cell. (8,9). $(CH_3NH_3)_2CuCl_4$, however, is an exception since it is isostructural with $(NH_4)_2CuCl_4$ and crystallises in the space group D_{2h}^{18} (10).

In the copper complexes there are sheets of nearly square planar $CuCl_4^{2-}$ ions separated from each other by two layers of alkylammonium groups. The bond lengths of the $CuCl_4^{2-}$ units in the methyl complex are not known but those in the isostructural $(NH_4)_2CuCl_4$ are not equal, two are 2.30 Å and the other two are 2.332 Å. In the ethyl complex the bond lengths are almost equal (2.277 Å and 2.28 Å) while they are all equal in the n-propyl complex (2.29 Å). These planar ions are held together in sheets which are mainly perpendicular to the planes of the ions by long CuCl bonds of 2.793 Å,

2.975 Å and 3.04 Å for the methyl, ethyl and n-propyl complexes respectively. Thus the Cu atoms have a (4+2) distorted octahedral configuration. The chlorine atom at a long distance from the copper atom belongs to the square co-ordination of a neighbouring copper atom (see Figure 4.1) The only forces holding successive copper-chlorine sheets together are van der Waals forces between terminal carbon atoms of the aliphatic chain. Because of this the crystals have excellent cleavages parallel to the planes of the sheets. In the ethyl complex the long CuCl bond is tipped 7.3° away from the z-axis while the Cu-Cl bond in the plane is tipped 5.1° out of the plane. The significant difference between the structure of the methyl complex and those of the ethyl and n-propyl complexes seems to be a slight shortening of the four equatorial Cu-Cl bonds and a considerable lengthening of the two axial Cu-Cl bonds in the latter. Thus the former is orthorhombically distorted and the latter tetragonally distorted from the regular octahedral geometry.

There is a possibility of hydrogen bonding arising from the location of the alkylammonium cations in the structure. "Holes" are formed at both sides of the sheets by eight neighbouring chlorine atoms and into these the NH_3 -groups sit. The nitrogen atom, however, lies particularly close to one chlorine atom to make it possible for a strong $\text{N-H}\cdots\text{Cl}$ type of hydrogen bonding. The stereochemical configuration, however, casts some doubt on this interpretation since, owing to the disorder in the aliphatic chain, there are no hopes of locating the hydrogen atoms directly.

Figure 4.1

CuCl₄²⁻The CuCl₄²⁻ Ion and Its Packing in (C₂H₅NH₃)₂-

Of the manganese salts only the structure of the n-propyl complex is known in detail at room temperature. This crystallises in the orthorhombic space group $Cmca$ ($= D_{2h}^{18}$) with $Z = 4$. (6). In this structure there is a two-dimensional metal-halogen framework formed by $MnCl_6$ octahedra sharing corners. Such an arrangement could be compared with a plane in the perovskite structure, the Mn atoms occupying the B-sites and the A-sites in the cavities between the octahedra occupied by the NH_3^- groups. By this, adjacent sheets are effectively isolated from each other. The interesting electrical and magnetic properties of these complexes may be dependent upon the spacing between the metal ions (11). The two non-bridging Mn-Cl distances are shorter than the four bridging ones which lie approximately in the plane of the Mn, giving a coordination sphere around the Mn of approximately D_{4h} symmetry. This structure is basically similar to the K_2CuF_4 structure (12). The existence of N-H...Cl hydrogen bonding causes the deformed octahedra to be tipped 8.0° away from the z-axis.

In both the copper and manganese structure there is a strong tetragonal pseudostructure and by small shifts of the mean positions of all the atoms except the hydrogens, whose positions are not definitely known, it is possible to generate the tetragonal space group D_{4h}^{17} with one formula unit in the primitive cell, a structure similar to K_2NiF_4 (13).

Structural phase transitions have recently been observed in the bis(alkylammonium)manganese tetrachloride complexes (14, 15, 16). There is a high temperature phase transition from orthorhombic to tetragonal at $393.6^\circ K$, $424.4^\circ K$ and $446.1^\circ K$

for the methyl, ethyl and n-propyl complexes respectively. A theoretical analysis based on the Landau-type group symmetry (17) has been carried out to investigate the symmetry and lattice dynamic aspects of this transition, which principally is of the order-disorder type (14). The room temperature phase is thus a frozen high temperature structure in which no disorder remains. Other structural phase transitions are reported for the methyl complex at low temperatures. (18).

The copper complexes are thermochromic changing colour from light yellow at room temperature to green at low temperature. The transition is near -40°C for both the methyl and ethyl complexes, although from DTA studies the transition is very broad covering a temperature range of nearly 50° (19) for the ethyl complex. The low temperature structural properties are not known.

Though this series of complexes has attracted considerable interest, it is mostly their magnetic properties which have been investigated (2,3); little attention has been given to their vibrational spectra. The far i.r. reflectance spectra (HT and RT) of $(\text{MeNH}_3)_2\text{MnCl}_4$ have been reported but no assignments could be made owing to twinning and phase change effects (18). From the mull i.r. spectra Adams (20) observed the $\nu(\text{Cu-Cl})$ at 284 cm^{-1} and 279 cm^{-1} for the $(\text{MeNH}_3)_2\text{CuCl}_4$ and $(\text{Et-NH}_3)_2\text{CuCl}_4$ respectively. Willet (21) however, considering the effective CuCl_4^{2-} geometry in the ethyl complex to be D_{2h} , observed the three i.r. frequencies for the B_{1u} , B_{2u} and B_{3u} modes which arise from the A_{2u} and E_u modes of D_{4h} symmetry when the latter is

lowered to D_{2h} . Single crystal Raman spectra of $(MeNH_3)_2CuCl_4$ has also been reported (22).

In the present studies Raman spectra have been recorded for the three copper complexes at RT, 195°K and 77°K but owing to fluorescence, the Raman spectra of the manganese complexes could not be recorded. The far i.r. reflectance spectra have been recorded at the three different temperatures at two orientations, E//X and E//Y for those complexes which grow as large crystals.

RESULTS AND DISCUSSION

Factor group analyses for the two structural types, namely D_{2h}^{18} and D_{2h}^{15} are presented in Tables 4.1 and 4.2 respectively. These analyses assume the alkylammonium cations to be point groups and neglect any rotatory lattice modes associated with the MCl_4 groups. This latter omission arises because of the quasi 2-D cross-linked layer structure of the MCl_4 groups such that any torsional motion around the M atom will, in fact, constitute a bending type of vibration. The translatory lattice modes are included (as opposed to treating these systems as a 3N-3 phonon problem) and may be regarded as vibrations of the alkylammonium groups against the semi-rigid metal-halogen lattices.

For the room temperature form of $(CH_3NH_3)_2CuCl_4$ and the manganese complexes, which have the space group $Cmca$ (D_{2h}^{18}), it can be seen that the optically active vibrations of the metal-chlorine layers are given by the representations (4.1) and (4.2):-

$$\Gamma_{\text{Raman}} = 3A_g + 3B_{1g} + 2B_{2g} + 4B_{3g} \quad (4.1)$$

$$\Gamma_{\text{i.r.}} = 4B_{1u} + 3B_{2u} + 3B_{3u} \quad (4.2)$$

while the translatory lattice modes and those rotatory lattice modes associated with the alkylammonium groups are given by the representations (4.3) and (4.4):-

$$\Gamma_{\text{translatory}} = 2A_g + B_{1g} + B_{2g} + 2B_{3g} + 3B_{1u} + 3B_{2u} + B_{3u} \quad (4.3)$$

$$\Gamma_{\text{rotatory (cations)}} = A_g + 2B_{1g} + 2B_{2g} + B_{3g} + B_{1u} + B_{2u} + 2B_{3u} \quad (4.4)$$

Table 4.1

Factor Group Analysis For the $(C_n H_{2n+1} NH_3)_2 MCl_4$ Complexes
of Space Group D_{2h}^{18} (Cmca).

	n_i	T_A	$T+T_A$	T	R	n_i'
A_g	5	0	2	2	1	3
B_{1g}	4	0	1	1	2	3
B_{2g}	3	0	1	1	2	2
B_{3g}	6	0	2	2	1	4
A_u	4	0	2	2	2	
B_{1u}	8	1	4	3	1	4
B_{2u}	7	1	4	3	1	3
B_{3u}	5	1	2	1	2	3

Table 4.2

Factor Group Analysis For the $(C_n H_{2n+1})_2 MCl_4$ of Space Group
 D_{2h}^{15} (Pbca).

	n_i	T_A	$T+T_A$	T	R	n_i'
A_g	9	0	3	3	3	6
B_{1g}	9	0	3	3	3	6
B_{2g}	9	0	3	3	3	6
B_{3g}	9	0	3	3	3	6
A_u	12	0	6	6	3	6
B_{1u}	12	1	6	5	3	6
B_{2u}	12	1	6	5	3	6
B_{3u}	12	1	6	5	3	6

For the other complexes having the space group $Pbca$ (D_{2h}^{15}) the equivalent representations are given by (4.5), (4.6) and (4.7).

$$\Gamma_{\text{internal}} = 6A_g + 6B_{1g} + 6B_{2g} + 6B_{3g} + 6B_{1u} + 6B_{2u} + 6B_{3u} \quad (4.5)$$

$$\Gamma_{\text{translatory}} = 3A_g + 3B_{1g} + 2B_{2g} + 3B_{3g} + 5B_{1u} + 5B_{2u} + 5B_{3u} \quad (4.6)$$

$$\Gamma_{\text{rotatory(cations)}} = 3A_g + 3B_{1g} + 3B_{2g} + 3B_{3g} + 3B_{1u} + 3B_{2u} + 3B_{3u} \quad (4.7)$$

In view of the pseudo-tetragonal structure of all these complexes, it is worthwhile including the group theoretical predictions for K_2CuF_4 which consists of 2-D cross-linked layers of CuF_6 octahedra. This complex has the tetragonal space group $I4/mmm$ (D_{4h}^{17}) with one molecule per Bravais unit cell and the optically active modes of vibration are given by the representation (4.8)

$$2A_g + 2E_g + 3A_{2u} + 4E_u \quad (4.8)$$

Considering only an isolated MX_4 unit of square planar (D_{4h}) geometry, five non-degenerate and two degenerate fundamental modes are expected as shown in Table 4.3 below.

Table 4.3 D_{4h} Square planar MX_4

	ν_1	ν_2	ν_3	ν_4	ν_5	ν_6	ν_7
Symmetry	A_{1g}	A_{2u}	B_{1g}	B_{1u}	B_{2g}	E_u	E_u
Activity	R	IR	R	Inact.	R	IR	IR

The M atom occupying the centre of the square represents a centre of symmetry so that the rule of mutual exclusion applies. A characteristic Raman spectrum of MX_4 square planar molecule has an intense totally symmetric stretching mode ($\nu_1 A_{1g}$), a weaker 'out-of-phase' symmetric stretch ($\nu_5 B_{2g}$) and an intense in plane deformation ($\nu_3 B_{1g}$). The frequency of the 'out-of-phase' stretching motion of the two pairs of opposite X atoms is expected to be very close to that of the symmetric stretching mode. If a simple valence force field, without the introduction of interaction terms is assumed, the frequencies of the two fundamentals would be the same. There is no Raman-active 'out-of-phase' deformation.

One of the E_u modes, ν_6 , is the only infrared-active stretching mode. The other E_u mode (ν_7) is an in-plane deformation while the other i.r.-active mode A_{2u} (ν_2) is an out-of-plane deformation.

Typical spectra that were obtained are shown in Figures (4.2) and (4.3) which are, respectively the Raman and i.r. spectra of $(\text{CH}_3\text{NH}_3)_2\text{CuCl}_4$ recorded at 300, 195 and 77°K; also in Figure (4.4) are shown the Raman spectra for $(\text{C}_2\text{H}_5\text{NH}_3)_2\text{CuCl}_4$. In Tables (4.4) - (4.11) are given the observed Raman frequencies and polarization data for the copper complexes recorded at various temperatures. Table (4.12) gives the observed i.r. frequencies of $(\text{CH}_3\text{NH}_3)_2\text{CuCl}_4$ at 300, 195 and 77°K. The observed i.r. frequencies for the various manganese complexes recorded at the various temperatures are given in Tables (4.13) - (4.15).

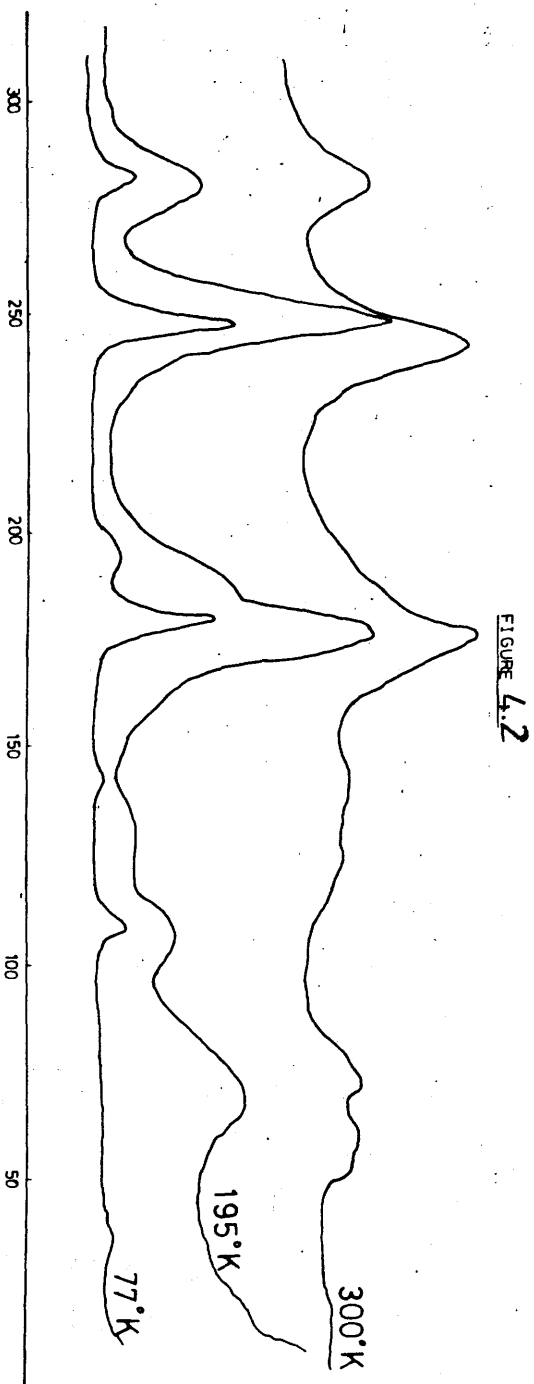


FIGURE 4.3

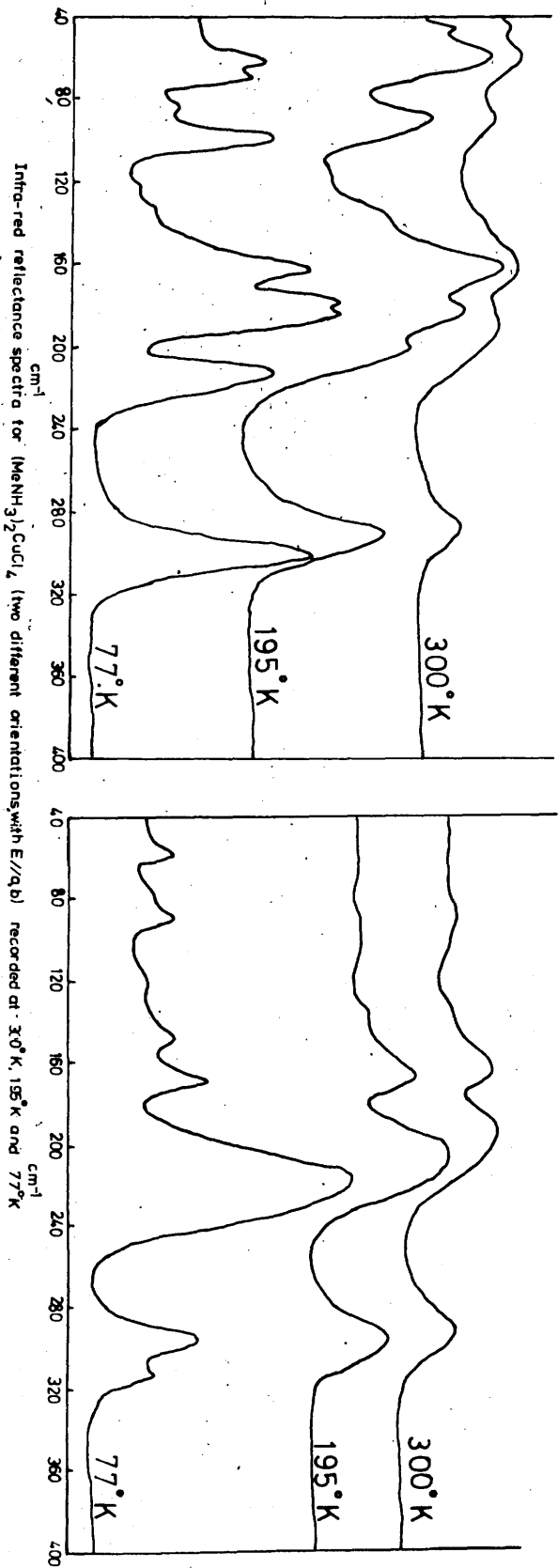
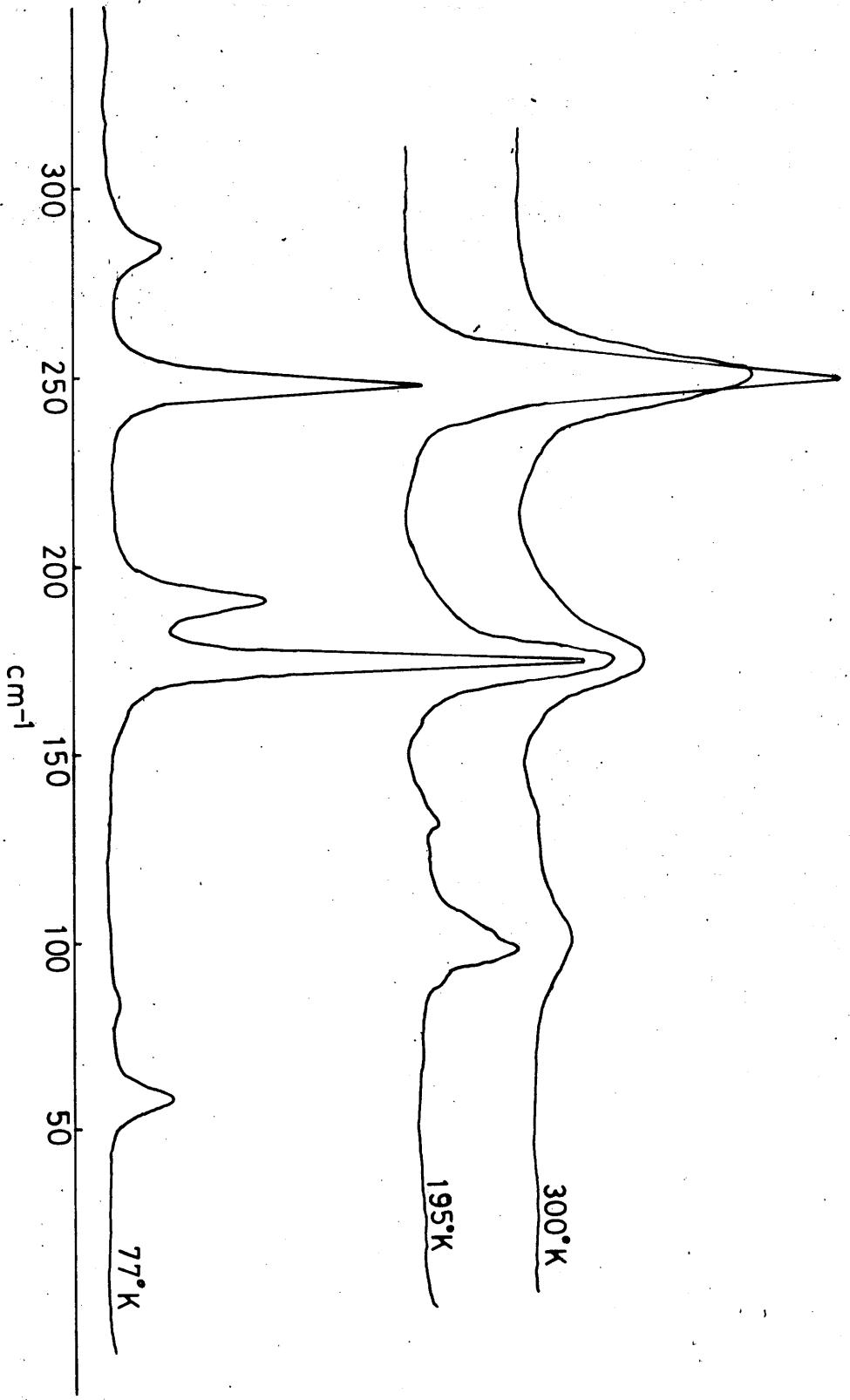


FIGURE 4.4



Raman spectra (zz tensor component) of $[\text{Et}(\text{NH}_2)_2]_2\text{CuCl}_4$
at 300°K, 195°K and 77°K

RESULTS

Table 4.4 Intensities of Raman Frequencies (RT) for $(MeNH_3)_2CuCl_4$

cm^{-1}	y(zz)x	y(zy)x	z(xx)y	z(xz)y	x(yy)z	x(yx)z		
281	32	33	22	103	30	103	(x^2, y^2, z^2)	(xy, xz, yz)
243	45	35	75	18	57	25	243	281
177	73	69	117	-	90	-	177	167
167				70	-	69	94	47
94					25		55	
55					128	23	49	
49					95			
47						15		

Table 4.5 Intensities of Raman frequencies (RT) for $(EtNH_3)_2CuCl_4$

cm^{-1}	y(xx)z	y(xy)z	x(zz)y	x(zx)y		
277	18	16	-	20	(x^2, y^2, z^2)	(xy, yz, xz)
249	41	26	20	-	249	277
173	105	50	50	25	173	173
58			65		58	56, 23
56				6		
23				10		

Table 4.6 Intensities of Raman Frequencies (RT) for $(n\text{-PrNH}_3)_2\text{CuCl}_4$

cm^{-1}	x(zz)y	x(zx)y	z(yy)x	z(yz)x		
278	4	9	-	4	(y^2, z^2)	(zx, yz)
247	8	4	71	10	247	278
189	-	-	-	9	172	189
172	20	20	53	19	89	172
89	-	-	31	-	55	41
55	32	-	-	-	47	25
47	15	-	-	-	41	
41	19	-	-	7	25	
25	-	-	13	9		

Table 4.7 Intensities of Raman Frequencies (195°K) for $(\text{MeNH}_3)_2\text{CuCl}_4$

cm^{-1}	z(yy)x	z(yz)x	y(xx)z	y(xy)z	x(zz)y	x(zx)y		
284	160	118	58	55	72	128	(x^2, y^2, z^2)	(xz, zy, xy)
246	153	88	132	46	98	51	246	284
198			54		32		198	188
192	59		56				192	168
188				49	46	38	179	152
179	165	134	190	79	155	74	168	70
168	80sh	80sh		50	82	73	156	64
156					48		152	60
152	27					17	124	
124	13						74	
74			14				70	
70		28			99		64	
64				9	80		60	
60	24	23						

Table 4.8 Intensities of Raman Frequencies (195°K) for $(EtNH_3)_2CuCl_4$

cm^{-1}	x(zz)y	x(zx)y	z(yy)x	z(yz)x	y(xx)z	y(xy)z		
279	10	20	-	2	26	83	$(x^2, y^2, z^2)(xy, xz, yz)$	
248	20	-	177	10	71	14	248	279
190			19				190	185
185				16			177	169
177	35	-	81	15	125	50	136	
169		14					125	
136			13				108	
125			8				67	
105			38				53	
67					10			
53			4					

Table 4.9 Intensities of Raman Frequencies (77°K) for $(MeNH_3)_2CuCl_4$

cm^{-1}	x(zz)y	x(zx)y	z(yy)x	z(yz)x	y(xx)z	y(xy)z				
285	51	72			9	24	$(x^2, y^2, z^2)(zx, yz, xy)$			
281			14	15			248	285	281	285
248	75	21	44	21	24	6	211	197	197	
211	22	7			9		192		188	
197	8	6		9			180	168	168	168
192			8				155		141	
188				8			106			
180	121	27	36	27	39	7	88			
168	32	31		5	10	11	75			
155	14	3			10					
141			5	4						
106	7		10	4						
88	13									
75	24				15					

Table 4.10 Intensities of Raman Frequencies (77°K) for $(C_3H_7NH_3)_2$

cm ⁻¹							<u>CuCl₄</u>			
	x(zz)y	x(zx)y	y(xx)z	y(xy)z	z(yy)x	z(yz)y				
273	51	80	78	58	59	56	(x ² , y ² , z ²)(zx, xy, yz)			
244	92	34	87	60	114	92	244	273	273	273
204			41	19	24		204		194	194
199	27		32				199			189
194				13		23	173			170
189					28	25	170	167	167	
173			121	91			164	164	164	
170	130				148	111	76	56		
167		70		13			70			
164			73	64		73	50			
76			32	18						
70	12									
56				11						
50			18							

Table 4.1f Intensities of Raman Frequencies for $(EtNH_3)_4CoCl_4$ 77°K

cm^{-1}	$z(yy)x$	$z(yz)x$	$y(xx)z$	$y(xy)z$	$x(zz)y$	$x(zx)y$	(x^2, y^2, z^2)	(yz)	(xy)	(zy)
283	18	103	20	81	10	18				
249	99	10	73	14	126	27	249	283	283	283
196	50	8	40	8	18	16	196	188	188	188
188		19		16		11	180	176	176	
180	151	25	118	24	86	39	145	166	166	166
176		33		27			110	94		
166		29		23	6	7	97	66	-	66
145				2	15	7	84	45	45	-
110					136	6	73			
97	11		3				56			
94		5								
73	55	13	14	-	6	8				
66						6				
56	5				4					
45		10		3						

Table 4.12 Far I R. Frequencies (cm^{-1}) for $(MeNH_3)_2CuCl_4$

RT		195°K		77°K	
E//X	E//Y	E//X	E//Y	E//X	E//Y
288	288	292	292	312	301
194	188	208	202	295	213
164	164	166	184	216	184
90b	90		164	168	178
	60		90	148	163
			60	120	99
				90	69
				59	62

Table 4.13 Far I.R. Frequencies for $(\text{MeNH}_3)_2\text{MnCl}_4$ (cm^{-1})

RT		(77°K)	
E//X	E//Y	E//X	E//Y
240m	236m	240m	244m
170v.b.	160v.b.	174	228
150v.b.	112v.b.		180
110b			100b.

At RT, apart from the two frequencies at 240m^{-1} and 236b cm^{-1} , from 200 cm^{-1} downwards the peaks are very broad.

Table 4.14 Far I.R. Frequencies for $(\text{EtNH}_3)_2\text{MnCl}_4$ (cm^{-1})

RT		77°K	
E//X	E//Y	E//X	E//Y
224	220v.b.	232	230
162	152 v.b.	178sh	192sh
100		172	180sh
74		140sh	164
		112	148
		100	112
		74	

Table 4.15 Far I.R. Frequencies for $(\text{C}_3\text{H}_7\text{NH}_3)_2\text{MnCl}_4$ (cm^{-1})

RT		(77°K)
E//X	E//Y	E//Y
No resolvable		236sh
peaks - very broad		214
band from 240 -		184
170 cm^{-1} , Lattice		198
region - very		126
broad - peak at		104sh
84 cm^{-1}		94

INTERPRETATION OF THE SPECTRA

a. Internal modes of the MCl_4 groups - the room temperature Raman spectra of all the three copper complexes are very similar, the main features being two distinct peaks in both the diagonal and off-diagonal tensor component spectra. These spectra are not characteristic of square planar MX_4 because of the 2-D sheets of linked CuCl_4^{2-} anions with an effective octahedral co-ordination for the copper atom. It is not easy to decide when a complex is truly square planar as opposed to a strongly tetragonally distorted octahedron. However, the tendency to achieve six-fold co-ordination around the metal atom is even more pronounced for square planar Cu(II) d^9 . In this case the influence of an asymmetrical d-electron arrangement can lead to severe distortion of the octahedron.

Earlier work (22) on $(\text{CH}_3\text{NH}_3)_2\text{CuCl}_4$ described the various vibrational modes in terms of a 'sheet' having D_{4h} symmetry. Accordingly the peaks at 243 cm^{-1} and 177 cm^{-1} in the room temperature spectrum of this complex were tentatively assigned to the terminal and bridging Cu-Cl stretching modes respectively; peaks at 281 cm^{-1} and 167 cm^{-1} were assigned to the out-of-phase terminal and bridging Cu-Cl stretching modes respectively.

From the similarity of the spectra of the three copper complexes, it is apparent that they are isostructural so that similar assignments could be made for the ethyl and n-propyl copper complexes. Willet (23), however, describes the effective geometry of the CuCl_4^{2-} unit in the ethyl as an orthorhombically distorted octahedron, i.e. D_{2h} . Apart from an additional peak at 189 cm^{-1} for the n-propyl copper complex almost the same frequencies, i.e. 277 cm^{-1} , 249 cm^{-1} and 173 cm^{-1}

are found in both ethyl and n-propyl complexes. The number of peaks found at room temperature in the Raman spectra of the three copper complexes are more in keeping with the factor-group analysis prediction for the space group D_{4h}^{17} .

The Raman spectra at low temperature are complicated. At 195°K new peaks appear in the Raman spectra. In the spectra of the methyl complex the two peaks above 200 cm^{-1} observed in the room temperature spectra shift upwards by 3 cm^{-1} while the two found at 177 cm^{-1} and 167 cm^{-1} remain unchanged. The reverse of the methyl complex is the case of the ethyl complex. Here the peaks above 200 cm^{-1} do not shift while those at 173 cm^{-1} shift to a higher frequency by 4 cm^{-1} .

More new peaks appear in the spectra of the three copper complexes at 77°K and the following general features are observed. In the methyl complex the peaks at 284 cm^{-1} and 246 cm^{-1} found in the spectra at 195°K remain unaltered but two more peaks appear in the region above 200 cm^{-1} . The ethyl and n-propyl complexes, apart from producing new peaks, shift all the peaks observed at -78°C by an average of 4 cm^{-1} . Interestingly, at -196°C, the highest frequency peak, which in the spectra at other temperatures was the same in all the off-diagonal spectra, appear at 285 cm^{-1} in the $x(zx)y$ and $z(y_z)x$ orientations while in the $y(xy)z$ orientation it is at 281 cm^{-1} . Such a feature is not observed in the other complexes.

For the copper complexes, the far i r. reflectance spectra could be recorded only for the methyl analogue. At room temperature, the spectra of the two orientations are identical

and apart from a distinct peak at 288 cm^{-1} , the remaining spectral features are rather broad. On recording the spectra at 195°K new peaks appear and the two orientations begin to differ since there are more peaks in one than in the other. However, the peaks are rather broad. They however become very sharp in the spectra at 77°K and the two spectra are very different. There are too many new peaks in the spectra, in addition to the lack of effective polarization, to enable unambiguous assignments to be made. Willet (23), however, reports that the planar CuCl_4^{2-} of D_{2h} symmetry in $(\text{C}_2\text{H}_5\text{NH}_3)_2\text{CuCl}_4$ shows a peak at 278 cm^{-1} with a shoulder at 294 cm^{-1} , corresponding to the B_{2u} and B_{3u} band in D_{2h} , and a weaker absorption at 182 cm^{-1} corresponding to the out-of-plane B_{1u} bend. The B_{2u} and B_{3u} modes arise from the splitting of the E_u mode in a D_{4h} geometry while the A_{2u} mode in D_{4h} becomes B_{1u} in D_{2h} geometry.

The far i.r. spectra of the manganese complexes show very broad peaks at RT. Here also the two orientations are similar. Earlier work (18) on the far i.r. reflectance spectra of the $(\text{CH}_3\text{NH}_3)_2\text{MnCl}_4$ complex explain the broad features observed in the spectra as a consequence of the increased number of long wave-length modes due to the doubling of the unit cell as the high temperature tetragonal phase is "frozen" to the room temperature ordered orthorhombic phase. Twinning makes polarization effects useless. The peaks are better resolved in the low temperature spectra and more new peaks are observed which is not surprising since it is reported (18) that there are further structural phase changes at low temperatures. No attempt has been made to assign the peaks owing to the complexity of the spectra.

LATTICE REGION

In both the Raman and i.r. spectra of the complexes, the main feature of the lattice region is the evidence of orientational disorder at room temperature. There are practically no defined peaks at room temperature. Distinct sharp peaks are observed only at low temperatures. The lattice region is composed of translatory and rotatory modes.

In these $(\text{RNH}_3)_2\text{MCl}_4$ complexes, together with the $(\text{R}_4\text{N})_2\text{MCl}_4$ and $(\text{DMA})_3\text{CuCl}_5$ complexes previously discussed, polarization differences at 300°K are almost non-existent reflecting the orientational disorder that is present. However, at certain temperatures below 300°K and provided no first order phase transition occurs, the atoms in these complexes should, theoretically, be located on those positions consistent with the space group inferred from room temperature X-ray studies. If this is the case, then the vibrational data obtained should be comparable to that for Cs_2MCl_4 complexes where spectral features are sharp and polarization leakage between different scattering geometries is almost negligible. However, in these $(\text{RNH}_3)_2\text{MCl}_4$ complexes, this is in no way the case; even at 77°K, when the systems should be almost 100% ordered polarization leakage is extensive making anything other than tentative vibrational assignments extremely difficult. In view of this anomaly it is worthwhile commenting upon the possible causal effects.

(a) Misalignment of the Crystal axes: This, the most common cause of polarization leakage, seems unlikely in view of our previous experience and the fact that almost identical results were obtained on frequent re-recording of the spectra. Crystal twinning has not been reported and not observed under the polarizing microscope.

- (b) Lack of ordering at 77°K: The thermal parameters listed for the alkylammonium ions are small so that orientational disorder of these ions at 77°K should be negligible.
- (c) Phase transitions: From n.m.r. studies two minor transitions occur below 300°K corresponding to hindered rotation of the methyl groups and the onset of -N-H...Cl hydrogen bonding. While these transitions may not cause structural phase changes, they could be responsible for the poor polarization data obtained for these complexes. If the final positions of the hydrogen bonds and the relative conformations of the methyl groups are not periodic, that is there is a degree of 'randomness', then this will impart a heterogeneity to these complexes which may be sufficient to cause scrambling of the incident polarized radiation.

This explanation of the extensive polarization leakage observed in these $(RNH_3)_2MCl_4$ and the other complexes previously mentioned must be regarded as being speculative. It is obvious that further structural studies are necessary. In particular, temperature dependent X-ray determinations would establish whether first order phase transitions occur and neutron diffraction studies would reveal the exact positions of the hydrogen bonds.

4.2 Thermochromism in the Copper Complexes

Thermochromic behaviour has been observed in some of the copper complexes studied, both in those containing distorted tetrahedra CuCl_4^{2-} and those containing square planar CuCl_4^{2-} .

Thermochromism may be defined as the reversible change in colour of a compound when it is heated (24). The colour change in inorganic solid complexes is usually very noticeable and sometimes occurs over a narrow temperature range. The transition may be due to a structural phase change in ligand geometry or a change in the number of molecules of solvent in the co-ordination sphere (24).

Of the complexes containing distorted tetrahedral CuCl_4^{2-} anions, tetramethylammonium and tetraethylammonium tetrachlorocuprates(II) are thermochromic changing colour from yellow at room temperature to green on cooling. Another complex containing distorted tetrahedral CuCl_4^{2-} which is also thermochromic is $(\text{DMA})_3\text{CuCl}_5$.

All the square planar CuCl_4^{2-} complexes studied, i.e. $(\text{C}_n\text{H}_{2n+1}\text{NH}_3)_2\text{CuCl}_4$ are thermochromic in the solid state, turning from yellow at RT to green at low temperatures. Extensive studies have been carried out on these systems by Willet who reports that the transition temperature is near -40°C for $(\text{MeNH}_3)_2\text{CuCl}_4$ and $(\text{EtNH}_3)_2\text{CuCl}_4$. (19)

Two types of thermochromic behaviour are reported (23). In one class are those in which there is phase transition which involves a change in the co-ordination geometry around the copper ion. The driving force for the changes being

the changes in the N-H...Cl hydrogen bonding scheme caused by the thermal motion of the organic cation. In the other class there is no phase change but the thermochromism is associated only with the temperature dependence of the line widths of the electronic absorption bands which might be due to vibronic coupling.

According to Willet (23) when there is no possibility of hydrogen bonding between the cation and the CuCl_4^{2-} anion, the trans Cl-Cu-Cl angle is always less than 132° and becomes larger as the extent of the bonding increases. In the $(\text{RNH}_3)_2\text{CuCl}_4$ complexes where Cu(II) assumes the (4+2) co-ordination the trans Cl-Cu-Cl angle is very large. See Table 4.15 below.

Table 4.15 Trans Cl-Cu-Cl angles in CuCl_4^{2-} (23)

Compound	trans Cl-Cu-Cl $^\circ$ A
Cs_2CuCl_4	124
$[(\text{CH}_3)_4\text{N}]_2\text{CuCl}_4$	128
$[(\text{CH}_3)_2\text{NH}_2]_3\text{CuCl}_5$ [(DMA) $_3\text{CuCl}_5$]	136

From the above it is evident that there is hydrogen bonding in the DMA complex and hence this may cause phase changes to occur. However, to date, no standard changes have been reported. There is evidence to support the claim that the thermochromism in the complex $[(\text{C}_2\text{H}_5)_2\text{NH}_2]_2\text{CuCl}_4$

involves a phase change (23).

The thermochromism in the complexes containing square planar CuCl_4^{2-} is thought (19) to result from a change in the co-ordination geometry of the copper ion, changing from D_{4h} to C_{4v} , but only slight changes are observed in the electronic spectra.

References

1. Foster and Gill, J. Chem. Soc. A., 2625 (1968)
2. Payen de la Garanderie, H. Ann. Phys., 9, 649 (1964)
3. Mostafa and Willet, Phys. Rev., B47, 2213 (1971)
4. Van Amstel and de Jongh, Solid State Comm., 11, 1423 (1972)
5. de Jongh, Physica, 58, 305 (1972)
6. Peterson and Willet, J. Chem. Phys., 56, 1879 (1972)
7. Steadman and Willet, Inorg. Chim. Acta, 4, 367 (1970)
8. Schenk, Physica, 49, 465 (1970)
9. Willet, J. Chem. Phys., 41, (8) 2243 (1964)
10. Willet, J. Chem. Phys., 56, 1879 (1972)
11. J. Koppen and Miedema, Phys. Letts., 25A, 376 (1967)
12. K. Knox, J. Chem. Phys., 30, 991 (1959)
13. D. Balz, Naturwissenschaften, 40, 241 (1953)
14. Heger G. et alia, Solid State Comm., 12, 1157 (1973)
15. Knorr, K. et alia, Solid State Comm., 15, 231 (1974)
16. Arend H. et alia, Ferroelectrics, 8 41 (1974), Solid State Comm., 13, 1629 (1973)
17. Landau and Lifshits, Statisfische Physic, pg. 472 (1966)
18. J. Petzett, J. Phys. Chem. Sol., 1975, 36, 1005
19. Willet et alia., Inorg. Chem., 6, 1885 (1967)
20. Adamas and Lock, J. Chem. Soc. A, 1967, 620.
21. Willet, Inorg. Chem., 13(12) 2919 (1974)
22. Beattie et alia., J. Chem. Soc. (A), 534 (1969)
23. Willet, Inorg. Chem., 13(10), 2510 (1974)
24. J.E. Day, Chem. Rev., 68, 649 (1968)

CHAPTER 5 - PEROVSKITE-TYPE NaMF_3 COMPLEXES

CHAPTER 5

NaMF₃ Complexes (M = Mn, Co, Ni, Zn)

The structure of complex halides having the general formula $A_x M_y X_{3x}$, in which the ratio of the halogen to the alkali metal is always 3:1, consists of a close-packed array of A and X atoms provided they are of approximately equal size. One of the largest groups of the AMX₃ complexes is the cubic perovskite-type compounds whose atomic arrangement was first found for the mineral perovskite, CaTiO₃, which is pseudocubic. The real symmetry of CaTiO₃ was later found to be orthorhombic with four molecules in the unit cell and space group D_{2h}^{16} (Pbnm). (1-3).

In the cubic AMF₃ complexes, the A ions are 12-co-ordinated; there are six F atoms in the same plane and two sets of three F atoms above and below all at equal A-F distances of $a/\sqrt{2}$ where a is the cubic unit cell dimension. The M ions at the corners of the unit cell occupy the octahedral holes with M-F distances of $a/2$. All MF₆-octahedron share corners and form a three-dimensional linear framework; it is found that the Bravais cell constitutes the cubic unit cell itself. Thus the A cation is normally found to be somewhat larger than the M cation. They are indeed, restricted to di-valent cations, M²⁺, and are stable almost exclusively to the first transition series only.

In order that the ions A, M and F have contact the following equation should hold

$$R_A + R_F = \sqrt{2} (R_M + R_F) \quad (5.1)$$

where R_A , R_M and R_F are the ionic radii. Goldschmidt (4) has

shown that the cubic perovskites are stable only if a tolerance factor, t , defined as

$$t = \frac{R_A + R_F}{\sqrt{2(R_M + R_F)}} \quad (5.2)$$

has an approximate value in the range 0.88 to 1.00.

If the tolerance factor becomes smaller an orthorhombic version of the perovskite lattice is formed, while larger tolerance factors than unity lead to various kinds of hexagonal perovskites.

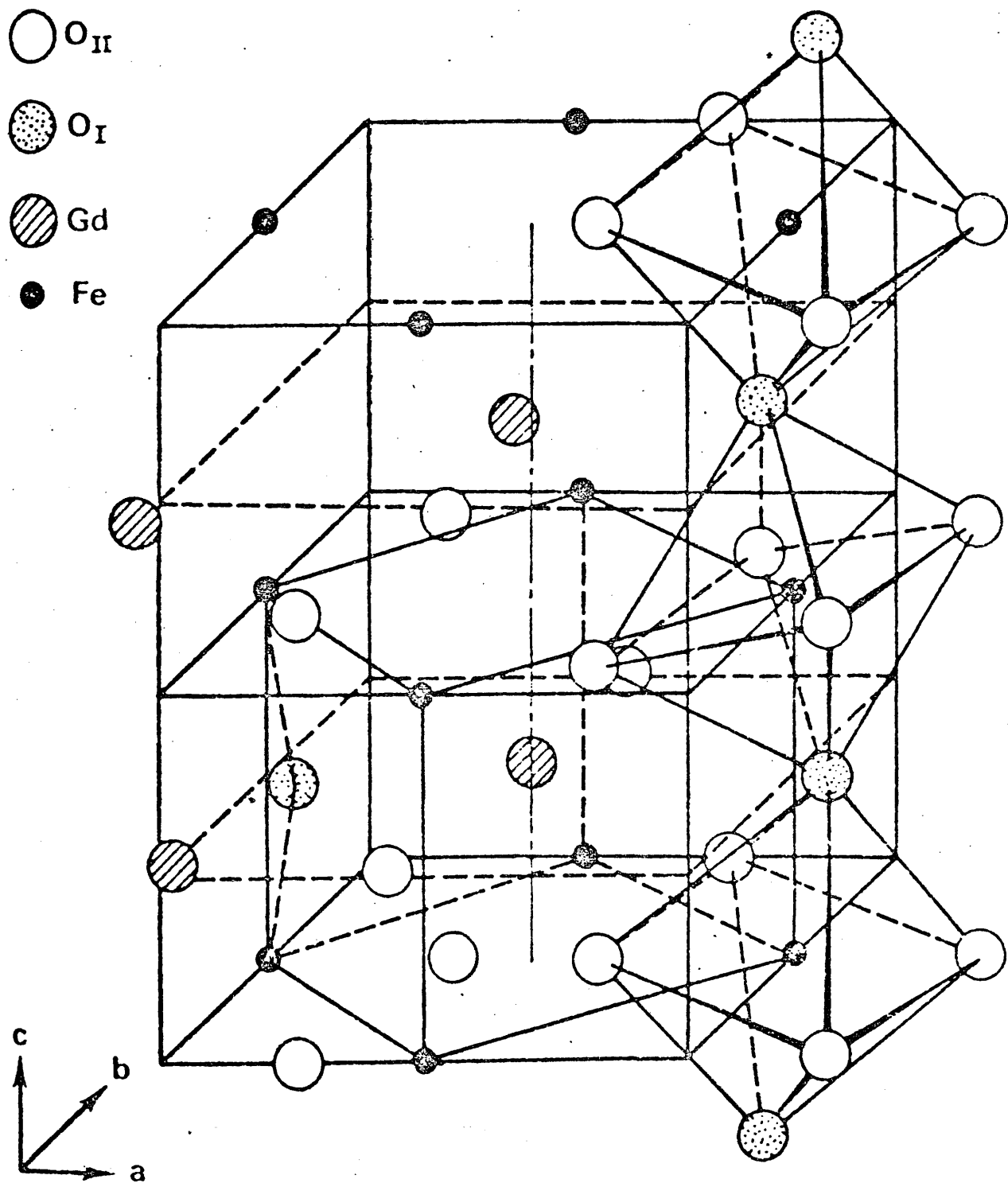
At room temperature, the strictly cubic structure is adopted by complexes such as KMF_3 where $M = Mn, Fe, Co, Ni, Zn$ and Mg (5), $RbMF_3$ where $M = Mn, Co$ and Zn and NH_4MF_3 with $M = Mn, Co, Ni$ and Mg . (6-8) In all these the cubic close-packed layers of AF_3 are formed provided the M^{2+} ions are not so small as to contract the octahedral framework too much. Very few perovskite-type oxides have the simple cubic structure at room temperature though many assume this structure at higher temperatures. Since the perovskite structure is a very tightly packed one, it is considered to be a favourable structure at high pressures and many perovskite-type oxides which are not stable at atmospheric pressure have been stabilised with the perovskite structure at high pressures (9,10).

It has been reported that the room temperature cubic perovskite structure of $KMnF_3$ transforms at $184^\circ K$ to an orthorhombic phase with a unit cell containing four formula units in the space group D_{2h}^{16} (Pbnm) (11). This is isostructural with the ternary oxide $GdFeO_3$ reported by Geller (12). There is a tetragonal pseudo cell with $c/a > 1$ in which the MF_6 octahedra remain essentially regular except

that they are tilted and twisted relative to the crystal axes. Figure 5.1 shows the GdFeO_3 structure. The structural phase change in KMnF_3 is caused by the decrease in unit cell size with temperature and there is a similar decrease in unit cell size when the potassium ions in KMF_3 complexes are replaced by the smaller sodium ions ($R_{\text{Na}^+} = 0.98 \text{ \AA}$; $R_{\text{K}^+} = 1.36 \text{ \AA}$). Not surprisingly Rudorff (8) has reported that the sodium fluoro complexes NaMF_3 ($M = \text{Mn, Co, Ni, Zn}$) have the GdFeO_3 type of structure and crystallize with four molecules in the unit cell with the centrosymmetric space group D_{2h}^{16} (Pbnm). However, essentially the same structure can also be described by the centrosymmetric space group C_{2v}^9 ($\text{Pbn}2_1$). These two space groups have the same crystallographic extinctions and detailed structure study is required to distinguish between the two possibilities. The tolerance factor for the GdFeO_3 type of structure falls in the range 0.78 to 0.88 and the tolerance factors for the NaMF_3 complexes do fall in this range, i.e. NaMnF_3 (0.78), NaCoF_3 (0.81), NaNiF_3 (0.83) and NaZnF_3 (0.82). Fluoroperovskites with tolerance factors less than 0.78 have not been observed. The distortion of the MF_6 octahedra in the NaMF_6 series is such that the three-dimensional linking of the octahedra is not linear but exhibit angles of about 150° at the fluorine atoms.

In the literature there are conflicting reports concerning the structures of the NaMF_3 series. Most distorted perovskites retain a strong pseudocubic character and this frequently makes it difficult to determine the true unit cell and the

Figure 5.1

— Structure of $GdFeO_3$.

symmetry of perovskite-type phases. NaNiF_3 and NaZnF_3 have been reported to be tetragonal (13) while NaCoF_3 and NaZnF_3 are reported by others not even to be of perovskite-type (14). Two different groups of workers have recently re-examined the crystal structures of NaNiF_3 and NaCoF_3 (15, 16, 17). Okazaki and co-workers (15,16) found NaNiF_3 and NaCoF_3 to belong to the space group D_2^4 ($P2_12_12_1$). The space group has been found for CaSnO_3 (18) from its single crystal study but a detailed structure determination is lacking. The more recent study by Carter (17) did not confirm the D_2^4 space group assignment but supported the space group of D_{2h}^{16} reported earlier by Rudorff (8). The Renniger effect or multiple Bragg scattering is suggested by Carter to be a possible explanation and this occurs when the Bragg condition is simultaneously satisfied for two or more reflections (18). It has also been shown recently that polysynthetic twinning can be responsible for additional weak reflections, which could lead to an erroneous space group assignment of D_2^4 ($P2_12_12_1$) (19). Further study on CaSnO_3 , NaCoF_3 and NaNiF_3 is therefore necessary. NaZnF_3 and NaMgF_3 undergo structural phase changes above room temperature (20,21) which almost precludes obtaining single crystals of these materials.

Up to the present the vibrational spectra of the distorted perovskite fluorides have been little studied. The infra-red absorption and reflectance spectra of the cubic perovskite fluorides have received extensive attention (22-27). The work done on the sodium perovskite fluorides include the infra-red spectra of NaCoF_3 (28), that of NaNiF_3 and NaCoF_3 (29,30) and that of NaMnF_3 , NaCoF_3 , NaNiF_3 , NaMgF_3 and NaZnF_3 (27).

The aim of the present studies was to employ both the Raman and infra-red reflectance spectra of single crystals to distinguish unambiguously between the two space groups reported. The reflectance spectra would be analysed by K-K relationship and classical analysis to obtain the true oscillator frequencies. The two space groups differ in the sense that D_{2h}^{16} is centrosymmetric and hence the rule of mutual exclusion would apply. The other space group D_2^4 is non-centrosymmetric which would be confirmed by the observation of the longitudinal optic and transverse optic modes (LO-TO splitting).

RESULTS AND DISCUSSION

Two different space groups have been suggested (17,15,16) for these sodium perovskites which have orthorhombic tetramolecular unit cells.

The factor group analysis for the centrosymmetric space group D_{2h}^{16} is given in Table 5.1. From this analysis the i.r. active modes of vibration are given by the representation (5.1) and therefore twenty-five bands should be observed in the infra-red spectrum:

$$\Gamma_{i,r.} = 7B_{1u} + 9B_{2u} + 9B_{2u} \quad (5.1)$$

The Raman-active modes are given by representation (5.2) and hence twenty-four bands are expected in the spectrum:

$$\Gamma_{Raman} = 7A_g + 7B_{1g} + 5B_{2g} + 5B_{3g} \quad (5.2)$$

The other suggested space group is the non-centrosymmetric D_2^4 - $P2_12_12_1$ and will give rise to fifty-two vibrations in the i.r. spectrum (27); the number and symmetry species of which are given by the representation (5.3):

$$\Gamma_{i,r.} = 16B_1 + 18B_2 + 18B_3 \quad (5.3)$$

In the Raman spectrum fifty-seven bands are predicted (27) and the number and symmetry species of the Raman-active modes are given by representation (5.4):

$$\Gamma_{\text{Raman}} = 5A + 16B_1 + 18B_2 + 18B_3 \quad (5.4)$$

The infra-red reflectance spectra were recorded for all the complexes NaMF_3 where $M = \text{Mn, Co, Ni}$ and Zn at both room temperature and liquid nitrogen temperature. For the manganese and cobalt complexes it was possible to identify all the three axes under the polarising microscope and thus enable recording of the spectra of the three different orientations with the electric vector parallel to each of the axes a, b and c , in turn. Only one of such orientations could be recorded in the case of the zinc and nickel complexes. This was due to the difficulty in identifying the other axes and thus the spectra obtained contained a mixture of the two orientations:

From the spectra recorded for all the complexes there was one orientation whose spectra was very similar in all the complexes as shown in Figure 5.2. Thus it can be assumed that they are all isostructural.

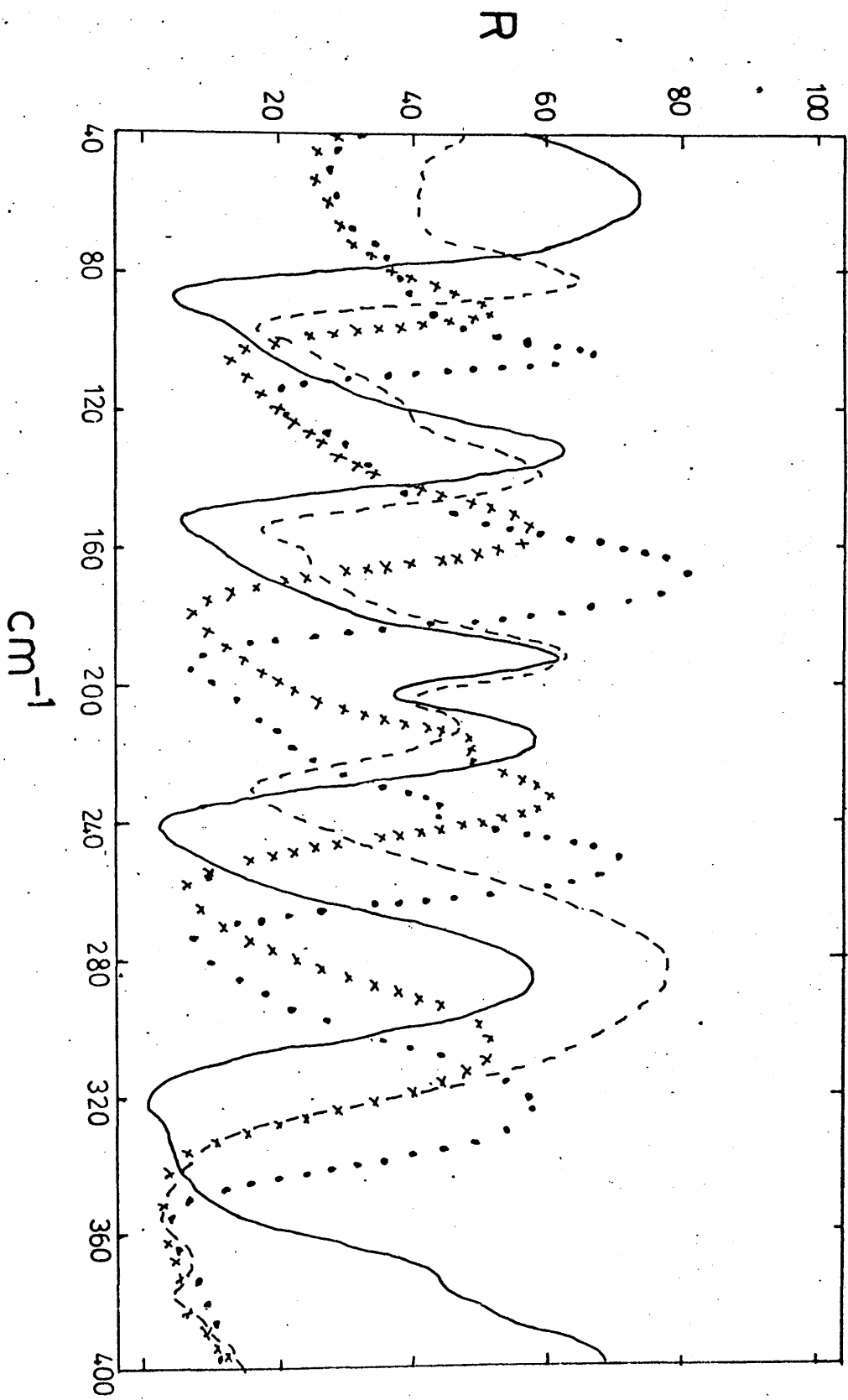
The crystals of NaMnF_3 had one face large enough to enable the room temperature reflectance spectra in two different orientations to be recorded above 400 cm^{-1} on the Perkin-Elmer 577 spectrophotometer which is fitted with a polariser. The reflectivity data obtained at room temperature for the manganese complex and for the cobalt complex were subjected to the Kramers-Kronig analysis to obtain the true oscillator frequencies.

From the initial K-K analysis (29) a trial set of dispersion parameters, ν_j , $4\pi\rho_j$ and γ_j , the frequency,

strength and damping constant respectively for each of the j oscillators and together with the high frequency dielectric constant ϵ_{∞} were obtained and these were adjusted to produce the best fit to the experimental data. These are shown in Figures 5.3a and 5.4a for NaMnF_3 and for NaCoF_3 respectively. The plots of the variation with frequency of both the real ϵ' and imaginary ϵ'' parts of the dielectric constant are shown in Figures 5.3b and 5.3c for NaMnF_3 and Figures 5.4b and 5.4c for NaCoF_3 . It is noted in the plot of ϵ'' with frequency for both manganese and cobalt complexes that the bands at 208 cm^{-1} for the manganese and at 225 cm^{-1} for the cobalt which are at the high frequency side of strong oscillators are weak oscillators and cause inversions of the latter (32) in the reflectance spectra. In the reflectance spectra there are shoulders on the high frequency side of the bands at 402.94 cm^{-1} , 281.97 cm^{-1} and 373.19 cm^{-1} for NaMnF_3 and at 326.61 cm^{-1} for NaCoF_3 . These shoulders are not observed in the ϵ'' spectra in which the frequency and intensity of the calculated maxima reflect respectively the true frequency and strength of the oscillators. They must therefore be very weak oscillators. However the addition of these very weak oscillators to represent the shoulders in the reflectance spectra improved the classical fits to the reflectance spectra (33).

The final set of dispersion parameters for the various orientations of the cobalt and manganese complexes are given in Tables 5.2 and 5.3 respectively. In Table 5.4 are the observed infra-red frequencies, recorded at 77°K for NaNiF_3 and NaZnF_3 . These were not subjected to K-K analysis and the frequencies quoted were taken at the minimum of the main reflectance band (32). To enable comparison to be made with the Raman spectra, the i.r. frequencies recorded at 77°K and

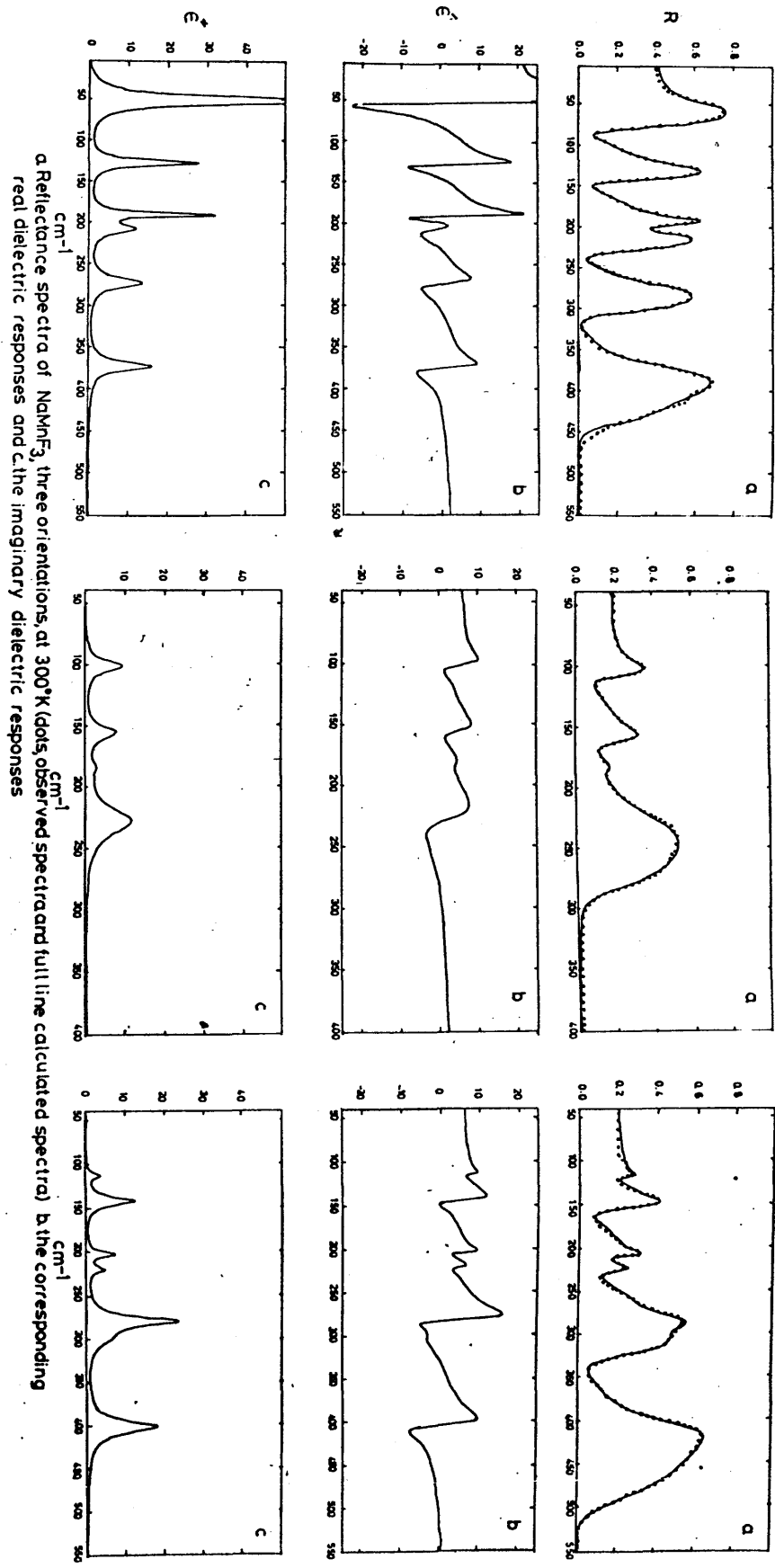
Figure 5.2



R

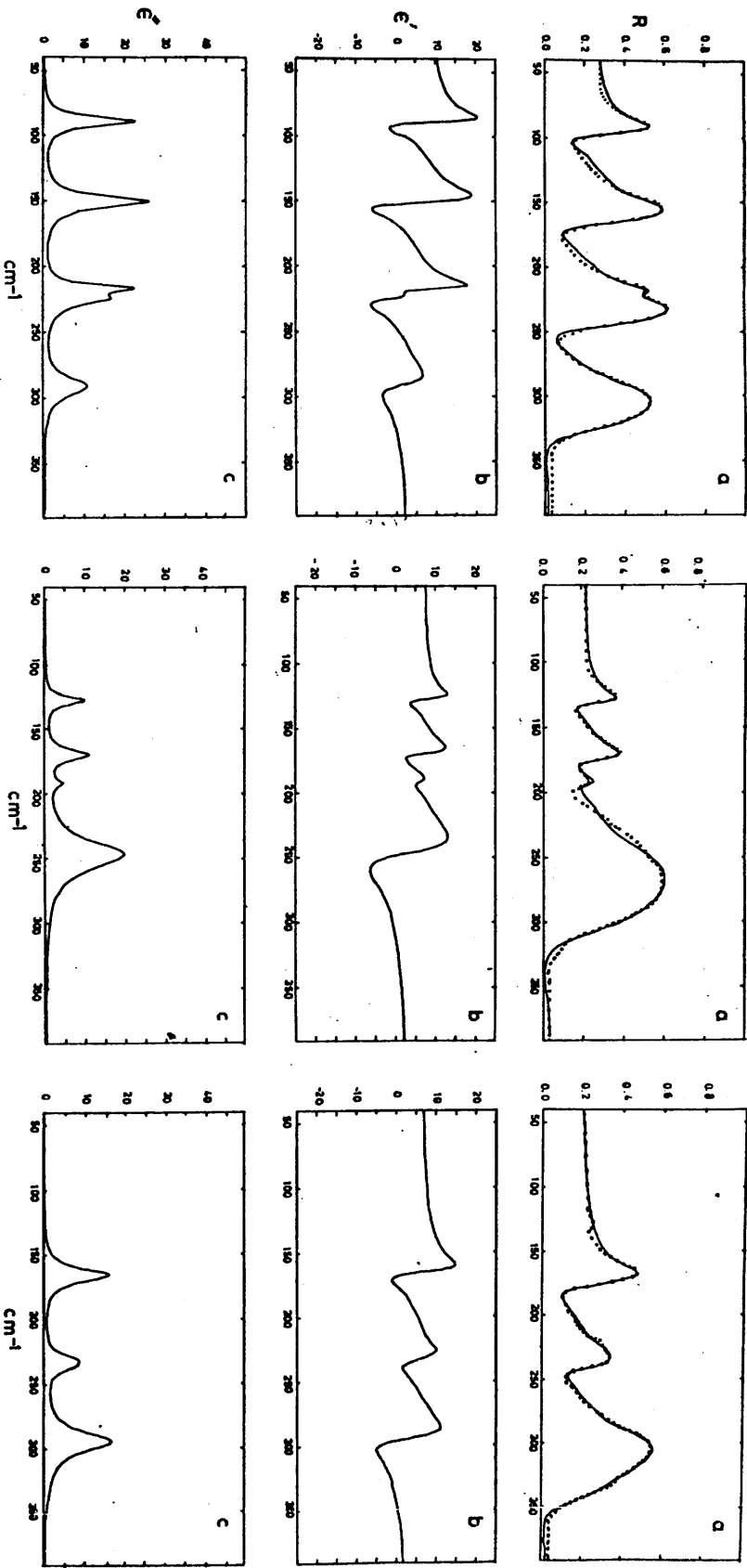
 cm^{-1} Infrared reflectance spectra of NaMnF_3 (—), NdZnF_3 (---), NaCoF_3 (***), and NdNiF_3 (....) [RT]

Figure 5.3



a) Reflectance spectra of NAMF₃, three orientations, at 300°K (dots observed spectra and full line calculated spectra) b) the corresponding real dielectric responses and c) the imaginary dielectric responses

Figure 5.4



a. Reflectance spectra of NaCoF_3 , three orientations, at 300K (dots, observed spectra and full line calculated spectra) b. the corresponding real dielectric responses and c. the imaginary dielectric responses.

Table 5.1

Factor Group Analysis for NaMF_3 with
Space Group D_{2h}^{16} - Pbnm ($z = 4$)

D_{2h}	n_i	T	T'	R	α	n_i'
A_g	7	0	2	0	3	5
B_{1g}	7	0	2	1	1	4
B_{2g}	5	0	1	1	1	3
B_{3g}	5	0	1	1	1	3
A_u	8	0	1	0	0	7
B_{1u}	8	1	1	0	0	6
B_{2u}	10	1	2	0	0	7
B_{3u}	10	1	2	0	0	7

Table 5.2

I R Frequencies, Strength, and Damping

Constants, Recorded at Room Temperature for NaCoF_3

$\nu(\text{cm}^{-1})$ Frequency	$4\pi_0$ Strength	$\gamma(\text{cm}^{-1})$ Damping	$\nu(\text{cm}^{-1})$ Frequency	$4\pi_0$ Strength	$\gamma(\text{cm}^{-1})$ Damping
89.88	2.1500	8.8355	127.32	0.5966	7.9070
151.70	1.3198	10.7833	169.06	0.6120	9.8942
217.64	0.4671	5.9335	191.21	0.1285	7.6787
225.68	0.7445	12.0045	246.49	2.0536	25.6614
291.92	0.6238	17.1563	$E_\infty = 3.785687$		

$\nu(\text{cm}^{-1})$	$4\pi_0$	$\gamma(\text{cm}^{-1})$
149.59	0.0197	12.9299
165.70	1.1868	12.1647
211.53	0.0081	11.5367
230.23	0.2459	10.1358
235.97	0.2331	10.7993
294.65	1.0754	19.0477
326.61	0.0827	37.1874

$$E_\infty = 3.908339$$

Table 5.3 I.R. Frequencies, Strength and Damping
 Constants Recorded at Room Temperature for
 NaMnF_3

ν (cm^{-1}) Frequency	$4\pi\rho$ Strength	γ (cm^{-1}) Damping	ν (cm^{-1}) Frequency	$4\pi\rho$ Strength	γ (cm^{-1}) Damping
52.19	13.7045	10.4711	102.18	0.9522	10.4942
128.28	1.7788	8.3395	155.88	0.5976	12.4316
190.97	0.9390	5.8071	184.47	0.1139	12.4259
208.36	0.6844	13.2373	228.60	1.3049	25.5243
273.54	0.6897	14.0295			
373.19	0.5351	12.4370			
415.45	0.0263	38.1128			

$$E_{\infty} = 2.708617$$

ν (cm^{-1})	$4\pi\rho$	γ (cm^{-1})
115.73	0.1745	5.8613
144.56	0.9751	11.3346
205.08	0.2289	6.6098
222.78	0.1518	7.8895
281.97	0.9451	12.3270
299.50	0.6151	27.3671
402.94	0.7369	16.8386
440.28	0.0994	79.4043

$$E_{\infty} = 2.693124$$

Table 5.4 Infra-red Frequencies (cm^{-1}) Recorded
at 77°K for NaNiF_3 and NaZnF_3

<u>NaNiF_3</u> <u>cm^{-1}</u>	<u>NaZnF_3</u> <u>cm^{-1}</u>
104	88
141	118
162	141
179	163
204	192
234	196
237	202
254	212
287	223
299	276
317	288
328	308
353	347
	382

Table 5.5 Infra-red Frequencies (cm^{-1}) Recorded at
 77°K for NaMnF_3

<u>cm^{-1}</u>	<u>cm^{-1}</u>	<u>cm^{-1}</u>
118	101	48
139	156	130
147	160	188
189	188	194
208	240	206
227	354	238
263		268
284		374

obtained from the K-K analysis for NaMnF_3 are given in Table 5.5. The frequencies for NaCoF_3 , recorded at 77°K are given in Table 5.6

From the number of bands obtained in the various complexes it seems reasonable to suggest that the space group is not $D_2^4 - P2_12_12_1$. Twenty-two bands are observed in the i.r. spectra of NaMnF_3 and twenty-five bands are predicted from the factor group analysis based on space group D_{2h}^{16} . The number observed is in closer agreement with the space group D_{2h}^{16} . The bands observed in the different orientations have not been assigned to their symmetry species. The difference between the room temperature spectra and that at 77°K was that the bands in the latter spectra were better resolved. Some of the bands were broad and asymmetric and this might consist of a number of bands having similar frequencies. This and the fact that some of the bands may lie above 400 cm^{-1} might explain the missing bands from the predicted number. It is of interest to note the rather unusual spectral features observed for NaZnF_3 . This complex has been reported (20) to undergo a phase transition from a tetragonal to an orthorhombic structure at 956°K. As a result, attempts to grow this complex from the melt give rise to a polycrystalline boule. An alternative method of flux growth according to the equation $2\text{NaCl} + 3\text{ZnF}_3 = 2\text{NaZnF}_3 + \text{ZnCl}_2$, was attempted and small crystals of poor optical quality were obtained. However, these were too small for infra-red reflectance work. Surprisingly the boule contained a cleavage plane, a certain direction in which when aligned with the electric vector gave rise to the infra-red

Table 5.6 Infra-red Frequencies (cm^{-1}) Recorded at
77°K for NaCoF_3

<u>cm^{-1}</u>	<u>cm^{-1}</u>	<u>cm^{-1}</u>
138	130	90
168	172	150
206	200	204
228	264	218
240		288
304		

reflectance spectrum shown in Figure 5.2. Spectra recorded at right angles to this plane were clearly mixtures of the other two orientations. These spectral features were also found in other boules of NaZnF_3 and must, therefore in some way reflect the mechanism by which the phase transition occurs. It is possible that the orthorhombic structure is formed by random torsional and twisting motions about a fixed direction in the tetragonal crystal.

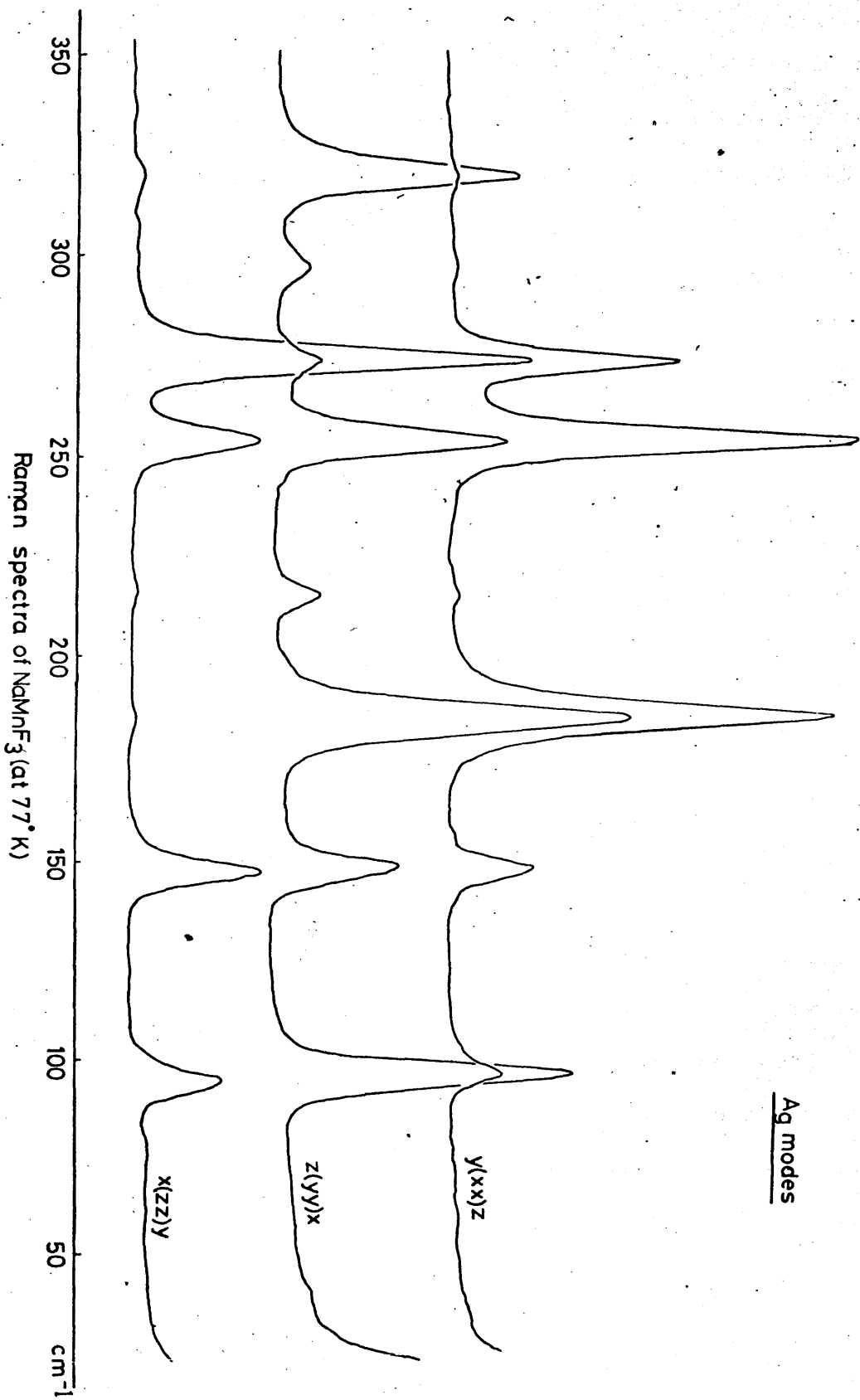
The Raman spectra could be recorded for only the manganese complex. The very deep red colouration of the cobalt complex made it impossible to record its Raman spectrum. The difficulty in locating the position of the axes in the zinc and nickel complexes contributed to the unsuccessful attempts to obtain their Raman spectra.

The frequencies (cm^{-1}) recorded at 77°K for NaMnF_3 , polarization intensity data together with the symmetry assignment based on space group D_{2h}^{16} are given in Table 5.7. The spectra obtained for the diagonal tensor components, recorded at 77°K are shown in Figure 5.5. Seven bands are observed in the diagonal tensor component spectra. This number is more than that predicted for the space group D_2^4 but is in good agreement with the factor group predictions based on D_{2h}^{16} . Though fewer bands are observed in the off-diagonal tensor components spectra, the number observed are far fewer than that predicted for D_2^4 but closer to that predicted for D_{2h}^{16} . In all sixteen bands are observed in the Raman spectra of NaMnF_3 recorded at 77°K . In the space group D_{2h}^{16} a total of twenty-four is predicted while in the D_2^4 space group a larger number of fifty-seven is predicted. Thus the number of bands observed does not support an orthorhombic structure based on

Table 5.7 Raman Frequencies (cm^{-1}), Recorded at 77°K ,
Polarization Intensity Data and Symmetry
Assignment Based on Space Group D_{2h}^{16} of NaMnF_3

Frequency cm^{-1}	Scattering Geometry						Assignment
	$y(xx)z$	$y(xy)z$	$x(zz)y$	$x(zx)y$	$z(yy)x$	$z(yz)x$	
321	4	0	6	0	102	0	A_g
313	0	0	0	0	0	8	B_{3g}
306	0	0	0	8	0	0	B_{2g}
298	0	121	16	7	0	0	$B_{1g} + B_{2g}$
275	94	0	163	0	21	0	A_g
254	166	0	52	0	96	0	A_g
231	0	4	0	0	0	0	B_{1g}
216	6	0	3	0	20	0	A_g
205	0	12	0	0	0	0	B_{1g}
186	157	10	2	0	147	0	A_g
164	0	0	0	0	0	47	B_{3g}
157	0	4	0	0	0	0	B_{1g}
148	35	0	53	0	53	0	A_g
145	0	29	0	0	0	0	B_{1g}
102	0	0	0	17	0	0	B_{2g}
95	21	0	38	0	123	0	

FIGURE 55



the space-group D_2^4 .

Since the space group D_{2h}^{16} is centrosymmetric, the rule of mutual exclusion should apply so that there should be no coincidences between the infra-red and Raman frequencies. Comparison of the frequencies from the low temperature i.r. spectra with those of the low temperature Raman spectra of NaMnF_3 reveal no appreciable coincidences. There are only three bands in the Raman spectrum which have frequencies almost coincident with three frequencies in the i.r. spectrum. They differ by only 1 cm^{-1} each. This near coincidence could be explained by the fact that the resolution in the Raman spectra was 4 cm^{-1} . It is therefore a fair conclusion that there are no coincidences and hence the centrosymmetric space group D_{2h}^{16} is confirmed for the sodium perovskite complexes.

In the non-centrosymmetric space group D_2^4 the observation of the longitudinal optic-transverse optic splitting should be observed. Attempts to observe this LO-TO splitting were unsuccessful.

The assignment of the Raman bands to the symmetry species of space group D_{2h}^{16} is quite straightforward. This was aided by the fact that polarization effects were perfect. The only difficulty arose with the band at 298 cm^{-1} which in addition to its being of B_{1g} symmetry species was also assigned to B_{3g} species although there was some leakage in the diagonal zz components.

From both the Raman and i.r. results of NaMnF_3 it is evident that the spectra are more complicated than that of KMnF_3 at low temperature with which it is isostructural. In the infrared transmission spectrum of KMnF_3 at 77°K (34) only four bands were observed which indicated that the triply

degenerate modes in the cubic system were not split. Many more bands are observed in the i.r. spectra of the sodium perovskite fluorides. The difference in the spectra of KMnF_3 and those of the sodium perovskite fluorides might be due to the fact that in the KMnF_3 complex the MnF_6 octahedra are not distorted while, for example in the NaNiF_3 complex the Ni-F-Ni band is not linear but bent conspicuously (8). The NaNiF_3 does not form a regular perovskite but shows a deformed structure resulting in a complication of the spectra. It is therefore difficult to describe the various vibrational modes since they will be mixtures of bending and stretching.

The features in the lattice region which generally is the region below 120 cm^{-1} , make it hard to break up the spectra into 'internal' and 'external' vibrations. It is better considered as phonon spectra.

EXPERIMENTAL

All the sodium perovskite fluorides were prepared from the melt. Stoichiometric amounts of 'Optran' grade alkali fluoride and the transition metal difluoride were dried and put into a carbon crucible which had been cleaned with aqua regia and dried 'in vacuo'. The carbon crucible containing the mixture was put into a platinum tube which was then sealed at both ends before going into the furnace.

The crystals obtained were cut along the axes and polished on the Logitech polishing machine using solder laps and a series of diamond paste abrasive down to 1μ mesh.

The 488.0 nm line of the Ar^+ laser was used as the exciting line for recording the Raman spectra of NaNiF_3 .

References

1. H.D. Megaw, Proc. Phys. Soc., 58, 133, 326 (1946)
2. H.F. Kay and P.C. Bailey, Acta Cryst., 10, 219 (1957)
3. R.S. Roth, J. Res. Natl. Bur. Std., 58, 75 (1957)
4. V.M. Goldschmidt, T. Barth, G. Lunde and W. Zachariasen, Die Gesetze der Krystallochemie, Skrifter Vidensk-Akad. Oslo 1-Mat-Naturv Klasse No. 2 (1926) 1.
5. K. Knox, Acta Cryst., 14, 583 (1961)
6. R. Hoppe, W. Liebe and W. Dahne, Z. anorg. chem., 307, 276 (1960)
7. D. Babel, Structure and Bonding 3, 1 (1967)
8. W. Rudorff, J. Kandler, G. Linke and D. Babel, Angew Chem., 71, 672 (1959), Z. Anorg. Chem., 317, 261, (1962)
9. F. Sugawara, S. Iida, Y. Syono and S. Akimoto, J. Phys. Soc. Japan, 20, 1529 (1965)
10. F. Sugawara Y. Syono and S. Akimoto, Mat. Res. Bull., 3 529 (1968)
11. O. Beckman and K. Knox, Phys. Rev., 121, 376 (1961)
12. S. Geller, J. Chem. Phys., 24, 1236 (1959)
13. W.L.W. Ludekin and A.J.E. Welch, Acta Cryst., 5, 841 (1952)
14. D.J. Machin and R.S. Nyholm, J. Chem. Soc., 3, 1500 (1963)
15. A. Okazaki, H. Iwanaga and N. Tsukuda, J. Phys. Soc., Japan, 24, 209 (1968)
16. A. Okazaki, N. Tsukuda, H. Iwanaga and M. Kawaminawi, Jap. J. Appl. Physics, 7, 977 (1968)

17. F.L. Carter, Solid State Comm., 7, 993 (1969)
18. W.H. Zachariasen, Acta Cryst., 18, 705 (1965)
19. M. Marezio, J.P. Remeika and P.D. Dernier, Acta Cryst., B26, 300 (1970)
20. B.V. Beznosikov and N.V. Beznosikova, Soviet Physics-Crystallography 13, 158 (1968)
21. Von O. Schmitz-Du Mont and H. Bornefeld, Z. anorgan. und allgem. Chem., 287, 3, 120 (1956)
22. G.R. Hunt, C.H. Perry and I. Ferguson, Phys. Rev., 134A, 688 (1964)
23. C.H. Perry, Jap. J. Appl. Phys., 4, Suppl. 1, 564, (1965)
24. M. Balkanski, P. Moch and M.K. Teng, J. Chem. Phys., 46, 1619 (1946)
25. C.H. Perry and E.F. Young, J. Appl. Phys., 38, 4616 (1967)
26. J.D. Axe and G.D. Petit, Phys. Rev., 157, 435 (1967)
27. A.P. Lane, D.W.A. Sharp, J.M. Barraclough, D.H. Brown, and D.A. Paterson, J. Chem. Soc. (A), (1971), 94.
28. N.N. Nesterova, I.G. Sinii, R.V. Pisarev and P.P. Syrnikov, Sov. Phys. - Solid State, 9, 15 (1967)
29. A.A. Karamyan, N.N. Nesterova and A.I. Stekhanov, Sov. Phys. - Solid State 11, 2148 (1970)
30. I. Nakagawa, T. Tsuchida and T. Shimanouchi, J. Chem. Phys., 47, 982 (1967)
31. W.G. Spitzer, R.C. Miller, D.A. Kleinman and L.E. Howarth, Phys. Rev., 126 1710 (1962)
32. W.G. Spitzer and D.A. Kleinman, Phys. Rev., 121, 1324 (1961)
33. J.M. Barraclough, D.H. Brown, A.P. Lane, D.W.A. Sharp and D.A. Paterson, Chem. Comm., 1969, 608.

CHAPTER 6 - K_2ZrF_6 AND K_2HfF_6 COMPLEXES

CHAPTER 6

K_2ZrF_6 and K_2HfF_6 Complexes

Complexes of the general formula A_2MF_6 (A = alkali metal) are known for all the elements of Group IVA and IVB. With the exception of K_2ZrF_6 and K_2HfF_6 , the presence of the octahedral MF_6^{2-} ions in the solids has been established by X-ray studies and they differ only in the packing arrangements of their lattices (1). However, when M is zirconium or hafnium other co-ordination numbers occur. The structure of the hexafluorozirconate(IV) anion varies with the nature of the cation and each of the salts of the hexafluorohafnates(IV) is isostructural with the hexafluorozirconate for the corresponding cation and has very similar lattice dimensions (2,3). Lithium hexafluorozirconate(IV) has a hexagonal lattice and contains ZrF_6^{2-} ions (4). The rubidium and cesium salts have been shown to have the trigonal form of the K_2GeF_6 structure (2). Potassium hexafluorozirconate(IV) on the other hand, crystallises in the orthorhombic system with space group $Cmcm$ (D_{2h}^{17}) having four molecules in the unit cell (3). These potassium complexes do not contain discrete ZrF_6^{2-} units but instead each Zr atom is bonded to eight fluorine atoms which surround it in a dodecahedral arrangement having the point group C_{2v} . Two edges of each ZrF_8 dodecahedron, on opposite sides of the Zr atom, are shared with adjacent dodecahedra, thereby forming chains along the c axis. There are, therefore, four bridging fluorine atoms in each ZrF_8 polyhedron. The structural unit can be thought of as a combination of two trapezoids and the

fluorine atoms which form one of the trapezoids act as bridges in the structure of K_2ZrF_6 . The lattice parameters for K_2ZrF_6 are $a = 6.58\text{\AA}$, $b = 11.4\text{\AA}$ and $c = 6.94\text{\AA}$, while those for K_2HfF_6 are $a = 6.58\text{\AA}$, $b = 11.4\text{\AA}$ and $c = 6.89\text{\AA}$ (2,3).

Previous infra-red and Raman studies have concentrated on those hexafluorometallates with discrete MF_6^{2-} units (5-9) and, for most of them, the i.r. active metal-fluorine stretching frequencies have been observed by Peacock and Sharp (5). Recently the single crystal infra-red and Raman spectra of some of the Group IV complex hexafluorometallates were reported by Forrest and Lane(10). Less work has been carried out on the vibrational spectra of K_2ZrF_6 and K_2HfF_6 and the data so far obtained were from powdered solids so that accurate symmetry assignments could not be made. It was therefore decided to use single crystals to study the infra-red and Raman spectra of K_2ZrF_6 and K_2HfF_6 thereby enabling more reliable assignments to be made.

Results and Discussion

The results of the factor group analysis on K_2ZrF_6 and K_2HfF_6 complexes are given in Table 6.1. In performing the analysis it was assumed that the Bravais unit cell, which is bimolecular, contained four potassium cations and one $(Zr_2F_{12})^{4-}$ polyhedral anion. From the analysis there should be twenty bands in the i.r. spectrum of which fourteen are internal modes associated with the $(Zr_2F_{12})^{4-}$ anion and the remaining six are lattice modes. The number and symmetry species of the i.r. active modes are given by the representations (6.1) and (6.2):

Table 6.1 Factor Group Analysis for K_2ZrF_6 and K_2HfF_6

D_{2h}	n_i	T	T'	R	α	n_i'	Activity
Ag	9	0	2	0	3	7	x^2, y^2, z^2
B_{1g}	7	0	2	1	1	4	xy
B_{2g}	4	0	0	1	1	3	xz
B_{3g}	7	0	2	1	1	4	yz
Au	4	0	0	0	0	4	
B_{1u}	7	1	2	0	0	4	z
B_{2u}	9	1	2	0	0	6	y
B_{3u}	7	1	2	0	0	4	x

Table 6.2 I.R. frequencies (cm^{-1}) for K_2ZrF_6 recorded at 77°K

B_{2u}	B_{1u} or B_{3u}
86	112
106	154
182	182
200	238
300	368
322	400
390	

$$\Gamma_{\text{internal}} = 4B_{1u} + 6B_{2u} + 4B_{3u} \quad (6.1)$$

$$\Gamma_{\text{external}} = 2B_{1u} + 2B_{2u} + 2B_{3u} \quad (6.2)$$

while those for the Raman active internal and external modes are given by representations (6.3) and (6.4):

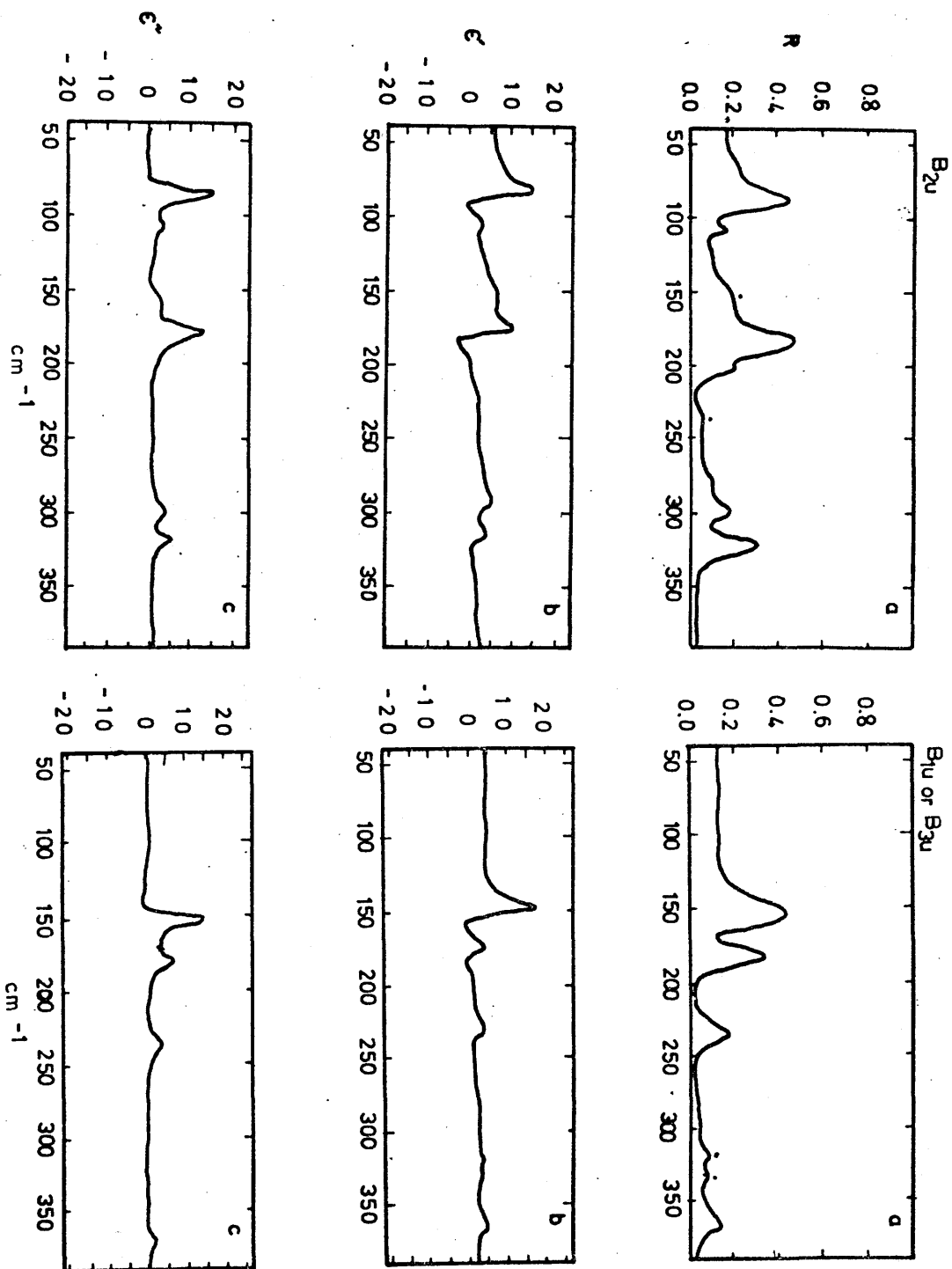
$$\Gamma_{\text{internal}} = 7A_g + 4B_{1g} + 3B_{2g} + 4B_{3g} \quad (6.3)$$

$$\Gamma_{\text{external}} = 2A_g + 3B_{1g} + B_{2g} + 3B_{3g} \quad (6.4)$$

These representations include three Raman active rotatory lattice modes of symmetry $B_{1g} + B_{2g} + B_{3g}$ which would correspond to torsional motions of the presumed $(Zr_2F_{12})^{4-}$ anion. However since the ZrF_8 polyhedra form infinite chains along the c axis, the torsional vibrations normally associated with isolated polyatomic groups cannot take place and these are better regarded as low energy internal twisting modes.

The optical quality of the crystals obtained was poor, and while both the Raman and the i.r. ($40 - 400\text{cm}^{-1}$) spectra could be recorded for K_2ZrF_6 only the Raman spectra could be recorded for K_2HfF_6 . Owing to the morphology of the K_2ZrF_6 crystals obtained, only two orientations could be recorded and the i.r. reflectance spectra obtained, recorded at 77°K are shown in Figure 6.1, from which the complexity of the spectra is evident. The poor optical quality of the crystals is reflected by the amount of polarization leakage (indicated) between the two spectra. The frequencies of the bands observed are given in Table 6.2. In view of the fact that seven bands are observed in one of the spectra, these are assigned to the B_{2u} modes of vibration since eight bands of this symmetry species are predicted as opposed to six in the other two orientations, the other spectrum contains either the B_{1u} or B_{3u} modes. A K-K analysis of the reflectivity data was carried out and is shown in Figure 6.1; little additional

FIGURE 6.1



Infrared Spectra and K-K Analysis of K_2ZrF_6 (at 77°K). a. Reflectance spectra b. Real dielectric response c. Imaginary dielectric response. (indicates polarization leakage)

information can be gained from the results owing to the polarization leakage but the B_{2u} bands at 154 cm^{-1} and 182 cm^{-1} are definitely separate modes and not the result of inversion caused by a weak oscillator. The observed frequencies are in good agreement with those previously reported (9) from powdered samples.

The frequencies observed in the Raman spectra of K_2ZrF_6 recorded at room temperature together with the polarization intensity data and symmetry assignments are given in Table 6.3. Owing to the lack of polarization effects in the Raman spectra of K_2HfF_6 , only the frequencies are given in Table 6.4. The Raman frequencies of the two complexes are very similar with those of the hafnium, complex slightly higher than those of the zirconium complex. This is a typical consequence of the lanthanide contraction. Nineteen bands are observed in the spectra of K_2ZrF_6 and only nine are observed for K_2HfF_6 . Here too, owing to polarization leakages, unambiguous symmetry assignments are difficult to make and too many A_g species are found. The most intense bands occur at 528 cm^{-1} for the zirconate and 538 cm^{-1} for the hafnate and are assigned to the terminal stretching modes ν_1 of species A_g . Since in the ZrF_8 polyhedron there are both terminal and bridging fluorines the vibrations involving the bridging framework will consist of both bending and stretching motions and this will result in a group of vibrations having a mixture of these characteristics. From the Raman results the frequencies can be grouped and thus allow the type of vibrations to be assigned. The two bands at 440 cm^{-1} and

Table 6.3 Raman Frequencies (cm^{-1}), Polarization Intensity Data and Symmetry Assignments, Recorded at Room Temperature for K_2ZrF_6

cm^{-1}	x(yy)x	x(yz)x	z(xx)z	z(xy)z	y(zz)y	y(zx)y	Symmetry Assignment
524	177	76	220	53	180	75	Ag
440	10	4	15	-	13	-	Ag
433	10			4			B_{1g}
383				8			B_{1g}
372	27	9	31	7	25	12	$Ag+B_{2g}$
349	19	7	46	9	18	10	Ag
314			10	15			B_{1g}
261	6						
235		5					B_{3g}
231	11				15		Ag
204	64	29	15	4	75	32	Ag
165	10	4					Ag
155			10	5			Ag
138			9				
122			19		35		Ag
119				4		8	$B_{1g}+B_{2g}$
111					27		Ag
102			26		55	7	Ag
90				5			B_{1g}

Table 6.4 Raman frequencies (cm^{-1}) for K_2HfF_6

538	v. strong
460	medium
388	medium
357	weak
325	weak
275	weak
248	weak
220	v. strong
171	weak

433 cm^{-1} are assigned as the bridge stretching modes of vibration while those between 261 cm^{-1} and 231 cm^{-1} are terminal bend and those between 204 - 138 cm^{-1} are the bridge bend modes of vibrations. Those bands below 110 cm^{-1} are assigned as lattice modes and the remaining bands are complex mixtures of terminal bend and bridge bend and stretching. Similar assignments can be made in the case of the observed i.r. frequencies. These assignments are made with reference to those made for the eight-co-ordinated anion TaF_8^{3-} (11) in Na_3TaF_8 although the TaF_8^{3-} anion is in the form of an isolated square Archimedian antiprism (12) whereas ZrF_8^{4-} dodecahedron involves fluorine bridges. The stretching mode ν_1 occurs at 622 cm^{-1} (11) for the TaF_8^{3-} anion and this higher value is not surprising since the average M-F bond strength will be less in ZrF_8^{4-} than in TaF_8^{3-} .

Experimental

Crystals of K_2ZrF_6 were obtained by slow evaporation of saturated 40% hydrofluoric acid solutions containing stoichiometric quantities of potassium fluoride and zirconium dioxide. The solutions were in platinum crucibles. Similar method was used to prepare K_2HfF_6 but the crystals obtained were of poor optical quality. Polarised Raman spectra were recorded at room temperature using 180° scattering geometry with the 641.0 nm lines of the Kr^+ laser as the exciting source.

References

1. A.G. Sharpe - in 'Advances in Fluorine Chemistry'
Vol. 1, Butterworths, London, 1960.
2. H. Bode and G. Teufer, Z. anorg. allgem. chem.,
283, 18, 1956.
3. H. Bode and G. Teufer, Acta Cryst., 1956, 9, 929.
4. R. Hoppe and W. Dahne, Naturwiss, 47, 397 (1960)
5. R.D. Peacock and D.W.A. Sharp, J. Chem. Soc. (1959),
2762.
6. D.H. Brown, K.R. Dixon, C.M. Livingston, R.H. Nuttal,
and D.W.A. Sharp, J. Chem. Soc. (A), 1967, 100.
7. P.A.W. Dean and D.F. Evans, J. Chem. Soc. (A), 1967, 698
8. P.W. Smith, R. Stoissinger and A.G. Turnbull, J. Chem.
Soc. (A), 1968, 3013.
9. A.P. Lane and D.W.A. Sharp, J. Chem. Soc. (A), 1969, 2942.
10. I.W. Forrest and A.P. Lane, Inorganic Chem., 15, 265, (1976)
11. K.O. Hartman and F.A. Miller, Spectrochim Acta., 1968, 24A
669
12. J.L. Hoard, W.J. Martin, M.E. Smith and J.F. Whitney,
J. Amer. Chem. Soc., 1954, 76, 3820.

CHAPTER 7 - PERCHLORATES

7.1 $M(ClO_4)_2 \cdot 6H_2O$ complexes

7.2 $Ni(ClO_4)_2 \cdot 6NH_3$ complexes

CHAPTER 7

Perchlorates: $M(\text{ClO}_4)_2 \cdot 6\text{H}_2\text{O}$

(M = Ni, Co, Fe, Mg) and $\text{Ni}(\text{NH}_3)_6 \cdot (\text{ClO}_4)_2$

1. $M(\text{ClO}_4)_2 \cdot 6\text{H}_2\text{O}$

INTRODUCTION

Wyckoff has reported that the perchlorates of general formula $M(\text{ClO}_4)_2 \cdot 6\text{H}_2\text{O}$ with M = Ni, Co, Fe and Mg are isostructural and crystallise in the orthorhombic space group C_{2v}^7 (Pmn) with two molecules in the unit cell (1). The divalent metal atom is octahedrally surrounded by the six water molecules and the perchlorate anion has tetrahedral symmetry with Cl-O distances of 1.46°A and 1.50°A .

However, recently these complexes have been reported to undergo phase transition from pseudo-hexagonal to monoclinic structure at $(230 \pm 15)^\circ\text{K}$ (2).

The infra-red and Raman spectra of several perchlorates have been studied by various workers both as powder and in solution (3-9). The i.r.-inactive ν_1 mode of T_d symmetry was observed in the i.r. spectra and in addition, the degenerate ν_3 and ν_4 modes were observed to be split. These observations have been interpreted as due to the loss of the T_d symmetry of the perchlorate anion in the solid.

The present studies aim at obtaining the single crystal Raman spectra from which an indication of the nature of the loss of the T_d symmetry would be evident. It is also hoped to observe the spectral changes occurring as a result of the reported phase transitions.

RESULTS AND DISCUSSION

The free perchlorate anion has nine modes of vibration giving rise to four fundamental frequencies. These have been established from Raman spectra of dilute solutions and occur at 935 cm^{-1} (ν_1), 462 cm^{-1} (ν_2), 1102 cm^{-1} (ν_3) and 628 cm^{-1} (ν_4) (10). Though the perchlorate ion has very little tendency to form complex compounds with metal ions, perchlorate complexes of transition metals are known (11). The appearance of the forbidden transition in the i.r. spectrum and the splitting of the degenerate modes could arise from three possible causes:

- (a) distortion of the ClO_4^- tetrahedron in the crystal lattice,
- (b) a non-uniform field due to the water molecules around the cation,
- (c) Covalent bonding of the perchlorate to the metal through one or more of the oxygen atoms,

Since the differences in the reported Cl-O distances (1) are too small to cause any appreciable effect on the spectrum and forbidden transitions have been observed even in the i.r. spectra of anhydrous perchlorates (12), it would appear that (a) and (b), listed above, are not responsible for the additional spectral features. Finally, if the perchlorate anion is to function as a unidentate ligand, then the co-ordinated oxygen atom will no longer be equivalent to the other three and the effective symmetry will be lowered to C_{3v} . The symmetry will be further lowered to C_{2v} when two oxygen atoms become co-ordinated either to the same or different ions.

The correlation between the unco-ordinated (T_d), unidentate (C_{3v}) and bidentate (C_{2v}) ClO_4^- anion is given in Table 7.1 together with the selection rules. Considering only the stretching modes of Cl-O, ν_1 and ν_3 , there should be, in the Raman spectra, two bands for the unco-ordinated anion, three and four bands for the unidentate and bidentate anions respectively. The frequencies observed in the Raman spectra of $Co(ClO_4)_2 \cdot 6H_2O$ and $Ni(ClO_4)_2 \cdot 6H_2O$ recorded as single crystals at room temperature with their assignments are given in Table 7.2. In both complexes the ν_3 band occurred as a broad, weak band without any splitting. The weak intensity could be due to the fact that it is observed as a strong band in the i.r. spectra (8). The broadness could well be due to the overlapping of unresolved bands. A splitting of 6 cm^{-1} is observed for ν_4 in the cobalt complex whereas no splitting of ν_4 occurs in the nickel complex. In the spectra of the nickel complex there is a shoulder at 922 cm^{-1} which is of medium intensity. This is assigned to an overtone of the ν_2 mode since the high intensity ν_2 has a component having the same symmetry as the totally symmetric fundamental ν_1 whose frequency is observed at 935 cm^{-1} . This overtone, $2\nu_2$ appears with a medium intensity due to Fermi resonance due to the close proximity of the ν_1 frequency. Similar bands have been observed in the Raman spectra of $KClO_4$ (13,14) and in that of $Ni(NH_3)_6 \cdot (ClO_4)_2$ discussed below.

The band observed at 70 cm^{-1} in both complexes is assigned as lattice mode.

It is known that covalent perchlorates are unstable (12,13) so that bonding of this type could not wholly account

Table 7.1

State of ClO_4	Effective Symmetry	ν_1	ν_2	(ν_3, ν_4)
Unco-ordinated	T_d	$A_1(R)$	$E(R)$	$F_2(R, IR)$
Unidentate	C_{3v}	$A_1(R, IR)$	E	$A(R, IR) \quad E(R, IR)$
Bidentate	C_{2v}	$A_1(R, IR)$	$A_1 \quad A_2$ $(R, IR) \quad (R)$	$A_1(R, IR) \quad B_1 \quad B_2$ $(R, IR) \quad (R, IR) \quad (R, IR)$

Table 7.2 Raman Frequencies (cm^{-1}) and Assignments, recorded at RT for $\text{Co}(\text{ClO}_4)_2 \cdot 6\text{H}_2\text{O}$ and $\text{Ni}(\text{ClO}_4)_2 \cdot 6\text{H}_2\text{O}$

<u>$\text{Co}(\text{ClO}_4)_2 \cdot 6\text{H}_2\text{O}$</u>		<u>$\text{Ni}(\text{ClO}_4)_2 \cdot 6\text{H}_2\text{O}$</u>	
cm^{-1}	Assignment	cm^{-1}	Assignment
1092 weak, broad	ν_3	1110 weak, broad	ν_3
938 very strong	ν_1	935 very strong	ν_1
632 medium	ν_4	922 medium	$2\nu_2$
626 medium	ν_4	628 medium	ν_4
468 medium	ν_2	463 medium	ν_2
70 broad, weak	lattice	70 broad, weak	lattice

for the splitting of the degenerate modes. It is therefore likely that the small bond length differences, together with the other two factors, the extent of whose effects are not known, are the cause of the problem.

Attempts to record the low temperature single crystal Raman spectra in order to observe the phase change were not possible since the fragile needle-like crystals crumbled when cooled. However, the spectra could be recorded at 273°K and were found to be very similar to those obtained at room temperature.

7.2. $\text{Ni}(\text{NH}_3)_6 \cdot (\text{ClO}_4)_2$

$\text{Ni}(\text{NH}_3)_6 \cdot (\text{ClO}_4)_2$ belongs to the series of complexes of general formula $\text{Me}(\text{NH}_3)_6 \cdot \text{X}_2$ where $\text{Me} = \text{Co}, \text{Ni}$, and $\text{X} = \text{Cl}, \text{Br}, \text{BF}_4, \text{ClO}_4$ and PF_6 which are all isostructural and crystallize in the cubic system with the regular space group O_h^5 ($\text{Fm}\bar{3}\text{m}$) (15). The lattice constant for $\text{Ni}(\text{NH}_3)_6 \cdot (\text{ClO}_4)_2$ is 11.219°A.

Owing to their high symmetry many spectroscopic studies have been carried out (16-21). However, Raman studies are less numerous (20) and so far no single crystal work has been undertaken owing to the difficulty in obtaining single crystals.

In this work single crystal Raman spectra of $\text{Ni}(\text{NH}_3)_6 \cdot (\text{ClO}_4)_2$ were obtained with the aim of observing the splitting, if any, of the degenerate modes of the internal vibrations of the tetrahedral anion ClO_4^- .

RESULTS AND DISCUSSION

The Raman spectra were recorded at both room temperature and liquid nitrogen temperature and the observed frequencies together with their assignment to the tetrahedral modes of

vibrations are given in Table 7.3.

The room temperature spectrum was very similar to that of $\text{Ni}(\text{H}_2\text{O})_6 \cdot (\text{ClO}_4)_2$ except for the presence of some bands due to the internal vibrations of the $[\text{Ni}(\text{NH}_3)_6]^{2-}$ ion (21). The most intense band is at 923 cm^{-1} and is assigned to the ν_1 stretching mode of the tetrahedral ClO_4^- anion. Two bands at 624 cm^{-1} and 613 cm^{-1} are assigned to components of ν_4 and thus a splitting of 11 cm^{-1} is observed although this was absent in the $\text{Ni}(\text{H}_2\text{O})_6 \cdot (\text{ClO}_4)_2$ complex. The overtone of ν_2 is observed at 900 cm^{-1} and the intensity of this band is again attributed to Fermi resonance with ν_1 . Only one band is observed at 1076 cm^{-1} for ν_3 and the band at 459 cm^{-1} is assigned to the ν_2 mode. All the other bands belong to the internal vibration of the cation. The low temperature spectrum is very similar to that at room temperature, the only difference being the appearance of only one band at 932 cm^{-1} which might be due to an internal vibration of the cation. Because of the similarity of the room temperature spectrum to that of the low temperature it can be concluded that no structural phase change has occurred. However, structural phase change has been reported for $\text{Ni}(\text{NH}_3)_2(\text{BF}_4)_2$ (22,23).

EXPERIMENTAL

Crystals of the complexes $\text{M}(\text{H}_2\text{O})_6 \cdot (\text{ClO}_4)_2$ $\text{M} = \text{Co}, \text{Ni}$ were obtained from a solution of the metal carbonate in 40% perchloric acid and grew as very small needles. The crystals of $\text{Ni}(\text{NH}_3)_6 \cdot (\text{ClO}_4)_2$ were prepared in two steps. First by dissolving Nickel(II) carbonate in 40% perchloric acid at 110°C . On cooling down small crystallites (needles) of $\text{Ni}(\text{H}_2\text{O})_6$

Table 7.3 Raman Frequencies (cm^{-1}) and Assignments
for the Complex $\text{Ni}(\text{NH}_3)_6(\text{ClO}_4)_2$

RT	LT	Assignment T_d mode
221 w	227 w	
293 w	305 w	
390 w	399 w	
447 m	447 m	
459 m	459 m	ν_2
613 m	613 m	ν_4
624 m	624 m	ν_4
900 m	902 m	$2\nu_2$
923 s	921 s	ν_1
	932 m	
1076 w,b.	1072 w,b.	ν_3

$(\text{ClO}_4)_2$ were obtained. Secondly a solution of NH_4OH was added to the crystals of $\text{Ni}(\text{H}_2\text{O})_6 \cdot (\text{ClO}_4)_2$ at 50°C and on cooling down blue octahedric crystallites of $\text{Ni}(\text{NH}_3)_6 \cdot (\text{ClO}_4)_2$ were obtained the composition of which was confirmed by analysis.

The 457.9 nm (indigo) line of the Ar^+ laser was used as the exciting line to obtain the Raman spectra of $\text{Ni}(\text{NH}_3)_6 \cdot (\text{ClO}_4)_2$. In the case of the $\text{Ni}(\text{H}_2\text{O})_6 \cdot \text{ClO}_4$ the 514.5 nm (green) line was used while the 647.1 nm (red) line of the Kr^+ laser was used as the exciting line for the $\text{Co}(\text{H}_2\text{O})_6 \cdot (\text{ClO}_4)_2$ complex.

References

1. W.G. Wyckoff, Crystal Structures, Vol. 3, Interscience New York (1965)
2. B.K. Chaudhuri, Solid State Comm., 16, 767 (1975)
3. A.M. Taylor, Trans. Faraday Soc., 25, 856 (1929)
4. C. Schaefer and M. Schubert, Z. Physik, 7, 297 (1921)
5. F.A. Miller and C.H. Wilkins, Analy. Chem. 25, 1253 (1952)
6. J. Goubeau, Z. Physik. Chem. (Leipzig) B36, 45 (1937)
7. L.A. Woodward, Trans. Faraday Soc., 54, 1271 (1958)
8. S.D. Ross, Spectrochim. Acta 18 (1962) 225
9. B.J. Hathaway and A.E. Underhill, J. Chem. Soc. 3709 (1960)
10. G. Herzberg, 'I.R. and Raman Spectra of Polyatomic Molecules' Van Nostrand, N. York (1945)
11. F.A. Cotton and G. Wilkinson, - 'Advanced Inorg. Chem.' 3rd Edition, Interscience N. York (1972)
12. H.E. Roscoe, Ann. Chem. Liebigs 124, 124 (1862)
13. J. Meyer and W. Spermann, Z. Anorg. Chem., 228, 341 (1936)
14. N. Krishnamurthy, Proc. Indian Acad. Sc., A61, 118, (1965)
15. W.G. Wyckoff, 'Crystal Structures' Interscience, New York 1960, Chapt. X.
16. T. Simanondin and J. Nakagawa, Spectrochim Acta, 22 759, 1707 (1966)
17. Sacconi, A. Sabatini and P. Gaus, Inorg. Chem., 3, 1771 (1964)
18. G.F. Svatos, J. Amer. Chem. Soc., 77, 6159 (1955)
19. D.B. Powell, J. Chem. Soc., 78, 3108, (1956)
20. H. Poulet, J.M. Terasse and J.P. Mathieu, Spectrochim Acta., 20, 305 (1964)
21. T. Grzybek, J.M. Janik, A. Kulczyck and G. Pytasz, J. Raman Spectra, 3, 185 (1973).

22. J. Stankowski, J.M. Janik, A. Dezor and B. Szczaniecki,
Phys. Stat. Sol. (a), 16, K167 (1973).
23. E. Dynowska, Phys. Stat. Sol. (a), 31, K23 (1975)

CHAPTER 8 - GENERAL EXPERIMENTAL METHODS

- 8.1 Far infrared interferometer
- 8.2 Laser Raman spectrometer
- 8.3 Preparation of single crystals
- 8.4 Determination of crystallographic axes

CHAPTER 8GENERAL EXPERIMENTAL METHODS8.1 Far Infrared Interferometer

The 'far infrared' is generally accepted as that region between 400cm^{-1} and 10cm^{-1} . The two problems associated with this region have been the low intensity of the sources available and the insensitivity of detectors available for the low energies associated with these longer wavelengths. These problems have been alleviated by the general use of high pressure mercury lamps and Golay detectors. Advances in filter design have also helped to remove the higher order reflections from diffraction gratings.

In any spectroscopic technique, a polychromatic beam of radiation must in some way be ordered so that each frequency of the radiation is differentiated from the others. Conventionally, this differentiation is carried out by passing the beam through a prism or reflecting it from a grating so that each frequency is distinguished spatially. Recent research in far infrared spectroscopy, however, employs a different technique which involves interference. Chemists commonly use the Michelson type (1) of interferometers of which the Beckman-RIIC FS 720 Fourier Spectrophotometer used in this study is one. The source of radiation is a quartz jacketed high-pressure mercury lamp. This radiation is chopped, rendered parallel and then divided into two beams by a taut film of polyethylene terephthalate ('Mylar') which

acts as a beam splitter. By varying the thickness of this film, e.g. 12, 25, 60 or 100 μm , various parts of the region below 400 cm^{-1} can be covered with high efficiency. Part of the radiation is transmitted on to a fixed mirror while the other part is reflected to a movable mirror to which a motor is attached to enable the mirror to travel. The radiation travels back from the mirrors along its incident paths and is recombined at the beam splitter. The radiation which is rejoined after reflection by the mirrors has certain frequencies which either constructively or destructively interfere with each other. The interference arises because of the variable path difference between the two beams introduced by the movable mirror. After the rays are recombined, the radiation passes to a condenser consisting of convex and concave mirrors which focus the light on the sample. The rays, reflected from the sample, are focused by another condensing system onto a Golay detector. The signal from the Golay is amplified and demodulated and the trace of signal against path difference on a chart recorder is known as an 'interferogram'. There is no monochromator in the instrument. The radiation which is transmitted by the detector contains all the frequencies passed by the filter so that the signal-to-noise ratio is very large and this feature is known as Multiplex or Fellgett advantage (2). From the interferogram the spectral intensity $I(\nu)$ at each wavenumber is obtained by means of the Fourier transformation:

$$I(\nu) = \int_{-\infty}^{+\infty} F(X) \cos 2\pi\nu x dx$$

In practice $F(X)$ can only be obtained over a finite interval $-X$ to $+X$ so the calculated spectrum $I(\nu)$ is given by a truncated integral

$$I(\nu) = \int_{-X}^{+X} f(X) \cos 2\pi \nu x dx$$

The computation was carried out by an FTC 100 analogue - digital computer and the spectra plotted on a recording wave analyser. The normal range of the instrument is $40 - 400\text{cm}^{-1}$ but could be extended as far as 10cm^{-1} by using the appropriate thickness of beam splitter, suitable filter and sampling interval. To make it possible for reflectance measurements there is incorporated in the instrument an FS 7RF module for near normal incidence and an A.I.M. wire grid polariser was used to obtain the polarised spectra. A VTL2 variable temperature cell with the temperature monitored by a copper-constantan thermocouple fitted to the sample position was used to record spectra down to liquid nitrogen temperature. Since the spectrometer is single-beam runs had to be carried out on an aluminised mirror as background and on the sample separately and the two resultant spectra are ratioed out by the computer. The optimum resolution was 2.5cm^{-1} . The entire optical system is enclosed and has to be evacuated to a pressure less than 0.1mm Hg in order to prevent atmospheric water vapour absorption. Interferometric methods have certain important advantages over the conventional absorption spectroscopy. The most important is the light gathering power at any given spectroscopic resolution. No light is wasted on exit slits and all frequencies in the range of interest are incident on the

detector except those which are absorbed by the sample and those which destructively interfere. The large amount of signal passing to the detector increases signal-to-noise ratio and allows better spectra to be obtained. The resolution of an interferometer is proportional to the maximum path difference and hence to double the resolution of a given spectrum the mirror travel, i.e. the measuring time is doubled. This is an advantage over a grating instrument where both the entrance and exit slits must be halved, so reducing the energy four-fold, in order to double the resolution. The main disadvantage is due to the fact that it is more difficult to recognise unsatisfactory conditions during a run, for example, the decomposition of the sample. Also the occurrence of a single noise-spike in the interferogram will affect all the frequencies in the spectrum.

8.2 Laser Raman Spectrometer

The basic components of any instrument for measuring the Raman effect are: a source of radiation which nowadays is a laser source, a means of collecting the scattered light from the sample, i.e. sample optics, a monochromator and a detector/electronics/recorder system.

The advent of laser sources has led to a renaissance in the technique of Raman spectroscopy. The intensity of Raman scattering is very low. The intensity of the Stokes Raman lines for a $0 \rightarrow 1$ vibrational energy level transition is given by

$$I = (\nu_0 - \nu_m)^4 N_0 (P_{0 \rightarrow 1})^2$$

and for the anti-Stokes $1 \rightarrow 0$ transition:

$$I = (\nu_0 + \nu_m)^4 N_1 (P_{1 \rightarrow 0})^2$$

where I is the intensity of the scattered radiation, N is the number of molecules producing the scattering in the energy level indicated, and P is the probability of the given transition occurring. From the above two equations it is evident that to increase the magnitude of I either the intensity of the incident light must be increased or a greater number of scattering molecules must be present. Since the latter condition cannot easily be fulfilled it is necessary to increase the power of the incident radiation ν_0 for a higher Raman intensity. Laser sources are therefore ideal for the purpose. Most lasers in use for Raman spectroscopy are gas-filled devices although the more powerful ion lasers such as Ar^+ and Kr^+ are also in use. In this study Coherent Radiation 52G Ar^+ and Kr^+ lasers were used. The argon laser is composed of a gas discharge tube filled with argon which is strongly excited by the passage of an electric current. A small proportion of the input power is then available as a beam of highly coherent radiation from one end of the laser. The optical system incorporated in the laser uses a pair of mirrors to form an optical resonator or cavity and therefore the divergence of the beam of radiation is small. The windows which seal the ends of the discharge tube are set at the Brewster angle and this allows the radiation to have specific polarization. The Ar^+ laser may have an output of 1 watt or more and the collimated nature of the laser energy allows

focusing for excitation of extremely small volumes. Most of the total intensity of scattered radiation occurs at ν_0 (Rayleigh scatter) and only $10^{-7}I_0$ occurs as Raman scatter. Since the Raman radiation is mixed with relatively intense Rayleigh radiation of very similar wavelength it is very essential to use monochromators with very low stray-light. The 'Spex Ramalog 4' used in this work incorporates double grating monochromators.

To collect as much scattered light as possible the optical system involves focusing of the laser beam within the sample. This produces both an increase in illumination flux-density and also a small volume of illumination which makes it possible to collect efficiently radiation emitted over a wide angle. With the use of a lens, the laser emission which is both monochromatic and coherent can be finely focussed.

It is also necessary to use very sensitive detectors and the introduction of the photomultiplier cell in place of the photographic plate has contributed immensely to the advances in Raman spectroscopy. By cooling the photomultiplier, a marked enhancement in the signal-to-noise ratio results due to a decrease in the dark current. The Raman scattered radiation presented to the detector may range in power from that which may be easily detected to that which is below the level of the best detection techniques available ($10^{-14}W$). There is a fundamental distinction in the use of photographic emulsion and a photoelectric detector. The photographic emulsion is used in a nonscanning system where

the whole of the spectral data is presented to the detector during the total time of the measurement. Each spectral element is observed during the total time of the observation, T . The photoelectric detector, however, is used in a scanning system where only information in a given spectral bandwidth ($\Delta\nu$) is presented to the photomultiplier in a given time interval. That is, when N spectral elements are to be measured during a total time T , each spectral element is observed during a time (T/N) .

8.3 Preparation of Single Crystals

The single crystals used in the present work were prepared either from melts or from solutions.

8.3i Melt Growth - Stockbarger Technique

The Stockbarger technique (3) of preparing single crystals is based on the solidification of a stoichiometric melt and a number of complex halides with congruent melting points were prepared by this method. Stoichiometric amounts of the anhydrous constituent halides are sealed in an evacuated tube, the end of which, being an important parameter in starting a single crystal, is tapered. The basis of the process is to lower the molten complex at its melting point very slowly through a steep temperature gradient of about $2^{\circ}\text{C}/\text{mm}$; the top of the temperature gradient being at the melting point of the complex. For the process to be successful, there must be strict temperature control and no motion other than the steady downward progress of the tube.

The furnace used consisted of a silica tube about 60cm long and 7cm inside diameter which was wound with resistance wire and contained in an asbestos box filled with "Vermiculite", an electrical and thermal insulating material. The windings of the silica core were divided into two halves, connected in series, which gave a higher temperature in the upper section. The temperature at a given point was controlled by a Pt/Pt-Rh thermocouple connected to a thermostat. The furnaces were capable of maintaining temperatures in excess of 1000°C for protracted periods. The temperature at the centre of the furnace was set about 20°C above the melting point of the complex.

Silica or glass tubes, depending on the melting point were used for the chloride melts while for the fluorides, graphite or platinum crucibles in sealed platinum tubes were used. Pure starting materials were necessary since impurities would interfere with uniform crystallization. At high temperatures explosive pressures might build up due to the presence of volatiles such as moisture. 'Optran' grade reagents and wherever possible sublimed materials were used. Volatiles were removed by prolonged evacuation of the crucibles at about 300°C prior to sealing. Generally the starting materials were handled in a moisture-free inert atmosphere box. The sealed crucible containing the stoichiometric amounts of the constituent halides was suspended about 1cm above the centre of the furnace and after the set temperature had been reached the crucible containing the molten complex was allowed to equilibrate for about two hours before being lowered through the furnace at a rate of 2mm per hour. Crystallization begins at the tapered end of the crucible as it goes through the temperature

gradient. After four days the tube and contents were cooled slowly ($1^{\circ}\text{C}/\text{min}$) to room temperature to prevent strain on the crystals formed.

8.3iii Crystallization from Solution

A number of crystals were grown from solutions containing the stoichiometric amounts of the appropriate materials. These incongruently saturating complexes were grown by reference to the literature for the correct molar ratios. To obtain good quality crystals controlled evaporation of the solution was necessary. This was achieved by placing the beaker containing the saturated solution in a large Dewar flask with the top covered by cotton wool. The sizes of crystals obtained from solution differed but were generally suitable for Raman work. Elemental analysis was often employed to confirm the composition of the crystals, though this was not necessary for the crystals from the melt.

8.4 Determination of Crystallographic Axes

The directions of the crystallographic axes in the crystal were deduced from the angles between natural faces or intersecting cleavage planes, and the optical extinction positions between crossed polarisers in a polarising microscope. Most of the crystals had well developed natural faces or cleavage planes. However, especially with those from the melt, grinding and polishing of the faces were required. This was done either manually or on a Logitech PM2 polishing machine using a solder lap and diamond paste, (down to 1μ mesh).

Where the crystals were very small in size the effective sample area for i.r. reflectance was increased by mounting a number of the crystals of the same compound side by side.

Care, however, must be taken to ensure that the orientations were the same for each.

References

1. Michelson, A.A. "Studies in Optics", University of Chicago Press, Chicago 1927.
2. Fellgett, P., J. Phys. Radium, 19, 187, 237 (1958)
3. Stockbarger, D.C., Rev. Sci. Instrum. (1936), 10, 205